

9-12-2007

The Mechanism of High MR Thioredoxin Reductase Investigated by Semisynthesis and Crystallography

Brian E. Eckenroth
University of Vermont

Follow this and additional works at: <http://scholarworks.uvm.edu/graddis>

Recommended Citation

Eckenroth, Brian E., "The Mechanism of High MR Thioredoxin Reductase Investigated by Semisynthesis and Crystallography" (2007). *Graduate College Dissertations and Theses*. Paper 73.

This Dissertation is brought to you for free and open access by the Dissertations and Theses at ScholarWorks @ UVM. It has been accepted for inclusion in Graduate College Dissertations and Theses by an authorized administrator of ScholarWorks @ UVM. For more information, please contact donna.omalley@uvm.edu.

**THE MECHANISM OF HIGH M_r THIOREDOXIN REDUCTASE
INVESTIGATED BY SEMISYNTHESIS AND CRYSTALLOGRAPHY**

A Dissertation Presented

by

Brian E. Eckenroth

to

The Faculty of the Graduate College

of


The University of Vermont

**In Partial Fulfillment of the Requirements
for the Degree of Doctor of Philosophy
Specializing in Biochemistry**


May, 2007

Accepted by the Faculty of the Graduate College, The University of Vermont, in partial fulfillment of the requirements for the degree of Doctor of Philosophy, specializing in Biochemistry.

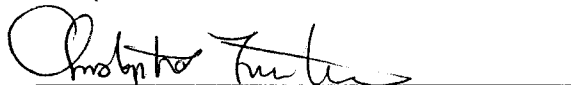
Dissertation Examination Committee:



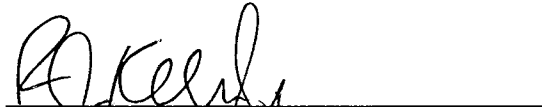
Robert J. Hondal, Ph.D. Advisor




Stephen J. Everse, Ph.D.



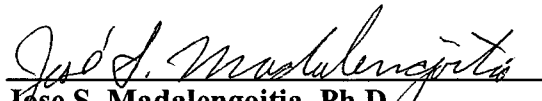
Christopher S. Francklyn, Ph.D.



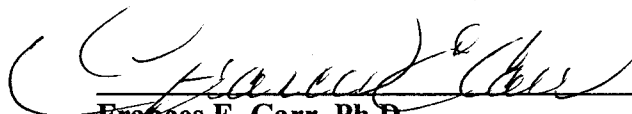
Robert J. Kelm, Ph.D.



Scott W. Morrival, Ph.D.



Jose S. Madalenoitia, Ph.D. Chairperson



Frances E. Carr, Ph.D. Vice President for Research
and Dean of Graduate Studies

Date: April 04, 2007

ABSTRACT

The high M_r (~55 kDa) thioredoxin reductases (TR) characteristic of higher eukaryotes are members of the glutathione reductase (GR) family of pyridine nucleotide disulfide oxidoreductases. These homodimeric enzymes catalyze the reduction of a cognate disulfide substrate. During the enzymatic cycle, reducing equivalents pass from NADPH to the conserved active site disulfide via an enzyme-bound FAD and then to the cognate substrate. TRs are unique in the family as electrons are then transferred to the C-terminal active site of the adjacent molecule as part of a 16 amino acid extension (in place of the cognate GR substrate GSSG), prior to transfer to the substrate thioredoxin. Each electron transfer step occurs via thiol-disulfide exchange in a multi-step process mediated by a conserved catalytic acid/base. Mammalian TRs require selenocysteine (Sec) incorporated into the Gly-Cys-Sec-Gly-OH (GCUG) C-terminal tetrapeptide motif, while the TR from *Drosophila melanogaster* (*Dm*TR) does not, and instead contains a Ser-Cys-Cys-Ser-OH (SCCS) tetrapeptide motif indicating that Sec is not universally necessary to catalyze the reduction of thioredoxin.

This project has achieved three major objectives; **1)** development of a semisynthetic method for production of mouse mitochondrial TR (mTR3) for structure-function studies, **2)** establishment of a new method to study the mechanism of TR by using tetrapeptides in the oxidized form equivalent to the C-terminal active sites as substrates for the truncated forms of both enzymes, **3)** determination of the crystal structure of *Dm*TR. The results show that the structure of *Dm*TR explains the biochemical data and has developed a new testable hypothesis in the field for the requirement of Sec in mammalian TR.

We demonstrate that the tetrapeptides tested in Aim 2 were all better substrates for *Dm*TR. The data also shows a far greater dependence on Sec for mTR3 than *Dm*TR, which is in agreement with that observed for the collection full-length mutants produced for each enzyme in Aim 1. As this method of investigation is more analogous to the other enzymes of the GR family, the structures of the tetrapeptides determined by NMR spectroscopy were oriented in the active site of the both enzymes using the diglutathione bound in the structure of GR as template. *Dm*TR appears to have a more open active site than observed in the known structure of mTR3. Residues from the helical face of the FAD-domain proximal to the FAD-associated active site are less bulky in *Dm*TR to accommodate the hydroxyls of the serines. This is likely to make the enzyme more amenable for the conformational switching of the SCCS peptide necessary to protonate the leaving group cysteine by the proposed catalytic acid/base. In contrast, mTR3 shows a more restricted interface by incorporating bulkier residues at the interface in conjunction with the smaller Gly residues of the C-terminal sequence GCUG. The tetrapeptides display a conformational preference not suitable for protonation of the first leaving group in mTR3.

CITATIONS

Material from this dissertation has been published in the following form:

Eckenroth, B.E., Harris, K., Turanov, A. A., Gladyshev, V. N., Raines, R. T., and Hondal, R. J. (2006) Semisynthesis and Characterization of Mammalian Thioredoxin Reductase. *Biochemistry* 45, 5158-5170.

Eckenroth, B. E., Rould, M. A., Hondal, R. J., and Everse, S. J. (2007) Structural and Biochemical Studies Reveal Differences in the Catalytic Mechanisms of Mammalian and *Drosophila melanogaster* Thioredoxin Reductases. *Biochemistry* 46, 4694-4705.

Material from this dissertation has been submitted for publication on March 9th, 2007 to *Biochemistry* in the following form:

Eckenroth, B. E., Harris, K. M., Lacey, B. M., Lothrop, A. P., and Hondal, R. J. (2007) Investigation of the C-Terminal Redox Center of High M_r Thioredoxin Reductase by Protein Engineering and Semisynthesis. *Biochemistry*, Submitted.

DEDICATION

This dissertation is dedicated to my family, especially my parents Dean and Nancy, for a lifetime of love and support for whatever I have chosen to pursue and for providing the foundation for character and integrity that has allowed me to develop and succeed. I would like to thank Amanda for all of her support, a new direction, and a means to escape. There are so many friends I would like to thank for their encouragement and camaraderie, and, of course, graduate school commiseration. One special person in particular whose years of friendship and support has been so important to me is Lisa. I would like to dedicate this to her, and her son Christopher, whose life and achievements in the face of tremendous challenges have been, and will continue to be, a source of inspiration.

ACKNOWLEDGMENTS

I would like to thank my advisor, Robert J. Hondal, for his scientific guidance, providing a technically diverse environment in which to study, and the opportunity to independently pursue elements of this project. I would also like to recognize all the members of the Hondal laboratory, past and present, for their support and contribution to the successes of this project, especially Brian Lacey and Erik Ruggles for their support throughout. Additional recognition is extended to Ms. Katharine Harris for her efforts towards developing the methods to produce the peptides used in this study and to P. Bruce Dekker for determining their NMR structures.

I would also like to thank Stephen J. Everse for all his time and the support dedicated to the crystallographic projects. I am grateful for the guidance and input from the members of my thesis studies committee and for the Department of Biochemistry's commitment to the progress and support of the students. I would also like to express my gratitude towards Mark A. Rould for his assistance and insight as well as the members of the Center for X-Ray crystallography and Vermont DOE EPSCoR for supporting the structural projects.

TABLE OF CONTENTS

CITATIONS	ii
DEDICATION	iii
ACKNOWLEDGMENTS	iv
LIST OF TABLES	viii
LIST OF FIGURES	ix
CHAPTER 1.	1
INTRODUCTION TO THE THIOREDOXIN SYSTEM.....	1
THIOREDOXIN REDUCTASE AND PHYSIOLOGY	2
THE GLUTATHIONE REDUCTASE FAMILY	5
Structural Overview.....	5
FAD Binding Domain.....	6
NAD(P) Binding Domain.....	9
The Dimerization Domain.....	10
Substrate Binding.....	13
SPECTRAL CHARACTERISTICS OF FLAVIN AND FLAVOPROTEINS	14
THE GLUTATHIONE REDUCTASE CATALYTIC CYCLE.....	16
Catalytic Overview.....	16
Flavin Spectra and Enzyme Kinetics.....	17
The Reductive Half-Reaction of GR.....	18
The Oxidative Half-Reaction of GR.....	19
THE HIGH M_r THIOREDOXIN REDUCTASE CATALYTIC CYCLE.....	21
SELENOCYSTEINE IS ESSENTIAL TO MAMMALIAN TR.....	24
SPECIFIC AIMS	27
CHAPTER 2:	40
SEMISYNTHESIS OF MAMMALIAN THIOREDOXIN REDUCTASE	40
Introduction to Semisynthesis.....	42
METHODS	44
Peptide Synthesis.....	44
Mutagenesis and Transformation.....	44
Thioredoxin Reductase Expression and Cleavage from Chitin Resin.....	46
Ligation of the CUG Peptide to Truncated Construct.....	47
Final Purification of Enzymes.....	47
Determination of the Selenium Content of the Semisynthetic TR.....	48
"Off-Resin" Ligation Efficiency.....	49
Enzymatic Characterization of Thioredoxin Reductase.....	49
DTNB Reductase Activity.....	50
Thioredoxin Reductase Activity.....	50
Peroxidase Activity.....	51
Production of Thioredoxin.....	51
Determination of the Mass of Truncated and Semisynthetic TRs.....	52

Peptide Mass Mapping of Tryptic Fragments.....	53
RESULTS AND DISCUSSION.....	54
Expression and Purification.....	54
Selenium Content of the Semisynthetic Enzyme.....	56
DTNB Reductase Activity.....	56
Activity toward Thioredoxin.....	57
Comparison of the Activity of Semisynthetic TR to That of Recombinant TR. ..	59
Peroxidase Activity.....	59
Ligation Efficiency for Off-Resin Ligations.....	60
Determination of the Mass of Truncated and Semisynthetic TRs.....	62
Peptide Mass Mapping of Tryptic Fragments.....	62
CHAPTER 3.....	82
STRUCTURE-FUNCTION STUDIES OF THE C-TERMINAL TETRAPEPTIDE MOTIF OF THIOREDOXIN REDUCTASE USING SEMISYNTHESIS	82
METHODS.....	85
Peptide Synthesis.....	85
Cloning and Expression of mTR3.....	86
Cloning and Expression of DmTR.....	86
Production of C-terminal Mutants of DmTR.....	87
Thioredoxin Activity pH Optima.....	88
RESULTS AND DISCUSSION.....	89
Production of TR.....	89
Activity of mTR3 Towards Thioredoxin.....	91
Low Activity TR Trx Assays and Consumption of NADPH.....	93
Activity for DmTR Towards Thioredoxin.....	94
Comparison of DTNB Reductase Activities.....	95
Peroxidase Activity of Semisynthetic mTR3.....	97
Interpretation of Structure-Function Study.....	98
From interpretation to hypothesis.....	100
CHAPTER 4.....	114
TRUNCATED THIOREDOXIN REDUCTASE AS A DISULFIDE OXIDOREDUCTASE INVESTIGATED BY PEPTIDE COMPLEMENTATION	114
METHODS.....	116
Activity of truncated TR towards C-terminal Tetrapeptide Substrates.....	116
RESULTS AND DISCUSSION.....	116
Truncated TR as a Disulfide Reductase.....	117
Indication of a Critical Leaving Group Effect for mTR3.....	119
Correlation to C-terminal Structure-Function Results.....	120
CHAPTER 5.....	132
THE CRYSTAL STRUCTURE OF THIOREDOXIN REDUCTASE FROM <i>DROSOPHILA MELANOGASTER</i> WITH TETRAPEPTIDE MODELING FOR COMPARISON WITH MAMMALIAN THIOREDOXIN REDUCTASE.....	132
METHODS.....	135
Crystallization of TR from <i>Drosophila</i>	135
Crystallization of TR from Mouse.....	135

Data Collection, Structure Determination and Refinement for DmTR.	136
C-terminal Peptide Structure and Docking	136
RESULTS AND DISCUSSION	138
Crystallization of TR.....	138
Crystal Structure of TR from Drosophila.	140
Electrostatic Surface Potential of DmTR.....	143
Alignment of Tetrapeptides with GSSG.....	144
Structural Explanation for the Peptide Complementation Data.....	148
Other crystallization trials.....	150
CHAPTER 6.	172
CONCLUSION AND MODEL.....	172
KEEPING MECHANISMS IN PERSPECTIVE.....	174
MODEL FOR THE REQUIREMENT OF SEC IN MAMMALIAN TR	175
BINDING OR CHEMISTRY (k_{cat}/K_m).....	178
OUR MODEL AND A MECHANISTIC EVOLUTIONARY ADVANTAGE	179
SUPPORT FROM THE STOPPED-FLOW TR LITERATURE	180
CONTRADICTIONS TO THE TR LITERATURE	182
SEC AS LEAVING GROUP OR INTERCHANGE.....	183
SUPPORTING EXPERIMENTS	184
REFERENCES	192
APPENDIXES	209
A. ABBREVIATIONS	209
B. COMPREHENSIVE LIST OF MATERIALS.....	211
C. LIST OF PCR PRIMERS.....	212
CLONING OF MOUSE TR3 WITH pTYB3.....	212
CLONING OF DROSOPHILA TR WITH pTYB1.....	212
CLONING OF THIOREDOXIN.....	214

LIST OF TABLES

Table 1. Spectral properties of mTR3.....	69
Table 2. DTNB reductase activity of mTR3 semisynthetic and mutant enzymes.....	70
Table 3. DTNB reductase activity reported for homodimeric TR in the literature.....	71
Table 4. Activity of semisynthetic and mutant mTR3 towards thioredoxin.....	72
Table 5. Comparison of methods used to construct a semisynthetic TR.....	76
Table 6. Semisynthetic mTR3 thioredoxin reductase activity.....	104
Table 7. <i>Dm</i> TR thioredoxin reductase activity.....	106
Table 8. DTNB reductase activity for semisynthetic mTR3.....	108
Table 9. DTNB reductase activity for <i>Dm</i> TR.....	109
Table 10. Peroxidase activity of semisynthetic mTR3.....	111
Table 11. Summary of TR/Ac-GCUG peptide ^a complementation kinetics.....	124
Table 12. Summary of activities toward tetrapeptides for the truncated TRs.....	126
Table 13. Ratio of peptide turnover rates for the truncated TRs.....	127
Table 14. Rates of ring opening step compared to full-length TR activities.....	131
Table 15. Crystallographic statistics for ^a mTR3-G.....	154
Table 16. Crystallographic statistics for ^a <i>Dm</i> TR-S.....	157
Table 17. Least squares structural comparison of the ^a GR family.....	162
Table 18. Tetrapeptide conformer distribution.....	166
Table 19. Substrates for truncated TR.....	189
Table 20. Substrates for glutathione reductase.....	189

LIST OF FIGURES

Figure 1. The physiological reducing systems.....	1
Figure 2. Glutathione reductase family cognate substrates.	30
Figure 3. Diagrammatic representation of GR structure.....	31
Figure 4. Ribbon diagram of GR and TR.	32
Figure 5. Multiple sequence alignment (C-terminal).....	33
Figure 6. Multiple sequence alignment (FAD Domain).	34
Figure 7. The FAD domain topology.....	35
Figure 8. Spectral properties of flavin.	36
Figure 9. The catalytic cycle of GR.	37
Figure 10. The catalytic cycle of TR.	38
Figure 11. Decoding of the UGA codon.....	39
Figure 12. Representation of semisynthetic TR.....	40
Figure 13. Method for semisynthetic production of mTR3.....	64
Figure 14. Mechanism of expressed protein ligation.....	65
Figure 15. Native chemical ligation and expressed protein ligation.....	66
Figure 16. SDS-PAGE of semisynthetic and recombinant mTR3.....	67
Figure 17. Chromatographic elution profiles for semisynthetic mTR3.....	68
Figure 18. Flavon spectra for semisynthetic and recombinant mTR3.....	69
Figure 19. Trx activity plot for semisynthetic mTR3.	73
Figure 20. Trx activity of semisynthetic and engineered SECIS produced mTR3.....	74
Figure 21. Peroxidase activity plot for semisynthetic mTR3.	75
Figure 22. MALDI-MS of semisynthetic and truncated mTR3.....	77
Figure 23. ESI-MS of semisynthetic mTR3 C-terminal tryptic fragment.	78
Figure 24. ESI-MS-MS of semisynthetic mTR3 C-terminal tryptic fragment.	79
Figure 25. MALDI-TOF of semisynthetic mTR3 digested with trypsin.....	80
Figure 26. Mass spectrometry peptide mapping for trypsin digests of mTR3.....	81
Figure 27. The pathway for transfer of electrons to Trx by mTR3.....	82
Figure 28. SDS-PAGE of <i>Dm</i> TR cleavage from the intein.	103
Figure 29. Trx activity as a function of pH for mTR3.....	105
Figure 30. Trx activity as a function of pH for <i>Dm</i> TR.	107
Figure 31. Peroxidase activity for mTR3 mutants.....	110
Figure 32. Peroxidase activity as a function of NADPH concentration.	112
Figure 33. Steps of thiol-disulfide exchange for TR.....	113
Figure 34. Peptide complementation of TR.....	114
Figure 35. Cognate substrates revisited for truncated TR.....	123
Figure 36. Peptide complementation of mTR3 with CUG(ox).....	125
Figure 37. Rate of ring opening for tetrapeptides(ox).	128
Figure 38. Rate of ring opening Ac-GCAUG(ox) for mTR3.	129
Figure 39. Rate of ring opening for Ac-GC _D C _L G(ox) with <i>Dm</i> TR.	130

Figure 40. The crystal structure of mTR3.....	132
Figure 41. Crystal of mTR3 with x-ray diffraction pattern.	153
Figure 42. Hypernucleation of TR crystals.....	155
Figure 43. Crystal of <i>Dm</i> TR with x-ray diffraction pattern.....	156
Figure 44. Omit density map for <i>Dm</i> TR C-terminus.....	158
Figure 45. The crystal structure of <i>Dm</i> TR.....	159
Figure 46. The homodimeric model of <i>Dm</i> TR.	160
Figure 47. Structural alignment of <i>Dm</i> TR and GR.....	161
Figure 48. Tetrapeptide binding pocket ribbon overlay.....	163
Figure 49. GR, TryR structural overlay.....	164
Figure 50. Electrostatic surface potentials.....	165
Figure 51. SCCS(ox) aligned with GSSG.....	167
Figure 52. <i>Dm</i> TR and mTR3 surface potentials with peptide fits.....	168
Figure 53. Stereo-view of mTR3 with GCUG(ox) C+.....	169
Figure 54. Ribbon view of GC _D C _L G(ox) and GC _L C _D G(ox) fits.....	170
Figure 55. Co-crystallization trial of mTR3 and Trx.....	171
Figure 56. Model for the requirement of Sec in mammalian TR.....	172
Figure 57. Model for mTR3 ring opening steps.	186
Figure 58. Model for <i>Dm</i> TR ring opening steps.....	188
Figure 59. Orientation of flanking serine hydroxyls.....	190
Figure 60. Interpretation of human TR-SCCS.....	191

CHAPTER 1.

INTRODUCTION TO THE THIOREDOXIN SYSTEM

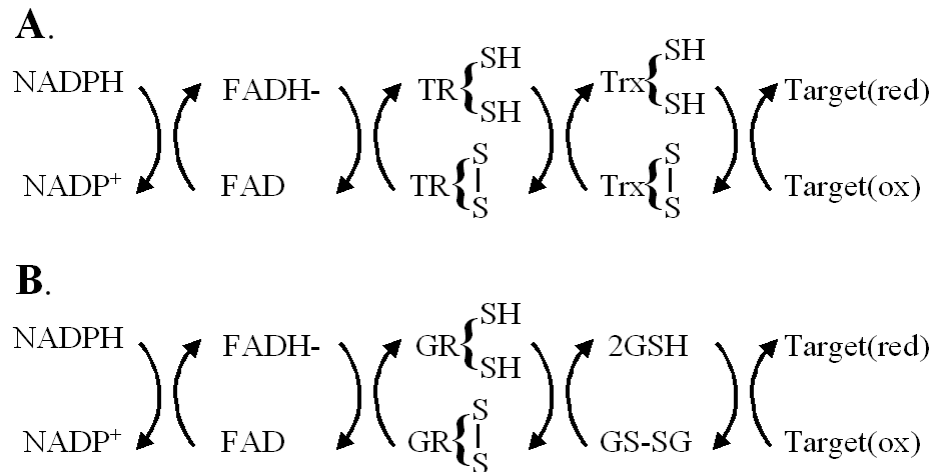


Figure 1. The physiological reducing systems.

The Thioredoxin system (A) and the Glutathione system (B) are each dependent on the system reductase, TR and GR respectively. These enzymes use a common modular architecture to perform the function of thiol-disulfide exchange. The unique properties of mammalian TR compared to the other related enzymes make understanding minor mechanistic differences essential to the development of therapeutics targeting TR.

THIOREDOXIN REDUCTASE AND PHYSIOLOGY

Oxygen...the key to life as we know it. Oxidation...an enemy of life as we know it. Oxidation is not just damage in the form of the rust on your car it is also damage incurred by all forms of biological macromolecules. This can lead to the inactivation of enzymes (1), oxidation of lipids contributing to atherosclerosis (2, 3), and DNA damage resulting in cancer (4, 5). While the extracellular environment is relatively oxygen rich, the intracellular environment is maintained in the reduced state. However, oxidation in both environments is also an essential process that occurs in many physiological reactions. The key for most oxidative processes to be beneficial rather than detrimental is that that the process be reversible. Because of this paradox, organisms have evolved systems to control and utilize oxidative processes.

The cellular environment is maintained in the reduced state by two primary systems, the glutathione system (sometimes referred to as the glutaredoxin system) and the thioredoxin system. The key enzymes are referred to as the system reductases, glutathione reductase (GR) and thioredoxin reductase (TR). *A comprehensive list of abbreviations used in this dissertation is available in **Appendix A**.* The reductase for each system utilizes reducing equivalents in the form of NADPH to reduce the system's respective cognate substrate, oxidized diglutathione (GSSG) or thioredoxin (Trx) (**Figure 1**). While Trx goes on directly to reduce a target substrate, there are two fates of reduced glutathione (GSH), the tripeptide γ -glutamylcysteinylglycine. Two molecules of GSH can be used to directly reduce a target or, more commonly, GSH will be used to reduce glutaredoxin or glutathione peroxidase (proteins similar to Trx). Many excellent reviews

are available on the physiological functions of both systems (6-9). The most common shared function between the two systems is the reduction of protein disulfides. Central to the function of these systems is the process of thiol-disulfide exchange mediating the directed transfer of electrons between reduced and oxidized species.

Both systems are nearly ubiquitous in all forms of life, however, there are certain organisms of which there are substitutions for these systems. For example, the parasite *Trypanosoma* utilizes the analogous trypanothione system rather than the glutathione system (10). The system reductase is trypanothione reductase (TryR) and cognate substrate is trypanothione. While GRs are functionally, structurally, and mechanistically homologous, TRs are divided into two classes: higher eukaryotes have the class I high M_r TR, which is the focus of this dissertation, while prokaryotes and lower eukaryotes have class II low M_r TRs. These two classes have partial homology on the basis of function and structure, but contain structural deviations and have distinct mechanisms. No GR has yet been identified in *Drosophila melanogaster* even though glutathione is utilized (11). In this system, the GSH pool is maintained by the thioredoxin system via Trx.

The essential nature of both systems makes the reductases a significant therapeutic target for a broad range of disease processes. For example, the protozoa of which TryR substitutes for GR are the cause of several tropical diseases. Therefore, TryR is a target under investigation as a therapeutic target (12-14). Similarly, active site distinctions between the high M_r TR of mammals and that of *Plasmodium falciparum*, the causative parasite of malaria, make the *Plasmodium falciparum* TR (PfTR) an attractive therapeutic target for treatment of malaria (15).

Both the glutathione and thioredoxin systems are reducing equivalent donors to ribonucleotide reductase (RNR) (8), the enzyme responsible for conversion of ribonucleotides to deoxyribonucleotides (dNTPs) for DNA synthesis (16). This enzyme is a target under investigation for cancer therapy, see Arnér and Holmgren for a TR-based review (17). Initial studies performed in *E. coli* showed Trx to have slightly lower activity than glutaredoxin (Grx) as electron donors to RNR. Though Trx was less active and showed ~10 fold higher K_m (18, 19), the cellular Trx concentration is considerably higher than Grx (20, 21). Trx knockout in yeast results in a 40% reduction of the dNTP pool *in vivo* (22). However, the impact for inhibition of these systems for higher eukaryotes in relation to ribonucleotide reductase has yet to be determined. Elevated levels of TR in human tumors have been reported (23, 24) but the degree of up-regulation and purpose of the elevated levels is uncertain (25).

The mammalian thioredoxin system is unique in its broad range of substrates compared to other systems. Transcription factors such as NF- κ B (26, 27) involved in oxidative stress and inflammatory responses have been demonstrated to be redox regulated by Trx. This redox control of transcription factors, and its involvement in the response to reactive oxygen species, implicate TR as a player in afflictions such as rheumatoid arthritis (28), cancer (17), aging, and HIV (29). Several other substrates unique to mammalian TR have been identified. The antioxidant ascorbate (vitamin C) can be reduced by TR (30) as can lipid peroxides (31). The unique roles that mammalian TR plays in so many physiological processes makes understanding the mechanistic differences of TR homologues and the related systems imperative.

THE GLUTATHIONE REDUCTASE FAMILY

Thioredoxin reductases from higher eukaryotes are members of the glutathione reductase (GR) family of pyridine nucleotide-disulfide oxidoreductases (32). The Structural Classification of Proteins (SCOP) identifies the protein family as FAD/NAD-linked reductases belonging to the FAD/NAD(P) binding domain Superfamily and Fold (33). Proteins in this family of which structures are available are GR (34), TR (35, 36), TryR (37), and LipDH (38). *There are many structures for most of these proteins, especially GR. The references given above are representative structures of each enzyme used in direct structural comparisons in this dissertation.* Glutathione, trypanothione, and lipoamide are all small-molecule substrates whereas thioredoxin is a 12 kDa protein (**Figure 2**). More distantly related family members include: alkyl hydroperoxide reductase, NADH peroxidase, NADH-dependent ferredoxin reductase, flavocytochrome C sulfide dehydrogenase, and apoptosis inducing factor (AIF). Although these proteins are generally related via the binding of FAD and/or NAD, their structural topologies are quite different from the GR family as reviewed by Dym and Eisenberg (39).

Structural Overview.

The proteins of the GR family are homodimeric (25) and have a three domain modular structure, which is diagramed in **Figure 3**. Each contains a N-terminal FAD binding domain followed by a NAD(P) binding domain. Each of these domains is structurally similar and composed of a three-layered sandwich, which will be described below. These two domains bind FAD and NAD(P) in a similar manner and are oriented

in a head to head fashion (**Figure 4**), essentially a mirror image, to place the flavin and nicotinamide in proper orientation for electron transfer. The domains are tethered by a two antiparallel β -strands with each strand representing the transition from one domain to the other. The C-terminal domain is the dimerization/interface domain for this class of proteins and is generally a five-stranded anti-parallel β -sheet with two alpha helices on either side. The high M_r TR (class I) characteristic of higher eukaryotes are ~55 kDa per monomer and have an additional C-terminal extension of 16 residues (compared to GR), which contains an additional active site disulfide (**Figure 5**). Prokaryotes and lower eukaryotes utilize class II TRs which are ~35 kDa per monomer. Class II TRs do not have the C-terminal domain characteristic of most members the GR family and dimerize via the FAD domain (40).

FAD Binding Domain.

The FAD binding domain is the most highly conserved domain among family members (alignment **Figure 6**). This is not unexpected as the FAD is permanently bound to the protein although non-covalently, with a few exceptions within the family such as fumarate reductase and sarcosine oxidase. The domain contains a variant of the Rossmann $\beta\alpha\beta\alpha\beta$ fold as the central motif in a three-layered sandwich; a five or six-stranded parallel central sheet, alpha helices on one face, and a three-stranded anti-parallel sheet on the other (**Figure 7**) (41). The anti-parallel sheet is the crossover connection to the directional change in the Rossmann fold. This retains the typical +3 topology of the Rossmann fold where strand number four in the sheet is strand seven within the sequence. Rossmann strand four is also the transition to the NAD(P) binding

domain such that stand five, six for some structures, follow the NAD(P) binding domain in the sequence.

The FAD molecule is divided into two modules connected via a pyrophosphate. The first module is the adenosine monophosphate (AMP) and lies within a well-defined groove created by the topological switch in the parallel β -sheet and a hydrophobic pocket between the two β -sheets. The adenine lies in the pocket with the N₆ coordinated by a backbone carbonyl in a conserved position at the N-terminus of strand one of the anti-parallel sheet. This residue is generally a small hydrophobic residue such as a glycine, alanine or valine. The ribose and phosphate extends through the groove with the phosphates coordinated by the highly conserved FAD binding motif. This motif is the most conserved sequence found within the domain. The motif is GxGxxGx(17)D/E and is located in the loop and N-terminal end of the helix between strands one and two of the Rossmann fold. The x represents any residue with some preference for hydrophobic residues in the 17-residue stretch. This motif provides both a structural platform and binding determinants for the adenosine monophosphate and pyrophosphate moieties. The backbone amides of the GxGxxG motif provide hydrogen bonds to the pyrophosphate and the D/E coordinates the 2'-OH of the ribose. In many structures, there is a conserved water molecule mediating the interaction with the pyrophosphate (42).

Charge stabilization of the pyrophosphate is believed to come from the positive helix dipole as the GxGxxG is the N-terminal end of helix 1 of the FAD domain (43). In the GR and TryR structures, the glutamate side chain hydrogen bonds to both the 2' and 3'-OH whereas in the *E. coli* TR structure it appears to be the backbone carbonyl of the Glu and the adjacent residue that provides these bonds. There is also a conserved Thr that

provides a hydrogen bond to the phosphate of the AMP. The second module of the FAD is the flavin mononucleotide, which contains the linear ribitol and the isoalloxazine ring of the flavin. The ribitol places the FAD in a linear conformation above the β -sheet platform, placing the flavin in contact with the alpha-helical face containing the active site.

The FAD domain contains the active site disulfide representative of the GR family, with exception of the small TR. It is located in the extended alpha-helical segment that connects strand two to strand three in the parallel β -sheet. The conserved redox active site sequence Cys-Val-Asn-Val-Gly-Cys (CVNVGC) sequence generates a short alpha helix followed by a longer helix, which is separated by a short loop created by the VNVG. This places the cysteines on the same face such that, when oxidized, the disulfide bond bridges across the loop. The N-terminal Cys is referred to as the interchange thiol and is responsible for electron exchange with the GSSG substrate (44). The C-terminal Cys is the charge-transfer Cys responsible for interacting with the Flavin. Reaction of reduced GR with iodoacetamide results in labeling of the interchange thiol while the C-terminal Cys is maintained in the charge-transfer state (44).

Immediately C-terminal to the active site is a conserved lysine that coordinates the N₅ of the flavin. Interestingly, the small TR has a similar short helix followed by a longer loop yet does not contain the active site motif. The local structure is maintained however, the small TR loop transitions to a helix that connects directly to the crossover β -sheet whereas the other members of the family extend towards the NAD(P) binding domain and reconnect to the FAD domain through an additional helix resulting in a sequence insertion of ~32 residues. This results in slightly different positioning of this

connecting helix in *E. coli* TR such that it occupies the substrate binding pocket representative of the other members of the family.

NAD(P) Binding Domain.

The NAD(P) binding domain demonstrates a similar architecture to that of the FAD domain although it is smaller and not as well conserved. While the FAD is permanently bound, the NAD(P) must bind and dissociate during the catalytic cycle. Therefore binding is less stringent and involves an induced fit (45). The domain architecture also contains a three-layered sandwich with the alpha helices being shorter and the parallel β -sheet containing only four strands. The GxGxxG motif is also conserved, although not as well as in the FAD binding domain. An important difference is the coordination of the ribose of the similar AMP module. Members of the family that bind NADP rather than NAD contain a pair of arginines in the loop where the D/E normally resides. These residues hydrogen bond to the phosphate on the 3'-OH and it appears that 2'-OH points toward the solvent. A series of mutations, including the Arg residues, allows for switching of substrate specificity from NADPH to NADH (46).

A conserved tyrosine from the NADP domain, Tyr197 in GR, shows a significant conformational change between the oxidized and reduced states of the enzyme (34, 47). Upon binding of NADPH, the Tyr rotates to allow the orientation of the flavin and nicotinamide for electron transfer. This same conformational change has also been reported for mouse mitochondrial TR (mTR3) (35). This residue was initially suggested to provide a cap to protect the flavin from access to solvent. However, mutagenesis to Phe, Ser, or Gly indicated the flavin is still protected. The latter two mutants, however,

resulted in a shift from the normal Ping-Pong Bi Bi mechanism to an Ordered-Sequential mechanism (48).

While the overall architecture is maintained within the family, there is a simple non-conserved sequence in a short alpha helix prior to the sequence returning to the FAD domain. This short helix contains the active disulfide for small TR. The end of this helix faces the FAD domain and contains the active-site sequence, CATC. The combined structures for *E. coli* TR demonstrate a significant conformational change that is unique to the Class II TR (49). The NAD(P) domain twists $\sim 60^\circ$ to expose the active disulfide to the open face of the structure, opposite the dimer interface, for interaction with thioredoxin. This sequence is GITS for GR and CISS or CITS for large TR, TryR and LipDH while the flanking regions are relatively well conserved. However, since this active site faces the dimer interface, it is inaccessible to a large substrate such as thioredoxin.

The Dimerization Domain.

The C-terminal dimerization domain represents $\sim 30\%$ of the sequence for the proteins of this family. As the name implies, it is this domain that is responsible for dimer formation thereby assembling the functional active site. It is this domain that provides the catalytic acid/base histidine for the active site of the enzyme. The conserved active site is composed of the FAD and the conserved disulfide (CVNVGC) from the FAD domain of Chain A, and the His-Glu dyad (His464 and Glu469 in **Figure 5**) from Chain B, as proposed from the crystal structures of GR (34, 50). Residues from chain B are given a prime designation. Implications for the His-Glu dyad will be discussed in more detail in

terms of the catalytic cycles covered in the next section. The His-Glu dyad is shown for the structures of GR and mouse TR3 in **Figure 4**. The communication between the FAD active site disulfide on Chain A and the catalytic acid/base on Chain B was verified by the preparation of heterodimeric GR from *E. coli* where one subunit contained the Cys47Ser mutant and the other subunit contained the His439Gln mutant (51, 52). Each mutant showed poor activity when prepared as a homodimer while the heterodimeric form showed ~50% of wild-type activity.

Proper dimer assembly is also a significant contributor to the catalytic mechanism. Several mutagenesis studies have been performed with GR targeting residues at the dimer interface. Though dimeric enzymes require elements from both monomers, cooperativity has not been reported for wild type enzymes under normal conditions. The *E. Coli* GR mutant Gly418Trp results in an enzyme having high cooperativity for GSSG binding with Hill coefficient of 1.76 (53). Mutations in this region can also disrupt the standard Ping Pong mechanism (54).

The additional thiol-disulfide exchange step characteristic of TR utilizes a 16 amino acid C-terminal extension (absent in GR) and typically contains a Cys-Cys dyad, which forms an *intramolecular* disulfide. Upon reduction of this dyad by the N-terminal redox center (on the opposite chain), the substrate (Trx) can then be reduced. The relationship between the N-terminal active site and the C-terminal active site was demonstrated using the heterodimer method developed for GR by Deonarain et al. mentioned above. In these experiments the interchange thiol Cys88 of *Plasmodium falciparum* (PfTR), was mutated to Ala in one construct while Cys535 was mutated to Ala in another (55). Each of the mutants, when produced as homodimers, showed very

poor activity towards Trx while the heterodimers showed ~50% of wild-type activity. This provided evidence that the N-terminal active site was in redox communication with the C-terminal active site.

With the exception of *PfTR*, which contains four intervening residues, the disulfide forms between adjacent Cys residues of the C-terminal dyad. This vicinal disulfide bond has a very low frequency in the Brookhaven Protein Data Bank (PDB) as is discussed by Perczel and coworkers (56, 57) and results in a type VII β -turn (58). Only TR has been identified as having a catalytically competent vicinal disulfide. Examples of proteins containing a vicinal disulfide include bacterial toxins (59), the nicotinic acetylcholine receptor (58), hepcidin (60), and methanol dehydrogenase (61). For these proteins it is suspected that the vicinal disulfide has a structural function. Mercuric ion reductase also contains a C-terminal vicinal disulfide but it does not appear essential for enzyme function (62).

Mammalian TRs (mTR) are distinguished in this group since they contain the rare amino acid selenocysteine (Sec, U) as part of the C-terminal dyad forming the redox-active motif Gly-Cys-Sec-Gly (GCUG) (63, 64). *Drosophila melanogaster* TR (*DmTR*) lacks Sec as part of this motif and has the C-terminal sequence Ser-Cys-Cys-Ser (SCCS) (11, 65) (**Figure 5**). Thus, high M_r TRs can be divided into enzymes that contain Sec and those that have a conventional Cys residue (66). TryR is interesting in that it also has a C-terminal extension, but the sequence is not conserved in comparison to TR and does not contain the active disulfide.

Substrate Binding.

Glutathione reductase is the structural model for the family and has been extensively studied. Both the alpha helical face of the FAD domain and the C-terminal end of the dimerization domain provide substrate-binding determinants for GSSG (34). Most of the binding contacts for GSSG in the structural complex appear water mediated with the most significant direct contacts formed between Chain A and GSII. Many of the substrate-binding residues are conserved in TR yet the enzyme cannot reduce glutathione or trypanothione. The arginine in position 37 for GR serves to anchor the carboxyl group of GSII. Trypanothione does not have carboxyl groups at both ends of the molecule and therefore has hydrophobic substitutions at position 37 and 106 and an acidic substitution at position 117. The extensive structural investigations of substrate binding residues for GR and TryR have allowed for engineering of trypanothione specificity in human GR (67) as 14 of 19 amino acids suggested to bind GSSG in GR are identical in TryR.

In the case of TR, the C-terminal tail is essentially the substrate for the FAD domain-conserved active site substituting for GSSG (68). Since glutaredoxin and glutathione peroxidase are the primary targets for GSH and are similar to Trx, it is as if TR has evolved by incorporating the GSSG-like moiety into the protein. The size of thioredoxin makes it inaccessible to the active site of GR, TryR and LipDH. Alternatively, the C-terminal extension of rat TR occupies the binding site making it inaccessible to glutathione, trypanothione, and lipoamide. The conservative substitution to Lys in TR for Arg37 of GR was suggested to serve a similar purpose with respect to

coordination of the C-terminal carboxylate of rat TR1 (36). There is no current data pertaining to the residues involved in Trx binding for large M_r TRs.

SPECTRAL CHARACTERISTICS OF FLAVIN AND FLAVOPROTEINS

To better understand the methods currently used for investigating mechanistic details within the GR family, an introduction to the spectral characteristics of flavin must be presented. Much of the work describing the electronic states of flavin derivatives was pioneered by Vincent Massey as reviewed in (69) and has been used to distinguish between free flavin and flavoproteins and their mechanisms (70, 71). Many classes of enzymes utilize a flavin moiety, which can participate in either one-electron or two-electron processes as investigated potentiometrically by Michaelis *et al.* (72). It is this characteristic that allows the flavin to be so versatile and results in several electronic states (73). Each of these states has specific spectral properties as shown in **Figure 8** (74) using Old Yellow Enzyme as the example showing all four electronic states. The simplified equation most commonly shown for the reduction of FAD is described in equation 1.



The yellow color associated with a flavin derivative is indicative of the moiety in the oxidized state. The color comes from an absorbance peak at ~448 nm that is shifted to longer wavelengths for flavoproteins, ~460 nm for GR and TR (71). This peak for flavoproteins also has a pronounced shoulder at ~430 nm and another at ~480 nm. These

shoulders were determined to be a function of the hydrogen-bonding environment between the protein and the isoalloxazine ring (71). As with most species with an aromatic nature, there is also an absorbance maxima in the near ultraviolet. This peak is ~375 nm for flavin and a slightly shorter wavelength for flavoproteins, ~370 nm for GR and TR. Complete reduction of flavin to FADH₂ results in a decrease in extinction for the UV peak and a loss of visible color. This loss of color upon reduction, however, is not observed in all flavoproteins (70).

As free flavin and flavoproteins have unique properties, the same can be said for the GR and TR compared to enzymes such as glucose oxidase (71, 73). For example, photoreduction and reoxidation experiments with glucose oxidase results in all flavin species being observable (75). The reduction of GR, however, under physiological conditions displays different properties (**Figure 8 inset**) (76). While the spectra of the oxidized enzyme (spectra 1) resembles that of the free flavin, it is clear that the reduced form of the enzyme using NADPH (spectra 2) or sodium borohydride (spectra 3) does not resemble that of the reduced free flavin in the form of FADH₂. The characteristic reduced spectrum is not typically seen in GR family proteins under normal conditions. To achieve this state, long incubations in excess NADPH or chemical reducing agents such as dithionite are most commonly required (70, 77-79). The reduced spectrum of GR instead appears to be a hybrid between the oxidized and anionic semiquinone states (73).

The most notable characteristic of NADPH-reduced GR or TR is a red color that is demonstrated by the absorbance change at 540 nm in the inset of **Figure 8**. This color indicates the essential species and primary intermediate of the mechanism of these proteins, the thiolate – flavin charge-transfer complex. There is a transient covalent

adduct with the C4a position of the isoalloxazine ring of the flavin and active site cysteine. An adduct intermediate with substrate at this position is also proposed for many other classes of enzymes (69). This transient species becomes the primary charge-transfer intermediate upon reduction of the disulfide. Preliminary investigations for spectral characteristics of the GR protein family were performed using LipDH (80-83). The two-electron reduced enzyme showed the same red color mentioned above with proton inventories suggesting a proton from dihydrolipoamide being taken by the catalytic acid/base. The adduct formed between the cysteine and FAD with the subsequent formation of the charge-transfer complex as the reduced intermediate for the GR results in equation 2, which is typically how the FAD in the reaction cycle is represented for GR and TR.



THE GLUTATHIONE REDUCTASE CATALYTIC CYCLE

Catalytic Overview.

GR is a two-substrate, two-product (or three, with a GSSG producing 2 GSH) enzyme, shown in equation 3, following Ping-Pong Bi-Bi kinetics similar to that of LipDH (84, 85), as reviewed in (86). Massey and Williams (87) originally proposed the catalytic cycle of GR which has since been divided into two phases: a reductive half-reaction and an oxidative half-reaction. In the reductive half-reaction, the enzyme is

reduced by the consumption of NADPH resulting in the formation of the thiolate-flavin charge-transfer complex. The enzyme is re-oxidized upon consumption of GSSG in the oxidative half-reaction, which is the prototypical enzymatic thiol-disulfide exchange. The steps in each half-reaction have been studied extensively by stopped-flow kinetics, as best described in (88, 89) using the spectral characteristics of the flavin. The reaction was predicted to be acid/base catalyzed with the residue identified in the C-terminal region of GR (90). A representation of the GR catalytic cycle is shown in **Figure 9**.



His467' for human GR (His439' for *E. coli*.) from chain B has since been identified as the acid/base catalyst in GR and is conserved throughout the protein family. It has been shown to be essential in both the reductive half-reaction and oxidative half-reaction for GR (48, 88, 91), LipDH (80, 92), and PfTR (93). His467' is activated by Glu472' (human GR) forming a catalytic dyad that acts as a potential charge-relay system between the dyad and the N-terminal thiol of the active site disulfide, as first proposed from the crystal structure of GR (50). For the discussion of the catalytic cycle, I have chosen to use the GR comparison as it functions to reduce a disulfide like TR rather than to oxidize a dithiol as is the case for LipDH.

Flavin Spectra and Enzyme Kinetics.

In the previous section we introduced the spectral characteristics of flavin and flavoproteins in terms of the redox state of the flavin in three states - oxidized, reduced, and charge-transfer. In terms of the catalytic cycle shown in **Figure 9**, there are three

primary flavin states but more than three steps. As can be seen in the flavin spectra in **Figure 8**, differences in the redox state results in changes throughout the spectrum. Therefore, a subset of relevant wavelengths has been established for kinetic analysis (88, 89). The easiest to understand is the thiolate-flavin charge-transfer complex observed at 540 nm. The second is a charge-transfer complex between FADH⁻ and NADP⁺ at 670 nm. The complete oxidation of flavin results in an absorbance maxima at ~460 nm but partial oxidation is a characteristic of these proteins during each half-reaction. Therefore this state is followed at 440 nm.

The method developed at The University of Michigan by Ballou and Arscott utilizes a stopped-flow spectrophotometer adapted for anaerobic conditions. These conditions are necessary to prevent auto-oxidation of the flavin. While the rapid reaction kinetics using flavin spectra provides more details than steady state kinetics, it is not without limitations. There are several species that are spectrally equivalent and cannot be distinguished for GR (88) or TR (78, 79, 93). Of special interest are the catalytic intermediates involving the thiol-flavin charge-transfer.

The Reductive Half-Reaction of GR.

During the reductive half-reaction (E_{ox} to $EH_2(B)$), the FAD-associated disulfide from chain A is reduced upon consumption of electrons from NADPH. Three primary phases have been spectrally observed for this reaction (88, 89). The first phase, binding of NADPH and formation of the NADPH - FAD charge-transfer complex is complete within the dead time of the stopped-flow instrument. The second phase includes the reduction of FAD to form the FADH⁻ - NADP⁺ charge-transfer complex. The third phase

transfers electrons to the N-terminal disulfide and occurs via the thiolate-FAD charge-transfer complex. The mutant His439'Ala (*E. coli* GR), was reported to result in a modest 16 fold decrease in the overall rate for the reductive half-reaction. A closer inspection reveals different spectra upon NADPH reduction of the wild type and mutant enzymes (88). The mutant enzyme at the end of the reaction has much more reduced flavin characteristic and less charge-transfer absorbance indicating the two proteins are in significantly different states. While the rate differences are addressed in the discussion, the magnitude of the difference in the spectra (especially at 440 nm) is not.

The Oxidative Half-Reaction of GR.

The oxidative half-reaction ($\text{EH}_2(\text{B})$ to E_{ox}) is the reduction of GSSG that results in the re-oxidation of GR. For each NADPH consumed in the reductive half-reaction, two GSH molecules are produced from a single GSSG in the oxidative half-reaction. The intermediate of the oxidative half-reaction ($\text{EH}_2(\text{C})$) is a mixed disulfide formed between the cysteine of GSH I and the active site interchange thiol (Cys58) from chain A (94). This step is referred to as interchange. This intermediate is seen crystallographically in PDB 1GRE compared with the bound oxidized GSSG in PDB 1GRA (34) now at $<2 \text{ \AA}$ refined from the initial 3 \AA structures (47). The high temperature factors of GSGII and the fewer direct contacts to GSHII from GR in combination with GSHI as the interchange moiety indicates that GSHII is likely the first leaving group. The significance of this intermediate is biochemically supported by GSH/GSSG equilibrium experiments and is hypothesized to be the major form of GR physiologically (94). Unlike the reductive half-reaction where multiple spectral states are observed, the oxidative half-reaction is

followed by a single state as $\text{EH}_2(\text{B})$ and $\text{EH}_2(\text{C})$ are spectrally equivalent. This means: 1) formation of the mixed disulfide, 2) protonation of the first leaving group, 3) resolution of the mixed disulfide, and 4) protonation of the second leaving group are incorporated into a single rate constant (88).

This challenge was partially addressed by earlier experiments using mixed-disulfide substrates (95). The substrates GS-SNB (mixed disulfide of glutathione and 5-thio-2-nitrobenzoic acid) and GS-SNP (mixed disulfide and 2-thio-4-nitropyridine) were evaluated as substrates for GR using kinetic isotope effects on k_{cat} with varying deuterium concentrations. The mixed disulfide substrates have an aromatic thiol group with a low $\text{p}K_{\text{a}}$ and would not require protonation, unlike GSH. Each substrate indicated a proton transfer step as partially rate-limiting and results from either substrate indicated that the same rate-limiting step was being observed. While the aromatic thiol should be the first leaving group (94) with GSH as the interchange mixed disulfide, it was hypothesized from this data that the GSH was the first leaving group. The rationale provided is that for the system to be in equilibrium, the GSH would have to be the first leaving group. At equilibrium, the free GSH would be able to re-attack the interchange mixed disulfide. If, however, the aromatic disulfide were the first leaving group, the reaction should be irreversible. Why the aromatic disulfide would be the second leaving group in this experiment is not quite clear. One possibility could be a function of binding or orientation of this modified substrate in the active site (96), which is not accounted for.

His439' has been shown to be essential to the oxidative half-reaction for protonation of the first leaving group, the thiol of GSHII (88). This half-reaction was shown to be 600 fold slower in the His439' mutant. This indicates that protonation of the

leaving group is essential in the oxidative half-reaction. Protonation and subsequent dissociation is essential to prevent the re-attack of the interchange mixed-disulfide by GSIII and thereby driving the reverse reaction (88). The final step of the oxidative half-reaction is the resolution step. The resolving thiol, Cys63, attacks the interchange mixed disulfide and reforms the enzyme Cys58-Cys63 disulfide with release of the second molecule of glutathione (GSHI). Thus, the enzymatic thiol-disulfide exchange process characteristic of this family of proteins involves an interchange step (requiring an interchange cysteine) and a resolution step (requiring a resolving cysteine).

THE HIGH M_r THIOREDOXIN REDUCTASE CATALYTIC CYCLE

The addition of a second thiol-disulfide exchange in TR results in a significantly more complicated reaction cycle (**Figure 10**) as best described for *PfTR* (93) and *DmTR* (78) with partial insight from mammalian TR (79). The reductive half-reaction of TR includes transfer of electrons from the N-terminal dithiol to the C-terminal disulfide (this is equivalent to the combination of the reductive and oxidative half-reactions in GR) as well as the consumption of an additional equivalent of NADPH. The oxidative half-reaction of TR is the thiol-disulfide exchange between the C-terminal dithiol and the disulfide of Trx. The steady state cycle therefore alternates between two-electron and four-electron reduced states of TR, EH_2 to EH_4 , as shown for *DmTR* (78) and *PfTR* (93). It is assumed from this work that $\text{EH}_4(\text{B})$ is the predominant product of the reductive half-reaction and demonstrates an enhanced flavin-thiolate charge-transfer complex.

As much mechanistic detail as is inferred from this work, only three discernable rate constants have been determined for the entire reductive half-reaction (93) from a model with at least eight steps. The first constant is the consumption of the first equivalent of NADPH forming the FADH⁻ - NADP⁺ charge-transfer complex and the second rate constant being the formation of the thiolate-FAD charge-transfer complex. This is similar to the analysis for GR. This means the third rate constant represents the thiol-disulfide exchange between the N-terminus and C-terminus with the spectra complicated by the consumption of the second equivalent of NADPH. Referring to **Figure 10**, these are the steps from EH₂(B) to EH₄(B).

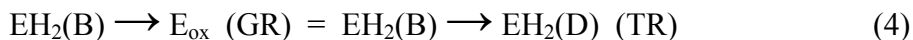
Mutation of either residue of the His-Glu catalytic dyad for *Pf*TR results in significant decreases in rate for both the reductive half-reaction and the oxidative half-reaction (93) with the His mutation almost completely destabilizing the thiolate-flavin charge-transfer complex. Similar results are seen by the authors for the equivalent mutations in *Dm*TR, but have yet to be published. This is in agreement with that observed for the equivalent mutants in GR (88, 89) and LipDH (97, 98). Similarly, mutation of the equivalent Glu477 in human TR results in a 6 fold reduction in k_{cat} (99). The perturbation of the reductive half-reaction appears greater in magnitude for the His mutation in *Pf*TR than mentioned above for GR. These results indicate 1) the importance of the catalytic acid/base in both half-reactions for GR and TR; 2) could imply the catalytic acid/base is also involved in thiol-disulfide exchange between the C-terminus of TR and the disulfide of Trx. The latter has been proposed in a mathematical model for mammalian TR (100) where the His would be directly involved in the exchange by deprotonation of the

attacking thiolate of TR and/or protonation of the leaving group thiol of Trx. However there is currently no experimental evidence for this.

It is quite possible that the decrease in rate for the His and Glu mutants of *Pf*TR (93, 101) represents the unfavorable formation of $\text{EH}_2(\text{B})$ rather than catalytic association with Trx. The authors note that the thiolate charge-transfer complex in the His mutant is nearly absent. If the model of the catalytic cycle is correct and $\text{EH}_2(\text{B})$ is formed prior to E_{ox} during reoxidation in these experiments, the His mutation could be a function of reoxidation of the N-terminal disulfide instead. Like the reductive half-reaction, three rate constants were determined for the oxidative half-reaction of *Pf*TR. The first rate constant for the His or Glu mutants is 50% of the wild type enzyme and is attributed to the thiol disulfide exchange with Trx indicating these residues are not directly involved with Trx. The second rate constant is attributed to the reaction of $\text{EH}_2(\text{D})$ with the excess Trx in the experiment. This rate would reflect conversion from $\text{EH}_2(\text{B})$ to $\text{EH}_2(\text{D})$ and is significantly slower in the His and Glu mutants. The third rate constant is the slowest of the three and reflects the complete reoxidation of the flavin.

It can be interpreted from this data that the decrease in rate for the His and Glu mutants for *Pf*TR in the oxidative half-reaction are actually steps in the reductive half-reaction. Each of the three rate constants for the oxidative half-reaction is significantly lower than the rates determined for the reductive half-reaction (93). This is consistent with results for *Dm*TR where the single determined rate constant of 11 s^{-1} was suggested to be the conversion of $\text{EH}_2(\text{B})$ to $\text{EH}_2(\text{D})$ during the oxidative half-reaction (78). The overall rate constant of 5 s^{-1} for reduction of Trx was determined, indicating this step is the major contributor to the overall rate of *Dm*TR. An interpretation that is completely

consistent for what is observed for GR where the protonation of the first leaving group in the oxidative half-reaction is the overall rate-limiting step (88, 95). The only caveat being that GSSG is now replaced by the C-terminal disulfide in TR. This may sound confusing at first, but it can be better understood by comparing **Figure 9** to **Figure 10** and establishing the important relationship in equation 4.



SELENOCYSTEINE IS ESSENTIAL TO MAMMALIAN TR

Earlier in the Introduction, it was implied that mammalian TR has unique functional properties in comparison to the other proteins in the family. Yet we have not discussed what makes mammalian TR unique. For simplification purposes, TRs have been discussed in general terms of the catalytic cycle, since all high M_r TRs share the active site containing C-terminal extension. There are two major subclasses of this C-terminal active site. Looking more closely at the sequence alignment in **Figure 5**, the one letter code U (selenocysteine) is in the penultimate position for mammalian forms while others contain C (the one letter code for cysteine). Therefore the two classes are those whose active site contains a Cys-Cys dyad and that which contains a Cys-Sec dyad, where Sec is the three letter code for selenocysteine.

Sec containing proteins are found in prokaryotes, eukaryotes and archea but are relatively rare. In humans for example, only 25 proteins have currently been identified that contain Sec (102). Sec is inserted co-translationally at the ribosome during protein

synthesis but requires a unique *cis* element and several unique *trans* factors as the codon for Sec is the normal termination codon UGA (**Figure 11**). The *cis* element is the selenocysteine insertion sequence (SECIS), a specific stem loop structure in the mRNA. This sequence is adjacent to the UGA codon in prokaryotes but is found in the 3' untranslated region for eukaryotes (see (102) and references therein). It also requires specialized enzymes for the assimilation and incorporation of selenium into Sec (103, 104). The process is metabolically expensive for the organism and challenging to manipulate for the scientist interested in recombinant protein production.

Bacterial formate dehydrogenase was the first enzyme where selenium was demonstrated as required for function (105). Several other enzymes, such as glutathione peroxidase and 5' deiodinases, were also identified as requiring selenium though the nature of the selenium moiety was not clarified, as reviewed by (106). Enoch et al. demonstrated that selenium was likely a covalent component of formate dehydrogenase and suggested the presence of a selenol (107). In the following year, selenium was identified as incorporated into the selenoprotein A, an essential component of *clostridial* glycine reductase, as Sec by the Stadtman group at the NIH (108). The same group did not identify Sec as the penultimate residue in human TR (63) until 20 years later. Sec since has been shown to be essential to the function of mammalian TR. Replacement of the catalytic Sec residue in the mammalian enzyme with a Cys residue results in a large decrease (>100 fold) in catalytic activity towards the cognate substrate Trx (109). Sec is incorporated into the mammalian TR C-terminal sequence, Gly-Cys-Sec-Gly (GCUG) (63).

Selenium is an essential trace element and the key component of many biologically important selenocompounds (110, 111) but is also toxic at increased concentrations (112, 113). The incorporation of Sec into mammalian TR is responsible for expanding the substrate range to include peroxides and lipid peroxides (31, 114), ascorbate (30, 115) and seleno-compounds such as selenite (116), methylseleninate (117), selenodiglutathione (118). This indicates TR may also be a component of the systems regulating the seleno-metabolite pool (17). Sec incorporation into TR has also been proposed to be one of the links between selenium supplementation and cancer prevention (119) as reviewed by (120).

While the incorporation of Sec may provide a selective advantage by expanding the substrate range, it is not required to catalyze the reduction of Trx by TR. One such example is *DmTR*, which has high activity towards its cognate Trx and good activity towards Trx from *E. coli* (11, 65). Gromer *et al.* (65) proposed that it is the flanking serine residues in the Ser-Cys-Cys-Ser (SCCS) motif that aid in deprotonating the catalytic Cys residue, thus obviating the need for Sec in this enzyme. Yet, when the Ser were mutated to Gly residues, only a 7 fold reduction in activity is observed. This is not the >100 fold loss in activity for the mutation of Sec to Cys in the mammalian enzyme or for mutating the catalytic His in GR (88) or *PfTR* (93, 101). The same authors proposed the conserved His (His106) as a second catalytic acid/base in *DmTR* (65). However, mutation to Phe or Gln results in a similar 3-7 fold loss in activity as observed in the mutation of the C-terminal Ser residues (121) with the author's interpretation being that His106 was not essential to catalysis. Clearly there is a discrepancy in the interpretation of these very similar results. It was also recently reported that the mitochondrial TR from

Caenorhabditis elegans (*CeTR2*), which has a Gly-Cys-Cys-Gly (GCCG) motif, also has a high activity towards *E. coli* Trx (122). In *CeTR2* there are no flanking Ser residues. This is also the case for *PfTR* which has the sequence Gly-Cys-Gly-Gly-Gly-Lys-Cys-Gly (GCGGGKCG) (55, 123, 124).

SPECIFIC AIMS

The question this project addresses can be phrased based on the direction of the approach. For those who focus on mammalian TR, the question is “why selenocysteine?” Taking into consideration that other higher eukaryotes catalyze the same reaction without Sec, the question may also be phrased “why not cysteine?” It has been long inferred that Sec is essential for mammalian TR due to the low pK_a of Sec (~ 5.2) making it a better nucleophile than Cys which has a $pK_a \sim 8.3$ (125). This is the motivation behind the proposal of Gromer *et al.* on the function of the flanking Ser for *DmTR* (65). However *CeTR* and *PfTR* function without flanking Ser residues. It is also hypothesized that the low pK_a of Sec makes it a better leaving group. However the catalytic acid/base essential to both half-reactions is conserved throughout the protein family, so why would the low pK_a of Sec be essential to mammalian TR but not *DmTR*, *CeTR2*, or *PfTR*? The purpose of this project is to develop a testable hypothesis for the requirement of Sec in mammalian TR.

Aim 1 is to develop a method for semisynthetic production of mammalian TR. The method produces the full-length enzyme from a ligation of two separately produced modules using expressed protein (126-128). A truncated form of TR missing the three C-

terminal amino acids is produced for the first module as a TR-intein-chitin binding domain fusion protein in *E. coli*. The second module is a C-terminal peptide with a N-terminal Cys. Using this method we will generate C-terminal mutants for structure function studies to investigate the positional and sequence dependence of Sec in the C-terminal active site for mammalian TR. This method will allow 1) avoidance of the complications of Sec incorporation by recombinant methods, 2) the incorporation of synthetic functional groups or site-specific radiolabels that would not be possible using standard recombinant techniques.

Aim 2 is to develop a new technique, termed peptide complementation, to study the mechanism of TR. This technique will allow us to look at a specific reaction in the catalytic cycle in a manner similar to that of GR. The formation of an intramolecular disulfide bond between vicinal residues like that of the C-terminus of TR results in an eight-membered ring. This ring must be opened (reduced) by the FAD-associated active site during the catalytic cycle. Oxidized tetrapeptides, equivalent to the C-terminus of TR are used as substrate for the truncated form of TR missing the final three residues. These tetrapeptides are reduced by the FAD-associated active site just as GSSG is reduced by the same active site in GR. This approach will allow us to determine the activity of Cys-Cys and Cys-Sec peptides in this step of the catalytic cycle for correlation to activities of the semisynthetic mutants.

Aim 3 is to determine the crystal structure of *Dm*TR for comparison to mammalian TR. The NMR structures of the tetrapeptides established as substrates for the truncated TR are modeled into the active site by orientation of the Cys residues to the binding orientation of GSSG in the structure of GR. The structure and peptide modeling

is expected to correlate to the biochemical data collected from Aims 1 and 2 and develop a new hypothesis for the requirement of Sec for mammalian TR.

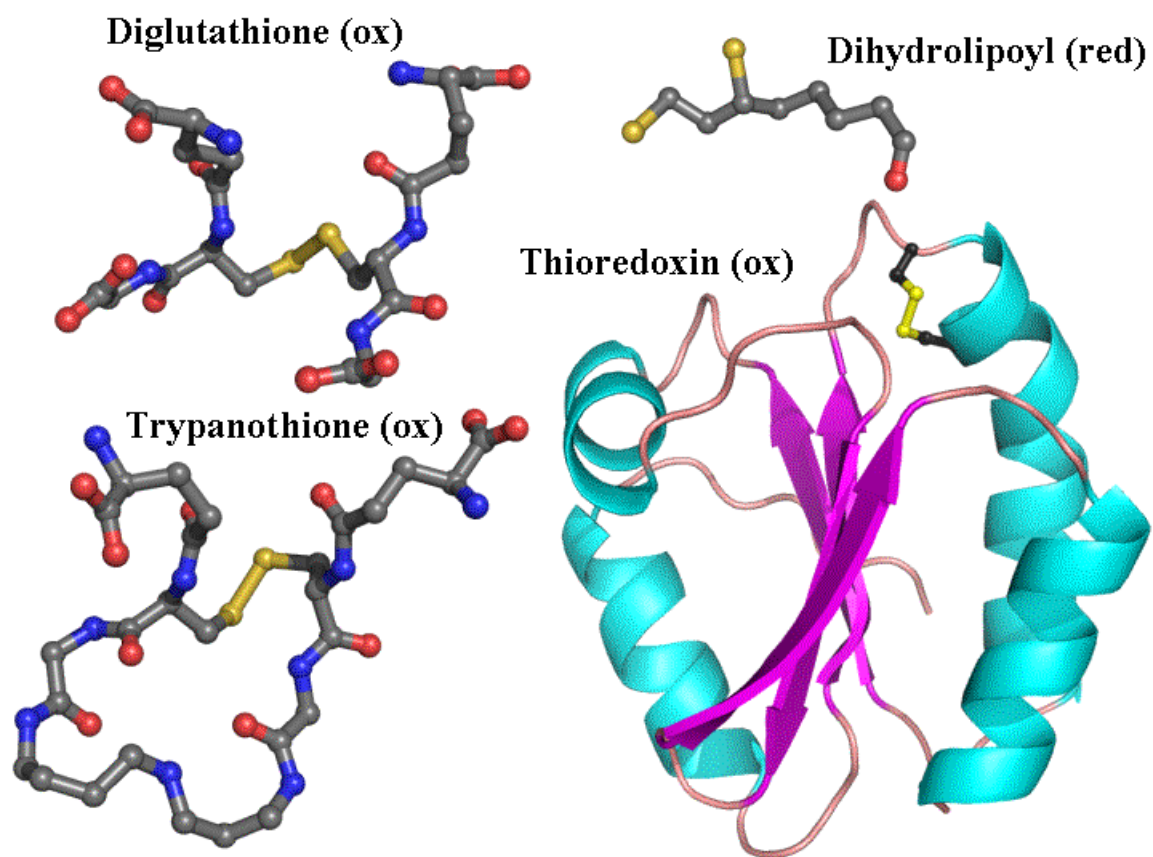


Figure 2. Glutathione reductase family cognate substrates.

Substrates of the Glutathione Reductase family of pyridine nucleotide disulfide oxidoreductases. The substrates are labeled with the shown redox state in parentheses. Diglutathione (GSSG) (34), trypanothione (37), and dihydrolipoyl (129) are small molecule substrates while thioredoxin (Trx) (130) is a ~12 kDa protein. The reversible disulfide of Trx with the conserved sequence Cys-Gly-Pro-Cys is shown.

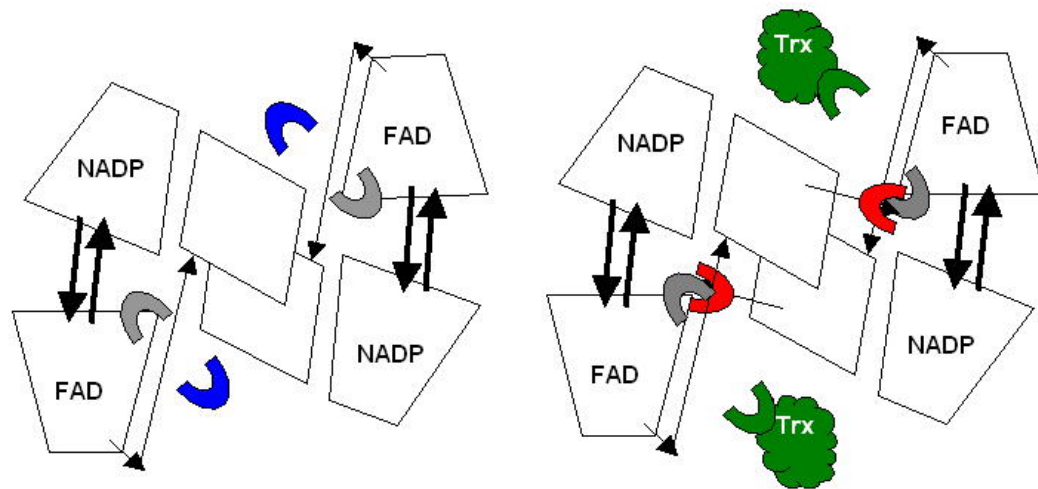


Figure 3. Diagrammatic representation of GR structure.

Glutathione reductase on the left is compared with thioredoxin reductase on the right. Each homodimer is assembled in a head to tail fashion. Each monomer has a N-terminal FAD domain, a central NADP domain, and a C-terminal dimerization domain. The conserved FAD-associated active site disulfide is indicated in gray. The GR substrate GSSG is shown in blue while the C-terminal disulfide active site for TR is in red.

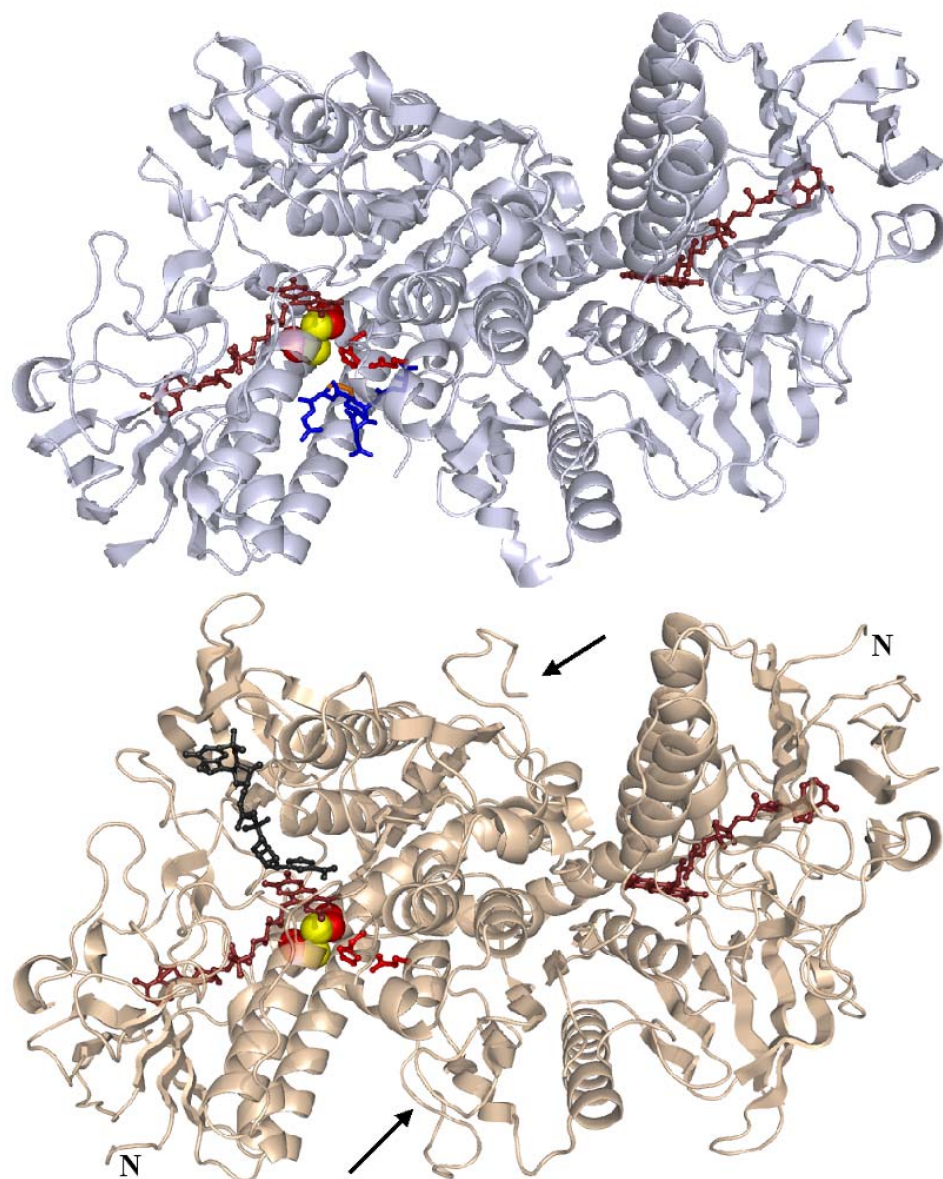


Figure 4. Ribbon diagram of GR and TR.

(Top) Ribbon diagram of glutathione reductase (34) showing the FAD (ruby), the bound GSSG (blue), catalytic residues (red). (Bottom) Ribbon diagram of mouse thioredoxin reductase 3 (35) showing the FAD (ruby), the bound NADP (black), catalytic residues (red), the arrows indicate the 16 amino acid C-terminal extension. The N indicates the N-terminus of each monomer.

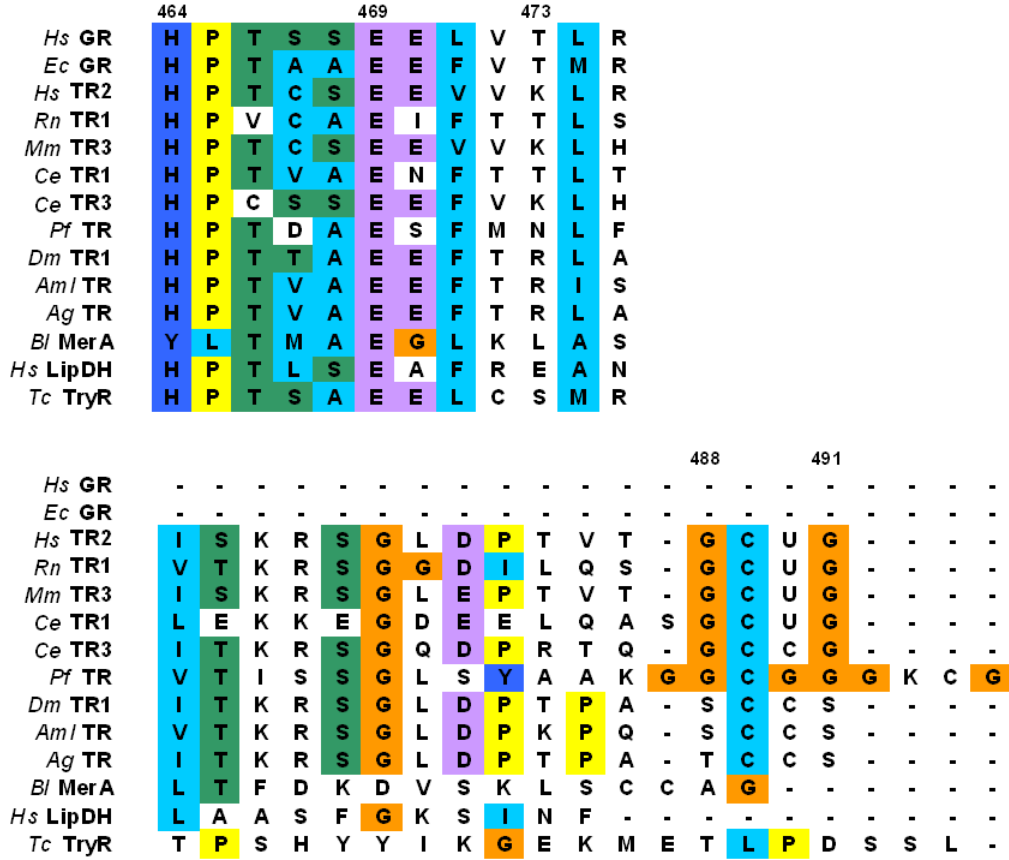


Figure 5. Multiple sequence alignment (C-terminal).

Multiple sequence alignment generated by Clustal W (131) of the C-terminal dimerization domain with either the PDB ID or accession number in parentheses. The sequences are glutathione reductase (GR) from *H. sapiens* (PDB 1GRA), GR from *E. coli* (PDB 1GER), Thioredoxin reductase (TR) 2 from *H. sapiens* (Q9NNW7), TR1 from *R. norvegicus* (PDB 1H6V), TR3 from *M. musculus* (PDB 1ZKQ), TR1 from *C. elegans* (AF148217_1), TR3 from *C. elegans* (NP_498971.1), TR from *P. falciparum* (NP_704777.1), TR1 from *D. melanogaster* (AF301144_1), TR from *A. mellifera linguistica* (AAP93583.1), TR from *A. gambie* (CAD30858.1), mercuric reductase (MerA) from *B. licheniformis* (CAC14663.1), dihydrolipoamide dehydrogenase (LipDH) from *H. sapiens* (EAL24389.1), trypanothione reductase (TryR) from *T. congolense* (AAA30258.1). The catalytic acid base dyad is His464 and Glu469 (*Drosophila* TR numbering).

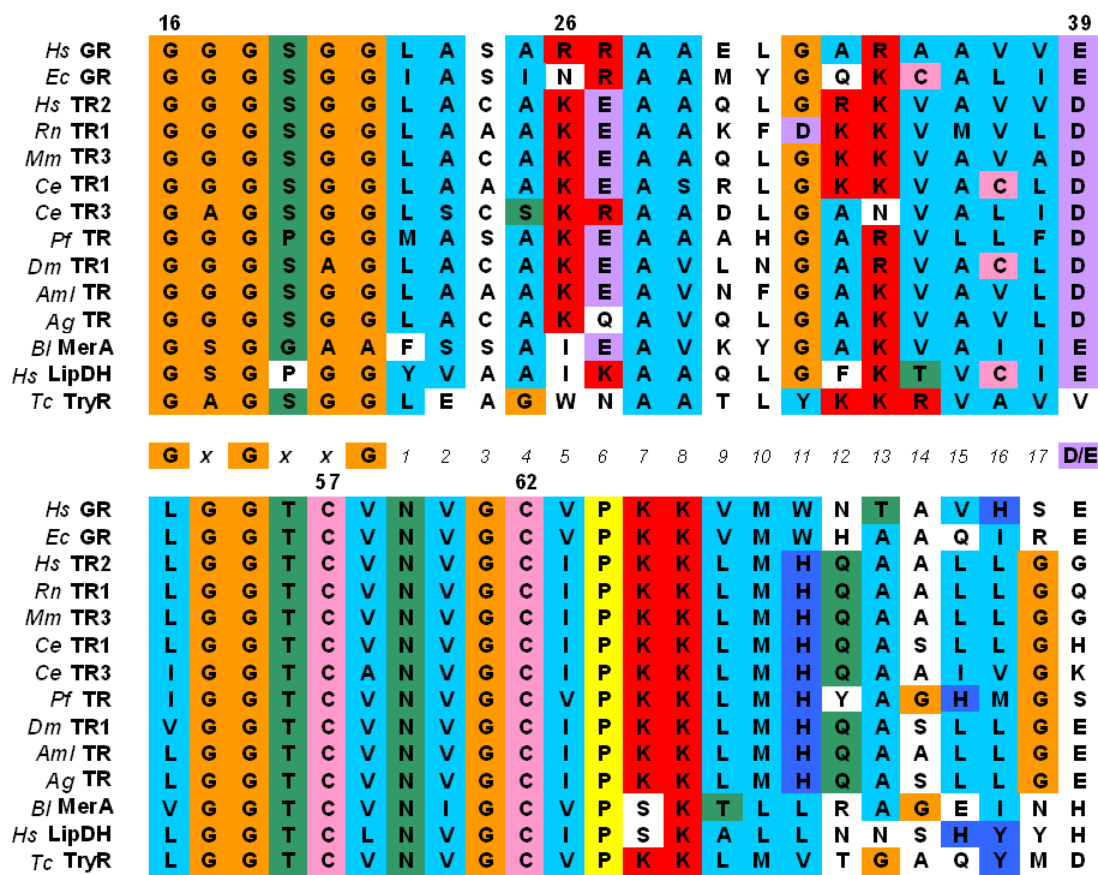


Figure 6. Multiple sequence alignment (FAD Domain).

Multiple sequence alignment generated by Clustal W (131) of the FAD domain with either the PDB ID or accession number in parentheses. The sequences are glutathione reductase (GR) from *H. sapiens* (PDB 1GRA), GR from *E. coli* (PDB 1GER), Thioredoxin reductase (TR) 2 from *H. sapiens* (Q9NNW7), TR1 from *R. norvegicus* (PDB 1H6V), TR3 from *M. musculus* (PDB 1ZKQ), TR1 from *C. elegans* (AF148217_1), TR3 from *C. elegans* (NP_498971.1), TR from *P. falciparum* (NP_704777.1), TR1 from *D. melanogaster* (AF301144_1), TR from *A. mellifera linguistica* (AAP93583.1), TR from *A. gambiae* (CAD30858.1), mercuric reductase (MerA) from *B. licheniformis* (CAC14663.1), dihydrolipoamide dehydrogenase (LipDH) from *H. sapiens* (EAL24389.1), trypanothione reductase (TryR) from *T. congolense* (AAA30258.1). The alignment shows the FAD binding motif (Top) and conserved FAD-associated active site sequence C₅₇VNVGC₆₂ (*Drosophila* TR numbering).

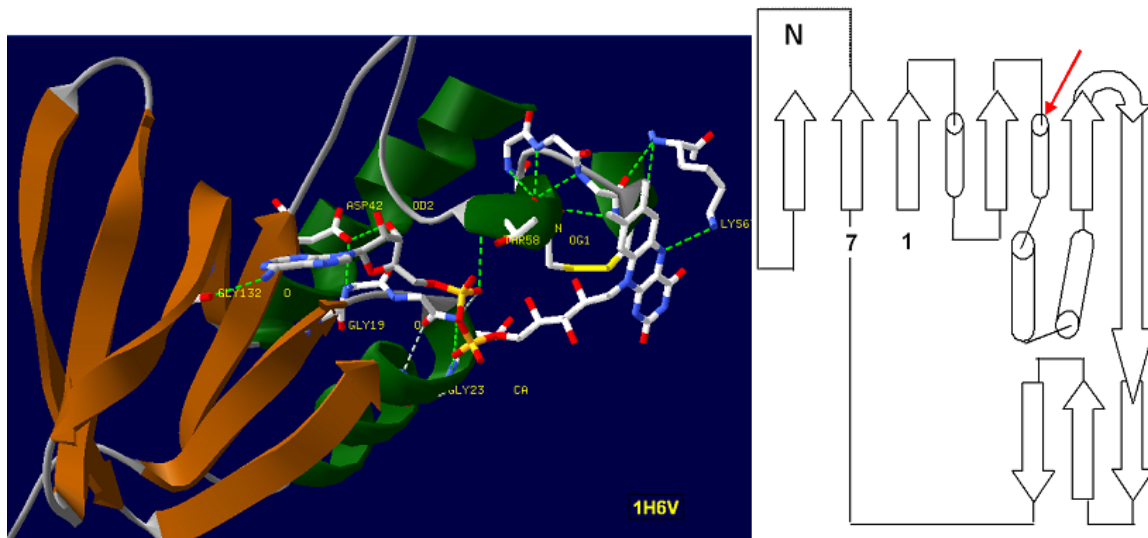


Figure 7. The FAD domain topology.

(Left) The Rossman Fold of the FAD-Binding Domain from rat thioredoxin reductase 1 (36). The conserved GxGxxGx(17)D/E is Gly19 to Gly23 as the phosphate binding motif and D-42 to coordinate the ribose of the adenosine. This is the Top panel of the alignment in **Figure 6**. (Right) The topology diagram of the domain shows arrows indicating strands and columns indicating helices. The N indicates the NADP domain and the red arrow indicates the active site CVNVGC.

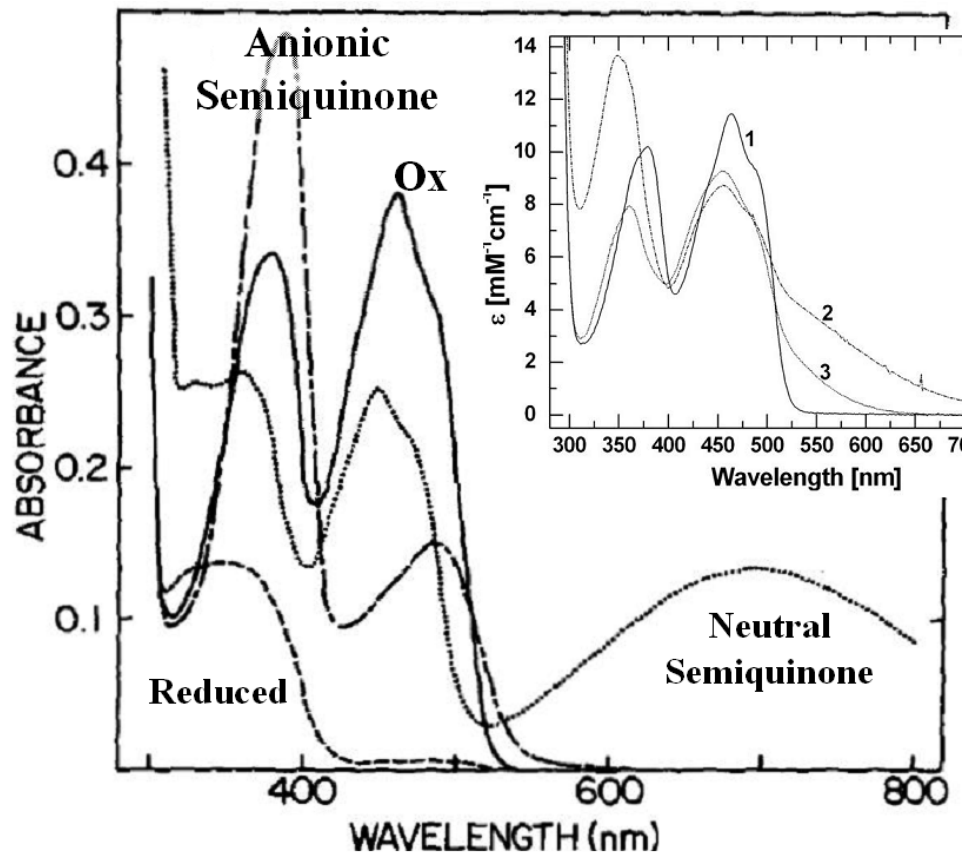


Figure 8. Spectral properties of flavin.

Spectral characteristics of the flavin moiety of Old Yellow Enzyme in various redox states taken from (74). The inset is of the human glutathione reductase taken from (76) in the oxidized form (1), NADPH reduced (2), and sodium borohydride reduced (3). The spectral characteristics of the reduced GR under normal conditions do not resemble that of the reduced flavin. It best represents a mixture between the oxidized and the anionic semiquinone. The shoulder at 540 nm (inset) is the charge-transfer complex between the flavin and the C-terminal Cys of the FAD-associated active site.

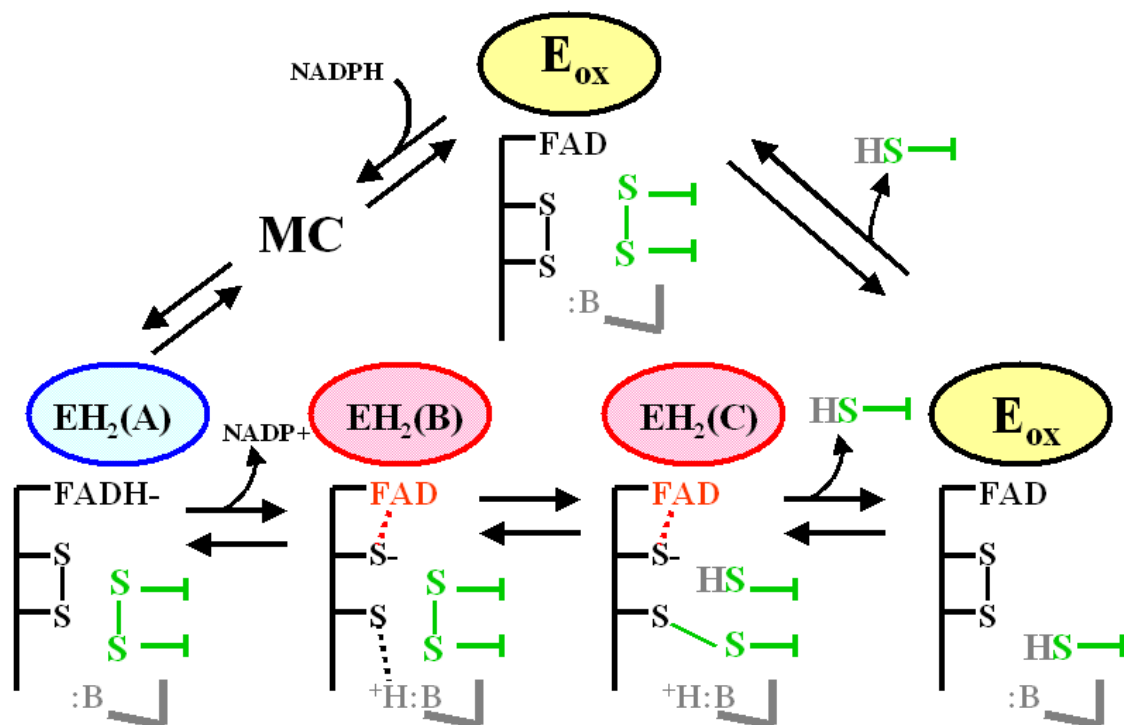


Figure 9. The catalytic cycle of GR.

The Catalytic cycle of Glutathione Reductase. The steady state cycles between E_{ox} and EH_2 . From E_{ox} to $EH_2(B)$ is the reductive half-reaction. From $EH_2(B)$ back to E_{ox} is the oxidative half-reaction. The colors for each enzyme species represent the characteristic wavelength: the oxidized enzyme is yellow (440 nm – 460 nm), the FADH⁻ - NADP⁺ charge-transfer complex is shown in blue (670 nm), and the thiolate-FAD charge-transfer complex is shown in red (525 nm – 540 nm). The GSSG substrate is shown in green, the catalytic acid/base from Chain B is shown in gray. Diagram adapted from (93).

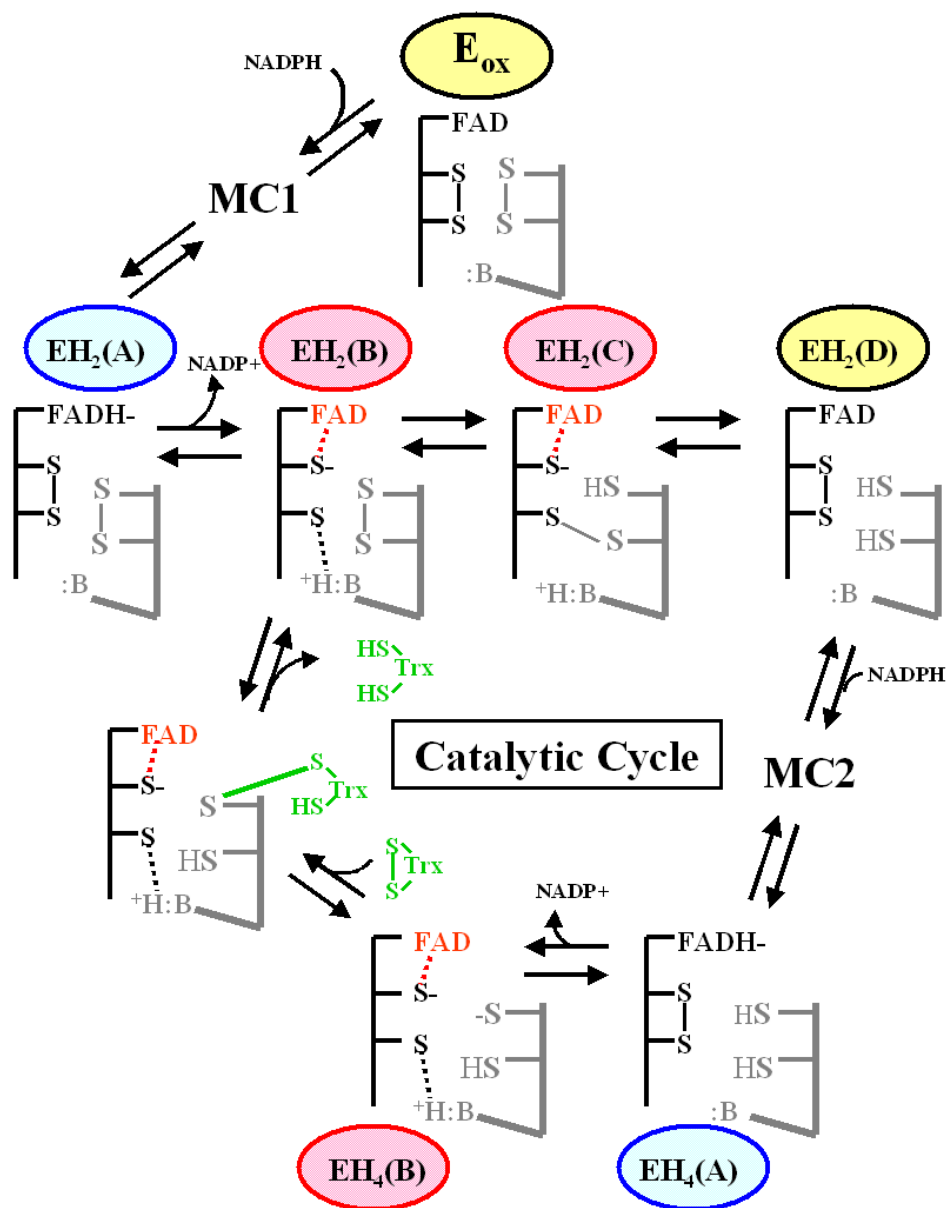


Figure 10. The catalytic cycle of TR.

The Catalytic cycle of Thioredoxin Reductase. The steady state is thought to cycle between EH_2 and EH_4 . From E_{ox} to $\text{EH}_4(\text{B})$ is the reductive half-reaction. From $\text{EH}_4(\text{B})$ back to $\text{EH}_2(\text{B})$ is the oxidative half-reaction. The enzyme species color code is as shown in figure 9. The C-terminal disulfide and the catalytic acid/base from Chain B are shown in gray. The substrate thioredoxin is shown in green. Diagram adapted from (93).

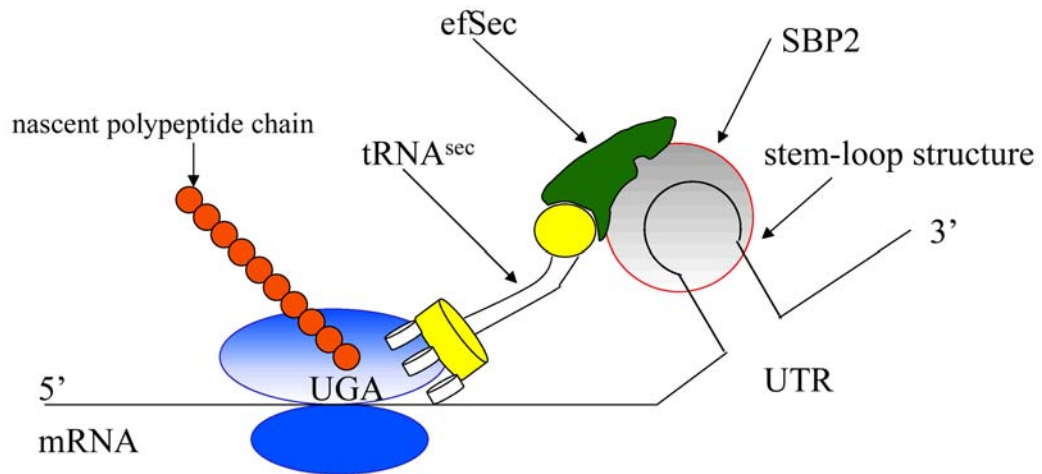


Figure 11. Decoding of the UGA codon.

Eukaryotic decoding of the UGA codon for the cotranslational incorporation of selenocysteine into proteins (132, 133).

CHAPTER 2:

SEMISYNTHESIS OF MAMMALIAN THIOREDOXIN REDUCTASE

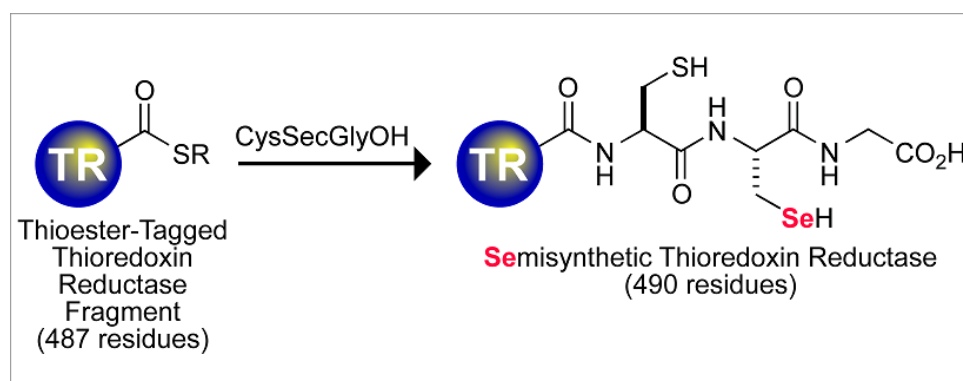


Figure 12. Representation of semisynthetic TR.

Semisynthesis of mammalian thioredoxin reductase. Selenoproteins are difficult to produce recombinantly due to the complicated cellular machinery, which must be manipulated for decoding of the UGA Sec codon. Semisynthesis produces the wild type enzyme by the ligation of two modules via a thioester intermediate: 1) the truncated form of the enzyme missing the three C-terminal amino acids and 2) the synthetically produced C-terminal tripeptide Cys-Sec-Gly.

Biochemistry 2006, Apr 25; 45(16): 5158-5170

**Semisynthesis and Characterization of Mammalian
Thioredoxin Reductase[†]**

Brian Eckenroth[‡], Katharine Harris[‡], Anton A. Turanov[§], Vadim N. Gladyshev[§],
Ronald T. Raines^{||}, and Robert J. Hondal^{*‡}

[‡]Department of Biochemistry, 89 Beaumont Ave, Given Laboratory, Room B413,
Burlington, VT 05405

^{||}Departments of Biochemistry and Chemistry, University of Wisconsin-Madison,
Madison, WI 53706

[§]Department of Biochemistry, University of Nebraska, Lincoln, NE 68588

[†]These studies were supported by National Institutes of Health Grants GM070742 to
RJH, GM044783 to RTR, and GM065204 to VNG.

*To whom correspondence should be addressed. Department of Biochemistry, University
of Vermont, College of Medicine. 89 Beaumont Ave, Given Laboratory, Room B413,
Burlington, VT 05405. Tel: 802-656-8282. FAX: 802-862-8339. E-mail:
Robert.Hondal@uvm.edu.

Here, we report the development of an alternative method for producing an active mammalian TR containing selenocysteine. This method uses expressed protein ligation to create a semisynthetic TR. TR contains selenocysteine in a C-terminal tripeptide with a Cys-Sec-Gly sequence, where the Sec residue is the penultimate amino acid (63). The location of the Sec residue in the C-terminus (**Figure 12**) makes TR an ideal candidate for semisynthesis. Our strategy for producing a semisynthetic TR is shown in **Figure 13**.

Introduction to Semisynthesis.

The term semisynthesis refers to the production of a functional entity, a single polypeptide chain enzyme for example, from two or more separately produced components. There are three categories of semisynthesis: 1) native chemical ligation (NCL), 2) expressed protein ligation (EPL) which is intein mediated, and 3) complementation. Unlike the first two techniques (127), complementation is a non-covalent association of the components. The best example of complementation is the production of functional ribonuclease from two separate polypeptide chains achieved by Richards (134). This technique will be addressed in Chapter 4.

The ligation methods both require the formation of a thioester intermediate at the C-terminal end of the N-terminal fragment, which is attacked by the N-terminal Cys of the C-terminal fragment. In native chemical ligation, the thioester is generated by synthetic means whereas in expressed protein ligation (**Figure 14**) the thioester is generated at the junction of a fusion protein. The fusion protein contains the N-terminal piece of the protein of interest followed by an intein. The thioester is formed at the fusion

protein junction by the N-terminal Cys of the intein. Like complementation, this technique has also been used successfully with ribonuclease (135), as well as for producing modified potassium channels (136, 137), and to investigate cell-signaling mechanisms (138) using modified phosphoproteins.

The intein is a naturally occurring self-splicing protein element found in several simple organisms such as certain bacteria as well as single-cellular eukaryotes (139). Analogous to RNA self-splicing introns, which join two flanking exons, the intein catalyzes the ligation of two flanking protein segments (140). This reaction is catalyzed via formation of a thioester intermediate formed by the N-terminal Cys of the intein. Upon ligation of the segments, the intein is released, as reviewed in (141).

Most often the two ligation techniques are used independently to assemble two fragments, as we have used with EPL to produce semisynthetic TR. However, the two methods can be used in combination to perform a two-step ligation product from three fragments (**Figure 15**). This has been utilized for the insertion of a fluorescent probe in between the Src homology domains 2 and 3 of a protein tyrosine kinase (142). In this method, the C-terminal domain (containing an N-terminal Cys) is produced recombinantly and purified. The label to be inserted is incorporated into a short, synthetically produced peptide. This peptide includes three features: a C-terminal thioester, the incorporated label, and a N-terminal factor Xa protease sequence. This peptide is mixed with the C-terminal domain to form the first ligated product by NCL. The product is treated with the factor Xa protease generating a new N-terminal Cys. The N-terminal domain is produced as the intein fusion protein of which the new N-terminal Cys will attack the thioester resulting in the final product by EPL.

METHODS

Peptide Synthesis.

Fmoc-selenocysteine(pMob)-OH was synthesized as reported previously(127, 128). This derivative of Sec was then used to make the Cys-Sec-Gly tripeptide (CUG) or the Ac-GCUG tetrapeptide using solid-phase peptide synthesis as described (143). Peptide were purified by preparative HPLC from the Shimadzu Corporation (Kyoto, Japan) and verified by Matrix Assisted Laser Desorption Time of Flight Mass Spectrometry on a Voyager DE PRO Workstation from Applied Biosystems (Framingham, MA). *A comprehensive list of materials used in this dissertation is available in Appendix B.*

Mutagenesis and Transformation.

DNA primers were purchased from Integrated DNA Technologies Inc. (Coralville, IA) for the mutation of the Sec residue (encoded by TGA) at position 489 to cysteine (encoded by TGT) (mutant Sec489Cys). *A comprehensive list of PCR primers used in this dissertation is available in Appendix C.* The template used was plasmid pTR3, which contained the full-length sequence of the mouse thioredoxin reductase-3 gene (mTR3 GenBank accession number [AF171053](#)) was a generous gift from Vadim N. Gladyshev. Mutagenesis was performed by PCR on the GeneAmp PCR System 2400 from Perkin-Elmer Life Sciences Inc. (Boston, MA) using Vent DNA polymerase. The

PCR product was purified using the QIAquick purification kit from Qiagen (Valencia, CA) according to product instructions. The PCR product containing the mutated sequence was inserted into the pTYB3 plasmid (New England Biolabs) by restriction digestion with Nco I and Sap I for 2 h at 37 °C followed by purification with a Qiagen spin column, and ligation with T4 DNA ligase at 16 °C for 16 h. The ligase was heat inactivated at 70 °C for 30 min, followed by incubation at 37 °C with Eco RI. Eco RI cuts only the plasmid that has not been ligated with the PCR insert, thus enriching the pool of positive clones. The resulting plasmid (pTYB3TR), also containing the gene for ampicillin resistance and a T7 promoter, was used to produce the thioredoxin reductase-intein-chitin binding domain fusion protein in *E. coli* ER2566 cells.

E. coli DH5 α cells, purchased from Stratagene (La Jolla, CA) were transformed with pTYB3TR by addition of 100 ng of plasmid to 200 μ L of cells and incubation on ice for 30 min. The cells were heat shocked at 37 °C for 2.5 min and placed back on ice for 5 min. A 1 mL aliquot of LB broth was added to the cells and the mixture incubated at 37 °C for 60 min. The cells were then plated onto LB-ampicillin agar and incubated overnight. Colonies were then picked and used to inoculate 3 mL of 2 \times YT medium containing 0.2 mg/mL ampicillin and grown in a shaking incubator for 24 h at 37 °C. The plasmid was purified from culture using the Perfectprep Plasmid Mini Kit from Eppendorf (Hamburg, Germany). Transformants were screened by restriction analysis and then analyzed by agarose gel electrophoresis. Positive clones were then sequenced to verify the complete coding sequence of mTR3.

An additional construct was also generated for the truncated form of TR missing the C-terminal tripeptide Cys-Sec-Gly (mTR3-G₄₈₇) using the method above. This

construct is used to produce either the truncated form of the enzyme or for ligation of the synthetic peptides to produce the wild type enzyme by semisynthesis.

Thioredoxin Reductase Expression and Cleavage from Chitin Resin.

The full-length U489C mutant and a truncated version of mTR3 that was missing the C-terminal CUG tripeptide were expressed in *E. coli* ER2566 cells (New England Biolabs). The cell culture (6 L) contained 0.2 mg/mL ampicillin, and cells were grown at 25 °C until an OD of 0.6 at 600 nm was achieved. Expression was then induced for 6 h by the addition of IPTG to a final concentration of 0.5 mM. Cells were harvested by centrifugation and frozen at -20 °C overnight. The cell pellet was homogenized with 300 mL of buffer containing 150 mM sodium chloride (NaCl) in 50 mM 3-(*N*-morpholino)propanesulfonic acid (MOPS) at pH 7.0 and probe-sonicated on ice for 20 min. The suspension was then centrifuged at 9000 rpm in a Beckman J21B preparative centrifuge (JA-14 rotor) from Beckman Coulter (Fullerton, CA).

The supernatant was gravity-loaded onto a column containing chitin resin (New England Biolabs) with a bed volume of 50 mL, and the column was washed with MOPS/NaCl until the absorbance at 280 nm of the eluant dropped to <0.1. For the truncated product and the full-length U489C mutant, the column was then equilibrated with cleavage buffer [50 mM MOPS, 150 mM NaCl, and 70 mM *N*-methylmercaptoacetamide (NMA) or β -ME (pH 7.2)]. The resin-bound TR-intein fusion protein was then incubated with this buffer at 4 °C overnight.

Ligation of the CUG Peptide to Truncated Construct.

The ligation of the synthetic CUG peptide to the truncated enzyme was performed with concomitant cleavage from the chitin resin. The resin-bound truncated construct was cleaved from the chitin resin with cleavage buffer containing 12 mM peptide (305 μ mol-100 mg) added directly to the chitin column. On the basis of typical protein yields, this represents a 3000:1 peptide:protein ratio. For a more optimized procedure with respect to ligation efficiency, the same amount of peptide (in cleavage buffer) was added to the chitin column in which only half the total amount of protein (supernatant from 3 L of cell culture instead of 6 L) was loaded onto the column. For a direct comparison of our methods of TR production, the peptide Cys-Cys-Gly (CCG) was also ligated to produce the Sec489Cys mutant by semisynthesis.

Final Purification of Enzymes.

The protein was batch eluted from the chitin resin with 1-3 column volumes of the cleavage buffer, depending on preparation scale. The ligated product was dialyzed extensively with the MOPS/NaCl buffer at pH 7.0 with a molecular mass cutoff of 6000 Da for removal of any unligated peptide. A separate control experiment was performed in which the truncated form of mTR3 was isolated in the same manner as the semisynthetic TR. Each step in the purification of the truncated mTR3 was the same except that tripeptide CUG was not added to the chitin column.

The pooled protein fractions were prepared for the next step in the purification by the addition of Tris to 50 mM and ammonium sulfate to 1.0 M, and the pH was adjusted

to 7.5. Samples were then gravity-loaded onto a column containing Fast Flow 6 Low Substitution Phenyl Sepharose from Pharmacia-Amersham Biosciences (Uppsala, Sweden) with a bed volume of 60 mL. Protein was eluted from the column with a 400 mL gradient of ammonium sulfate (from 1.0 to 0 M) with collection of 4 mL fractions. Collected fractions were evaluated by the absorbance at 280 nm and 460 nm, as well as 12% SDS-PAGE. Fractions containing mTR3 were pooled, dialyzed against 10 mM potassium phosphate and 10 mM NaCl (pH 7.8), and gravity-loaded onto DEAE-Sepharcel from Sigma Diagnostics (St. Louis, MO) with a bed volume of 60 mL. The protein was eluted with a 400 mL linear gradient of NaCl (from 10 to 300 mM), collecting 4 mL fractions. Fractions containing mTR3 were verified by SDS-PAGE, pooled, dialyzed against 100 mM potassium phosphate (pH 7.4), 1 mM EDTA, and 150 mM NaCl, and concentrated using Centriprep 10 concentrators from Millipore (Bedford, MA). The purification process was monitored via 12% Tris-glycine SDS-PAGE with Novex precast gels from Invitrogen (Carlsbad, CA) and stained as previously described (144).

Determination of the Selenium Content of the Semisynthetic TR.

Semisynthetic TR was analyzed by inductively coupled plasma mass spectrometry (ICP-MS) to determine the selenium content of the enzyme. The TR samples were in phosphate-buffered saline, and the corresponding buffer was also analyzed in parallel as a control. The selenium content (in parts per million) was then recalculated to the molar amount of the analyzed protein.

"Off-Resin" Ligation Efficiency.

The cell extract from 6 L of *E. coli* cells was loaded onto a chitin-agarose column as described above. After being extensively washed with column buffer, the resin was treated with cleavage buffer to elute the protein. The eluate was concentrated as before and then dialyzed against 50 mM MOPS buffer (pH 7.0) with 150 mM NaCl to remove excess NMA. The concentrated protein sample was then divided into four aliquots. The CUG tripeptide was added to each of three aliquots at a concentration of 5 mM: one aliquot received 50 mM NMA, the second aliquot received 50 mM NADPH, and the third aliquot received buffer. The fourth aliquot received only buffer, contained no peptide, and served as the negative control. The samples were allowed to incubate at room temperature for 4 h, after which they were dialyzed against 50 mM potassium phosphate buffer (pH 7.4) containing 150 mM NaCl and 1 mM EDTA to remove excess peptide and reagent. After dialysis, the samples were assayed using 90 μ M thioredoxin (Trx) to determine a specific activity.

Enzymatic Characterization of Thioredoxin Reductase.

The TR mutants were assayed for activity towards DTNB, Trx, and hydrogen peroxide as described by Arner (145). All assays were performed on a Cary 50 UV/VIS spectrophotometer from Varian (Walnut Creek, CA) at 25 °C, pH 7.0, and were initiated by addition of enzyme. Concentration of homodimeric TR was determined using the flavin extinction coefficient of 22.6 mM⁻¹cm⁻¹. Activity was monitored over two minutes and V_o determined from the linear fit. Plots of V_o/E_T vs. substrate concentration were fit

by the Michaelis-Menten equation using KaleidaGraph 4.02 from Synergy Software (Reading, PA) and activities reported as moles of NADPH consumed per minute per mole of homodimeric TR.

DTNB Reductase Activity.

The DTNB assay contained 0.2 mM NADPH and 10 mM EDTA in 100 mM potassium phosphate. For each concentration of DTNB, activity was corrected for background by addition of buffer only. Activity was measured by the increase in absorbance at 412 nm, calculated using the extinction coefficient for TNB^- , $13.6 \text{ mM}^{-1} \text{ cm}^{-1}$, and divided by two to account for the production of 2TNB^- per NADPH consumed. The concentration of TR in the assay was 2 nM.

Thioredoxin Reductase Activity.

The Trx assay contained 0.15 mM NADPH, 1 mM EDTA, and 10 mg/mL insulin in 50 mM potassium phosphate. Activity was background corrected for each concentration of Trx by addition of buffer only as well as in the absence of substrate. Activity was measured by the decrease in absorbance at 340 nm for the consumption of NADPH and calculated using the extinction coefficient of $6200 \text{ M}^{-1} \text{ cm}^{-1}$. The concentration of the semisynthetic mTR3 in the assay was 2 nM. The concentration of each mutant TR was adjusted to achieve a similar change in absorbance at 340 nm as that of semisynthetic TR.

Peroxidase Activity.

The hydrogen peroxide assay for semisynthetic mTR3 is formulated similar to that of the DTNB assay with activity measured at 340 nm and background corrected as with the previous assays. The concentration of semisynthetic TR in the assay was 50 nM and the concentration of each mutant TR was adjusted to achieve a similar change in absorbance 340 nm.

Production of Thioredoxin.

The clone containing the gene for Trx A from *Escherichia coli* was a gift from Ronald T. Raines (146) and was produced similar to methods previously described (32). Calcium chloride competent *E. coli* BL21DE3 cells were transformed with 50 ng of DNA and plated onto LB agar supplemented with 200 µg/mL ampicillin. Single colonies were used to inoculate 100 mL ampicillin-containing LB media and allowed to shake overnight at 37 °C.

One liter of LB media supplemented with 200 µg/mL ampicillin was inoculated with 10 mL of starter culture and grown to an OD of 0.6 at 600 nm while shaking at 37 °C in a C25KC Shaker Incubator from New Brunswick Scientific. The cells were induced for 3 hours at 37 °C with 0.5 mM IPTG then harvested by 10 minute centrifugation at 10,000 rpm in a JA-14 rotor using a Model J-21B centrifuge from Beckman and pellets frozen at -20 °C.

Cells were thawed on ice, homogenized in 20 mM Tris pH 8.4 containing 1 mM EDTA, and lysed by probe sonication using a Branson Sonifier. The lysis was

centrifuged as above for 90 minutes and the supernatant loaded onto DEAE sephacel, 70 mL bed volume, from Sigma-Aldrich equilibrated in the lysis buffer. After loading, the column was washed with buffer until the OD at 280 nm of the effluent was 0.05. The sample was eluted using two 400 mL gradients containing NaCl (0 mM to 0.1 mM and 0.1 mM to 0.25 mM). Fractions were collected and evaluated by absorbance at 280 nm and SDS-PAGE. Fractions containing Trx were pooled adjusted to 60% ammonium sulfate and centrifuged as above for 60 minutes. The pellet was solubilized in a minimal volume of 20 mM Tris pH 8.4, 250 mM NaCl, and 1 mM EDTA.

A 2mL sample was loaded onto a Sephacryl S-100 HR (98 cm X 3.3 cm) gel filtration column from Pharmacia-Amersham Biosciences (Uppsala, Sweden) equilibrated with sample buffer. Collected fractions were evaluated by absorbance at 280 nm and SDS-PAGE. The fractions containing Trx were pooled, concentrated using an Amicon Ultra with 5000 molecular weight cutoff from Millipore. Purity was >95% as judged by 15% SDS-PAGE and Trx concentration was calculated using the extinction coefficient at 280 nm of $13,700 \text{ M}^{-1}$.

Determination of the Mass of Truncated and Semisynthetic TRs.

The enzymes were concentrated to 1 mg/mL in 10 mM ammonium bicarbonate buffer (pH 8.0). The protein samples were then spotted on a 100-well plate at various dilutions. A solution of sinnapinic acid at 10 mg/mL was overlaid onto the protein spots, and the samples were left to air-dry. A Voyager-DE MALDI-TOF mass spectrometer in the linear mode was then used to analyze the samples. The instrument was externally calibrated using BSA.

Peptide Mass Mapping of Tryptic Fragments.

Purified thioredoxin reductase (truncated or semisynthetic) at a concentration of 0.3 mg/mL was digested using 10 µg/mL sequencing grade trypsin (Promega) in 150 mM ammonium bicarbonate at 37 °C for 16 h. The digested sample was stored frozen until mass spectrometric analysis. Samples for MALDI-TOF were prepared by serial dilution in 10 mg/mL matrix, 2,5-dihydroxybenzoic acid (DHB), or α -cyano-4-hydroxycinnamic acid (CHCA), with a 50% acetonitrile/0.05% TFA mixture as a diluent. Samples were applied to the MALDI plate as 1 µL spots and dried under vacuum.

A Voyager-DE PRO Workstation (Applied Biosystems) was used to analyze MALDI-TOF samples. Positive ion spectra (mass + H⁺) were collected in reflector mode with an accelerating voltage of 20 000 mV and a delayed extraction time of 175 ns. Data were collected as the accumulated spectra containing a minimum of 10 spectra at 50 laser shots per spectrum. Monoisotopic masses were corrected by external calibration using Applied Biosystems Calibration Mixture 2: angiotensin I (1296.6853), ACTH clip 1-17 (2093.0867), clip 18-39 (2465.1989), and clip 7-38 (3657.9294) prepared in the equivalent matrix. The resulting (mass + H⁺) data were compared to a theoretical digest generated using the ExPASy Peptide Mass Proteomics tool.

Digested samples were also analyzed by LC-MS using a Thermo-Finnigan LCQ Deca XP Plus liquid chromatograph via ion trap mass spectrometry with peaks subjected to MS/MS fragmentation sequencing by collision-induced dissociation. Full MS of parent ions and MS/MS fragmentation data were processed using the Turbo-SEQUENT database for peptide identification. The mass + H⁺ of the semisynthetic C-terminal tryptic

fragment (SGLEPTVTGCUG), molecular formula of $\text{Se}_1\text{C}_{44}\text{H}_{73}\text{N}_{12}\text{O}_{18}\text{S}_1$ representing the oxidized form, was compared to the theoretical isotope pattern generated using MS-Isotope from USCF ProteinProspector version 4.0.5.

RESULTS AND DISCUSSION

Expression and Purification.

We have constructed a fusion protein that consists of mouse thioredoxin reductase-3, intein, and chitin binding domain. The chitin binding domain is a small peptide that has a high affinity for the chitin-agarose fusion, and this resin provides a high level of purification of the fusion protein. The fusion construct is made so that glycine 487 of mTR3 is the amino acid at the junction between mTR3 and the intein. Addition of a cleavage buffer containing thiol (NMA, β -ME or DTT) causes elution of the thioester-tagged mTR3 from the affinity column. The fusion protein appears as a band near 110 kDa in the 12% SDS-PAGE gel. **Figure 16** shows a 12% SDS-PAGE gel of pooled protein fractions from each step in the purification process. As the chitin resin is an affinity resin, the purity of the eluted mTR3 (either truncated or semisynthetic) is very good with only minor contaminants showing. These contaminants are removed after the phenyl-sepharose and DEAE chromatographic steps as shown in **Figure 16**. The elution profile for semisynthetic mTR3 for each column is shown in **Figure 17**.

The purity of the truncated mTR3 is such that large crystals can be grown from the purified enzyme (**Chapter 5**). The purity of the semisynthetic enzyme is similar to

that of the truncated enzyme as shown in **Figure 16**. The purity is also verified by the characteristic absorbance spectra of TR. Three main peaks are observed for the oxidized enzyme (86). The 275 nm peak is the protein peak and the 370 nm and 460 nm peaks are the characteristic flavin peaks. The flavin spectra are shown in **Figure 18** and a summary of corresponding wavelengths in **Table 1**. For the oxidized form of the enzyme, the 460 nm peak is expected to be larger than the 370 nm peak at a ratio of ~1.1 which is what is typically observed for our proteins. A purity ratio of ~8.5 for the 275 nm to 460 nm peak has been established for rat TR1 (109). The rat TR1 and mTR3 have similar predicted extinction coefficients for the protein sequence (147), 59,205 and 60,110 $M^{-1}cm^{-1}$ respectively. Therefore, the 275 nm to 460 nm ratio should be similar for mTR3. Purified mTR3 also shows a 275 nm to 460 nm ratio of ~8.5.

The purified proteins have excellent stability when stored in the final dialysis buffer of 50 mM potassium phosphate pH 7.4, 150 mM NaCl, 1 mM EDTA. Storage at 4 °C shows no loss of activity for >12 months. Preparation of a 50% glycerol stock for storage at -20 °C showed no loss in DTNB reductase activity after 18 months. Protein solution is concentrated most effectively using the Millipore Amicon Ultra. The storage pH of 7.4 and the DEAE purification at pH 7.8 is to aid in the solubility. Concentrated protein stored at pH 7.0 tended to form precipitate which can partially be recovered by incubation with DTT. Precipitate was also observed for higher yield preps during the dialysis step prior to the DEAE purification, which was addressed by using pH 7.8 during this step. However, the protein must still remain dilute until bound to the column and 10 mM NaCl is added to help prevent the precipitation. These observations lead to the conclusion that the solubility is significantly dependent on salt concentration. At 150 mM

NaCl the limit of solubility is 10 – 15 mg/ml. Increasing to 300 mM NaCl allows for concentration to 30 mg/ml, which was critical to the crystallographic progress in Chapter 5.

Selenium Content of the Semisynthetic Enzyme.

The selenium content of the semisynthetic enzyme determined by ICP-MS was found to be 0.63 mol of selenium/mol of enzyme. Our yield of TR from this method was 24 mg from 6 L (4 mg/L) of cell culture. The selenium content of the semisynthetic enzyme using half the bound resin of the initial trial was found to be 0.91 mol of selenium/mol of enzyme, with a yield of 9 mg of enzyme from 3 L (3 mg/L) of cell culture. By comparison, the selenium content of the recombinant mTR3 prepared by fusing a bacterial SECIS element to the 3' end of the gene had a selenium content in the range of 0.4-0.5 mol of selenium/mol of enzyme depending on the preparation (148). In both cases, the final preparations of enzymes are a mixture of the truncated form and the full-length form. The ligation efficiency can be estimated from ICP-MS analysis since the ligated tripeptide is the only source of selenium for the enzyme.

DTNB Reductase Activity.

A summary of activities for DTNB is shown in **Table 2**. DTNB is a small molecule disulfide that is a non-physiological substrate as can be seen by the high micromolar to low millimolar values for K_m . These high values for K_m are consistent with reports in the literature, however unlike with the substrate Trx, k_{cat} is rarely reported for DTNB (**Table 3**). The wild type TR from rat and human shows significantly higher

activity towards DTNB than a Sec to Cys mutant (109) or a C-terminal truncation (149). Therefore, it is rather surprising to see that all of our mutant forms have very high DTNB reductase activity (>60% of wild type). However, for each of the mutants, the K_m is 3 to 7 fold higher, resulting in a significant decrease in catalytic efficiency, k_{cat}/K_m . The semisynthetic wild type at 63% and 91% selenium incorporation have similar activities. The 63% incorporation has ~5% greater activity than the 91% but the higher incorporation has the higher k_{cat}/K_m .

A similar phenomena has been reported for the non-selenium containing *DmTR* and *PfTR*. The C-terminal mutant Cys535Ala of *PfTR* shows 64% of wild type activity with ~2 fold increase in K_m , while mutation of the FAD associated Cys88 has essentially no activity (55). The same is the case for *DmTR* where the C-terminal mutants display DTNB reductase activity with a 7 fold increase in K_m (78). Unfortunately, no k_{cat} is reported for *DmTR* or *PfTR*. These results are similar to what we observe for mTR3. It is not clear why there is such a broad range of activities for DTNB by these proteins while the range of activities for Trx are rather narrow. Regardless of whether there is a relevant value for k_{cat} , it does provide an alternative means to semi-quantitatively assess the production of a functional protein for those mutants that are inactive to Trx. The questions regarding DTNB as a substrate for the truncated and mutant forms of TR will be further addressed in the following chapters.

Activity toward Thioredoxin.

The peptide complementation system described above led to the development of a semisynthetic enzyme that covalently links the tripeptide containing Sec to the main body

of the enzyme through a peptide linkage. The semisynthetic enzyme could be constructed by addition of peptide CUG to the cleavage buffer, as described above. Since this peptide has an N-terminal cysteine residue (and is not N-acylated), the sulfhydryl group of the cysteine residue can attack the C-terminal thioester group of the enzyme. Rearrangement then occurs to the amide form (141). To test whether the peptide becomes truly incorporated into the enzyme, we tested the ability of the semisynthetic enzyme to reduce Trx. The presence of a Sec residue has been shown to be necessary to reduce *E. coli* Trx with high efficiency (109). The semisynthetic enzyme at a concentration of 2 nM exhibited excellent activity toward *E. coli* Trx in comparison to both the truncated form and a mutant form of the enzyme in which a cysteine residue replaces Sec489 as part of a full-length construct. A Michaelis-Menten plot for our semisynthetic construct in comparison to the Sec489Cys mutant is shown in **Figure 19**, and a summary of our kinetic data is given in **Table 4**. As shown in Figure 7, the Sec489Cys mutant has much lower activity, as would be expected and as was reported previously (109). In contrast to the cysteine mutant enzyme, our semisynthetic enzyme shows very high activity, with values of k_{cat} ranging from 1500 to 2220 min^{-1} , depending on the preparation. This high activity strongly indicates that the C-terminal tripeptide was successfully ligated to the thioester-tagged enzyme. The enzyme preparation with a higher k_{cat} value resulted from using a higher peptide:protein ratio during the ligation and resulted with an enzyme with a higher selenium content (91% Se). The truncated enzyme (ending with amino acid 487 and missing the tripeptide) has no detectable activity toward oxidized Trx.

The thioredoxin reductase activity of our enzyme compares very favorably to the value of 3000 min^{-1} reported for rat TR1 (145, 150). The K_m for thioredoxin of our

semisynthetic enzyme is in the range of 35-70 μM . This is 10-20-fold higher than the K_m reported for rat TR1 with human Trx, but the sequences of the two enzymes are only 56% identical so some difference in K_m is to be expected (the difference is between the cytosolic form of the rat enzyme and the mitochondrial form of the mouse enzyme). This is nearly identical for that observed for the originally identified human TR (24) which showed a 3.7 μM K_m for rat Trx but 34.0 μM K_m for *E. coli* Trx as was the case for rat TR1 with *E. coli* Trx (145, 150). As was observed for the DTNB assays, the Sec489Cys produced recombinantly or by semisynthesis display similar kinetic parameters.

Comparison of the Activity of Semisynthetic TR to That of Recombinant TR.

The activity of the semisynthetic enzyme was compared to that of the recombinant mTR3. The latter protein was expressed in *E. coli* and contained 0.5 equiv of selenium (148). The recombinant TR enzyme is made by fusing a bacterial SECIS element to the 3' end of the TR3 gene. This allows for heterologous expression of the recombinant enzyme in *E. coli*. The results in **Figure 20** show that the recombinant mTR3 and the semisynthetic mTR3 have similar activities with both *E. coli* Trx and recombinant rat Trx2. The recombinant mTR3 has an estimated k_{cat} of 1770 min^{-1} . These data further verify that the semisynthetic method resulted in a functional TR.

Peroxidase Activity.

Mammalian thioredoxin reductases also exhibit hydrogen peroxidase activity. This activity is a characteristic feature of the mammalian enzymes because non-selenium-containing TRs have been shown to have little, if any, hydrogen peroxidase activity

(109). **Figure 21** shows the results of our hydrogen peroxidase activity assays with our semisynthetic enzyme and the Sec489Cys mutant. The mutant enzyme has barely detectable hydrogen peroxidase activity, while the semisynthetic enzyme shows high peroxidase activity with a k_{cat} of $71 \pm 7 \text{ min}^{-1}$ and a K_m of $6.6 \pm 0.50 \text{ mM}$. This rate was achieved with 200 nM semisynthetic enzyme present in the assay though the plot shows very poor saturation. The kinetic data derived from **Figure 21** compare favorably to the data reported by Zhong and Holmgren (109) for reduction of H_2O_2 by human placental TR1. The high peroxidase activity of our enzyme provides additional strong support for the incorporation of the selenocysteine-containing tripeptide by our semisynthetic approach.

Ligation Efficiency for Off-Resin Ligations.

As shown in **Figure 13**, our method of making a semisynthetic TR makes use of the addition of the oxidized tripeptide to a thiol-containing cleavage buffer, which is then added directly to the resin-bound protein. The thiol in the cleavage buffer can either liberate the protein from the resin to produce a thioester-tagged protein or reduce the oxidized tripeptide, which in turn could directly attack the resin-bound protein and become incorporated as part of the polypeptide chain. Alternatively, the liberated thioester-tagged protein can undergo a thioester exchange reaction with the reduced tripeptide and then be incorporated into the polypeptide via a stable amide bond. All three pathways lead to the eventual incorporation of the tripeptide into the larger polypeptide of mTR3. The key to ligating this tripeptide to the larger polypeptide of mTR3 is keeping this tripeptide reduced by using a large excess of thiol in the cleavage buffer. The thiol in

the cleavage buffer functions to effect cleavage of the resin-bound protein and also to keep the tripeptide reduced so that it can ligate to the liberated thioester-tagged protein.

We compared the efficiency of the ligation when the peptide is added directly to a slurry of resin-bound TR and cleavage buffer to that of addition of the peptide to a semipurified, concentrated form of the thioester-tagged TR off-resin. Concentrated thioester-tagged protein was treated with either oxidized peptide or oxidized peptide with 70 mM NMA. After dialysis to remove excess peptide and reagents, the resulting enzymes were assayed for thioredoxin reductase activity. The results are summarized in **Table 5** and clearly show that the efficiency of ligation is much higher when the peptide is added directly to the slurry of resin-bound TR and cleavage buffer. One reason for this decline in efficiency when the ligation is done off-resin is that the lifetime of the thioester-tagged TR may be short in this protein context. Hydrolysis of the thioester would yield the C-terminal carboxylate form of the protein, which is unproductive with respect to ligation. Second, the reduced tripeptide can directly attack the resin-bound TR-intein fusion protein with concomitant ligation. This process should be kinetically faster than when an intermediary thiol attacks first.

In the absence of thiol, the CUG peptide is likely to oxidize to form the intramolecular selenysulfide or dimeric peptides. Either fate will decrease the ligation efficiency. An interesting observation is that the NADPH ligation sample resulted in three fold higher activity than the buffer only ligation. This suggests that the enzyme can reduce the tripeptide to promote ligation. This would not be unexpected as the conserved FAD-associated active site functions to reduce the C-terminal selenysulfide during the catalytic cycle.

Determination of the Mass of Truncated and Semisynthetic TRs.

The mass spectrographs of the truncated and semisynthetic TRs are shown in **Figure 22**. The predicted masses of the truncated and semisynthetic enzymes are 52,857 (carboxylate form) and 53,164 Da, respectively. The experimentally observed masses were 52,787 and 53,144 Da, respectively, and are in good agreement with the expected values. An overlay of the two spectra shows a clear mass increase due to the presence of the ligated peptide. The experimental mass increase of the semisynthetic enzyme is 357 Da, which is very close to the expected mass increase of 329 Da.

Peptide Mass Mapping of Tryptic Fragments.

To unambiguously demonstrate that our peptide had been ligated to the C-terminus of mTR3, we undertook a peptide mass mapping experiment. In this experiment, both the truncated and semisynthetic enzymes were digested with trypsin and analyzed by MALDI-TOF MS and ESI-MS. **Figure 23** shows a peptide with a sequence of SGLEPTVTGCUG found in the ESI-MS experiment, which is at m/z 1169.3 (calculated value of m/z 1169.4). The mass of this peptide corresponds exactly to the mass of the C-terminal peptide containing Sec. Further proof of the identity of this peptide is provided by a MS/MS experiment shown in **Figure 24**. In this experiment, the peptide is fragmented by collision-induced dissociation (CID), and the resulting ions unambiguously identify the sequence of the peptide as the peptide corresponding to the C-terminus. This data in combination with the enzymatic activity data indicate successful semisynthetic production of mTR3. Identification of the C-terminal tryptic fragment

SGLEPTVTGCUG is very difficult using MALDI-TOF. The sequence is very hydrophobic and, as trypsin cut C-terminal to Lys and Arg, is less likely to hold a positive charge. Should this technique be used for future analysis, the protease LysC would be a better choice. LysC will cut C-terminal to Lys only and the sequence preceding our C-terminal Fragment is Lys-Arg. Digesting with LysC would leave the N-terminal Arg and likely improving the ionization using MALDI. Approximately 70% of the total peptides were identified by mass mapping (**Figure 25**). A summary of all of the identified peptides is available in **Figure 26**.

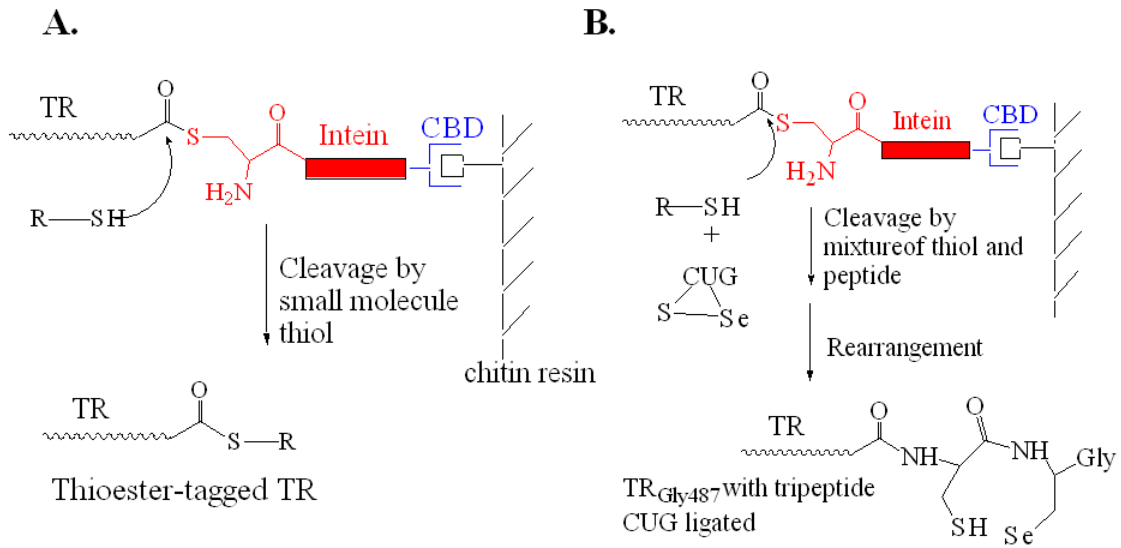


Figure 13. Method for semisynthetic production of mTR3.

Thiol-mediated cleavage of the mTR3-intein fusion construct by addition of exogenous thiol. The junction between mTR3 and the intein exists in equilibrium between amide and thioester forms. Addition of exogenous thiol causes cleavage of the target protein from the thioester form of the fusion protein. (B) Mechanism of incorporation of tripeptide CUG into the mTR3-intein fusion protein. The ligation is achieved by adding oxidized tripeptide to the cleavage buffer containing 70 mM thiol. The excess thiol both reduces the tripeptide and causes cleavage of mTR3 from the intein fusion. The reduced peptide can then attack the thioester-tagged protein and become stably ligated to the protein because of the presence of the N-terminal amino group, which enables rapid rearrangement to the amide form of the protein.

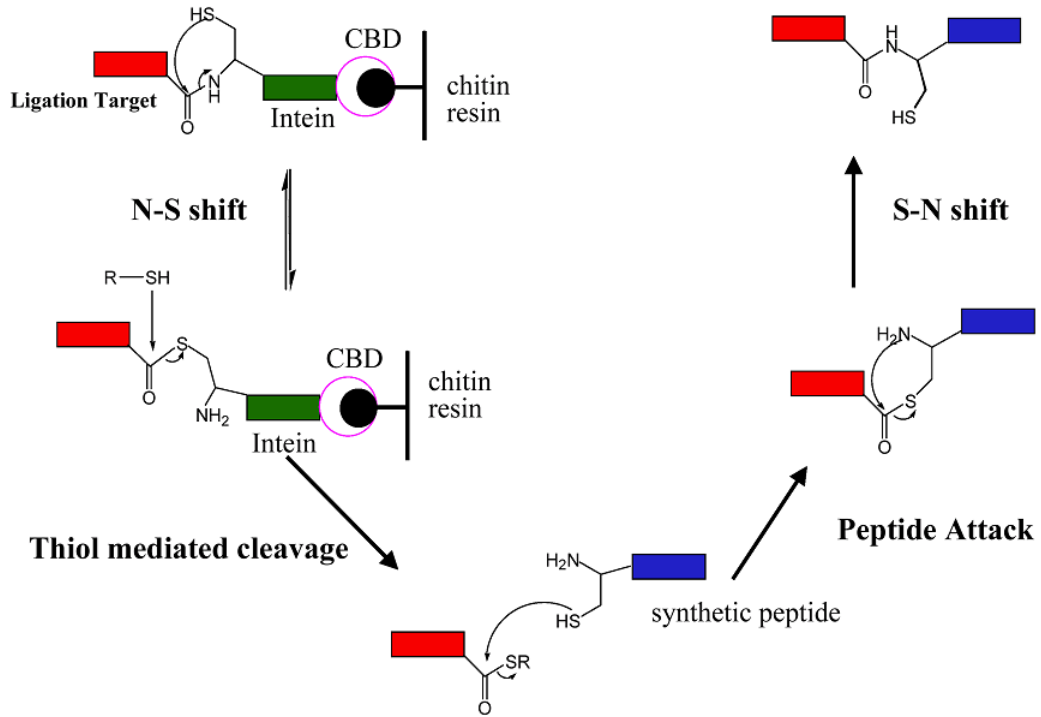


Figure 14. Mechanism of expressed protein ligation.

Example of semisynthesis using expressed protein ligation utilizes a target-intein-chitin binding domain fusion protein. Generation of the thioester at the ligation junction is catalyzed by the N-terminal Cys of the intein. Figure adapted from (135, 139).

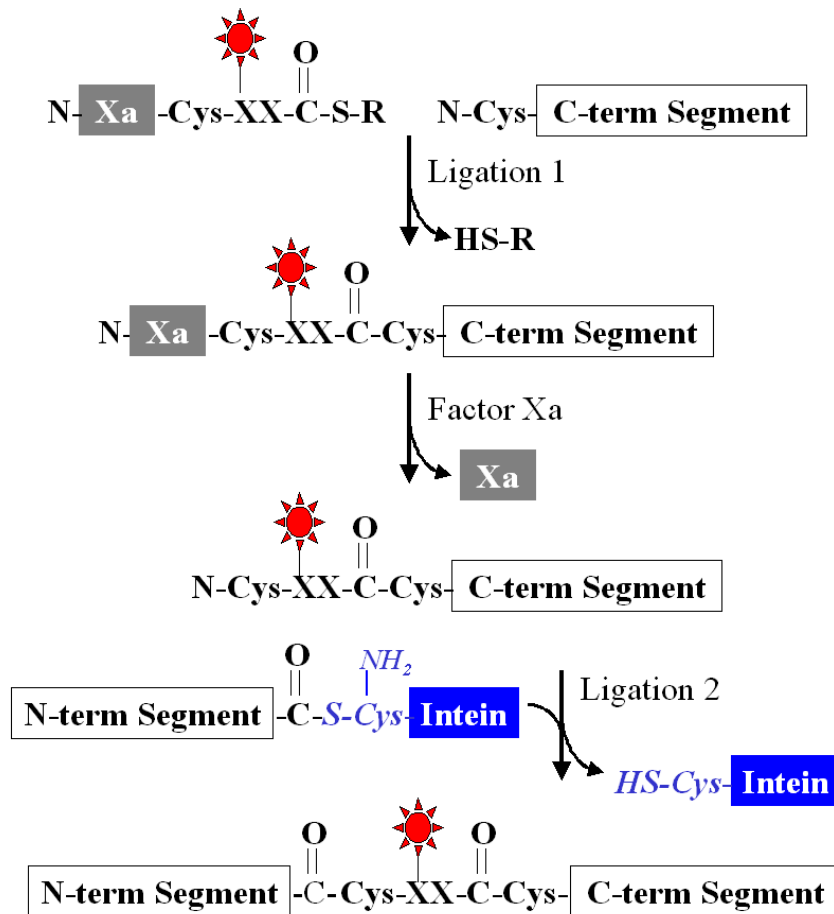


Figure 15. Native chemical ligation and expressed protein ligation.

Example of Semisynthesis using native chemical ligation (Ligation 1) and expressed protein ligation (Ligation 2) to insert a label in between two protein domains adapted from (142). Both protein domains are produced recombinantly, with the N-terminal domain produced as the intein fusion protein. The factor Xa protease cleavage site produces a new N-terminal Cys for Ligation 2

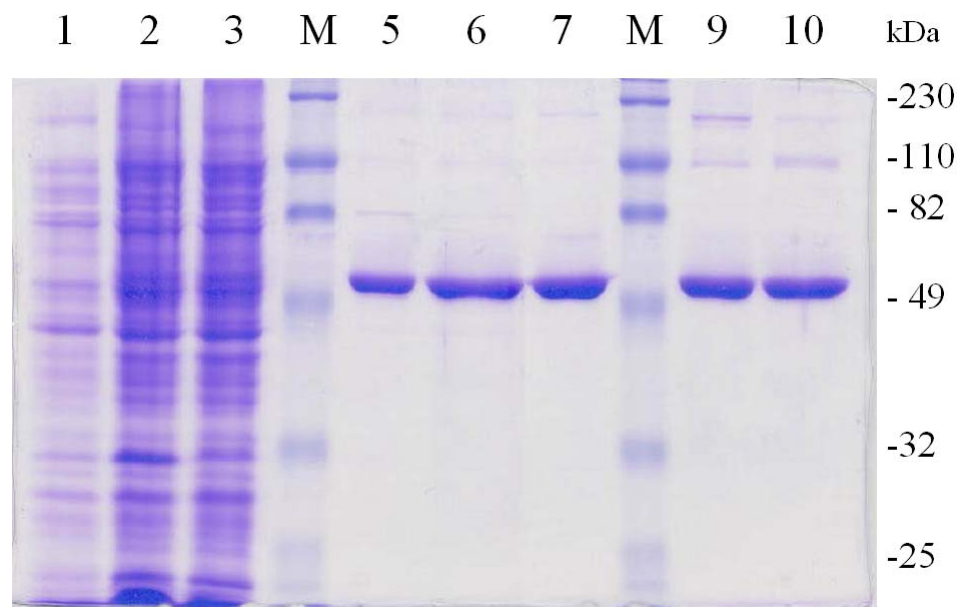


Figure 16. SDS-PAGE of semisynthetic and recombinant mTR3.

SDS (12%)-PAGE characterization of recombinant mouse thioredoxin reductase 3: lane 1, cell culture pre-induction; lane 2, IPTG-induced cell culture; lane 3, supernatant of the cell lysate; lanes 4 and 8, molecular mass markers; lane 5, truncated TR cleaved from the intein on-resin by 2-mercaptoethanol and eluted from the chitin resin; lane 6, truncated TR eluted from the phenyl-Sepharose column; lane 7, truncated TR after elution from the DEAE column; lane 9, purified semisynthetic TR after elution from the DEAE column; and lane 10, purified truncated TR cleaved from the intein on-resin by the amino acid cysteine.

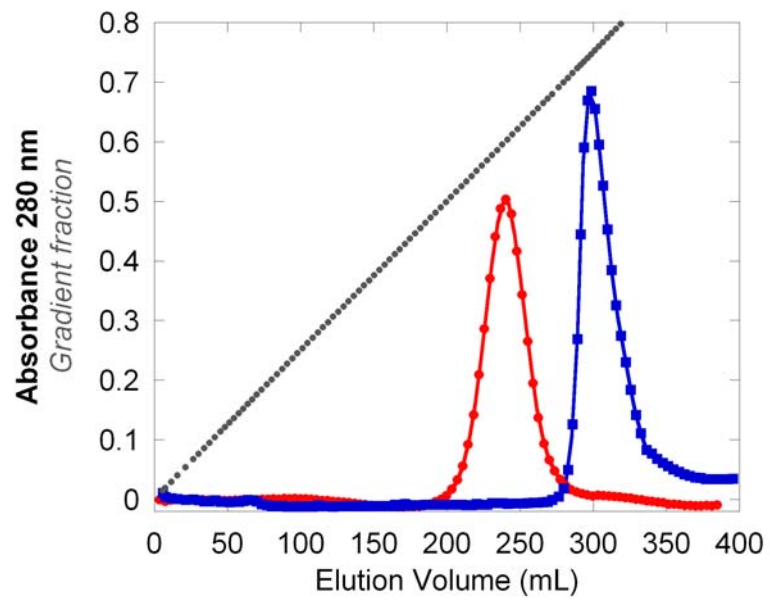


Figure 17. Chromatographic elution profiles for semisynthetic mTR3.

Elution profile of semisynthetic mTR3 from phenyl sepharose (■) and DEAE Sephacel (●). The plot also shows the fraction of the elution gradient (—).

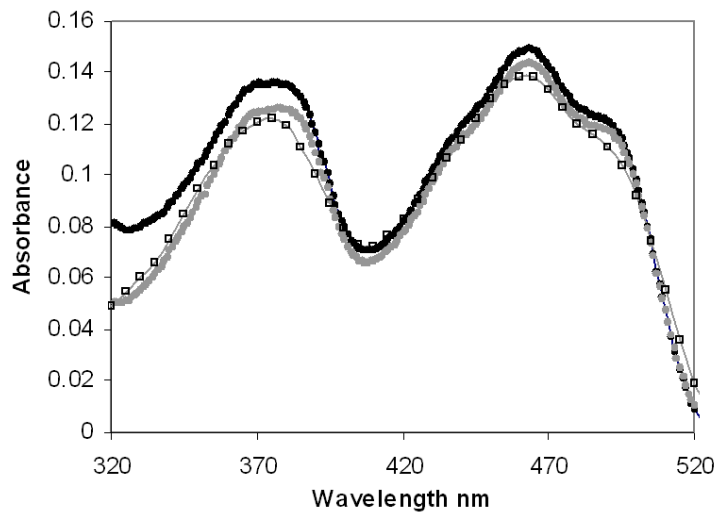


Figure 18. Flavin spectra for semisynthetic and recombinant mTR3.

Absorbance spectra for semisynthetic (●), Sec489Cys mutant (□), and truncated (●) thioredoxin reductase 2 in 50 mM potassium phosphate pH 7.4, 150 mM NaCl, 1 mM EDTA

Table 1. Spectral properties of mTR3.

<u>Enzyme</u>	λ_{\max} nm			λ_{\max} Absorbance Ratio ^a	
	1	2	3	(1) / (2)	(3) / (1)
Semisynthetic	463	376	275	1.04 ± 0.11	8.55 ± 0.91
Sec489Cys	462	375	276	1.00 ± 0.15	8.10 ± 0.22
Truncated	463	377	276	1.11 ± 0.05	8.66 ± 0.65

^aRatios are averages for 3 preparations of the semisynthetic, 3 preparations of the Sec489Cys mutant, and 6 preparations of truncated.

Table 2. DTNB reductase activity of mTR3 semisynthetic and mutant enzymes.

Enzyme	k_{cat} (min^{-1})	K_m (mM)	k_{cat} / K_m ($\text{s}^{-1} \text{M}^{-1}$)
^a TR-Gly487	856 ± 43	2.72 ± 0.43	5.2 x 10 ³
^b TRSec489Cys	794 ± 78	1.75 ± 0.41	7.6 x 10 ³
^c TR-semisynthetic Sec489Cys	908 ± 37	3.08 ± 0.32	4.9 x 10 ³
TR-semisynthetic (63% Se)	1307 ± 102	0.59 ± 0.16	3.7 x 10 ⁴
^d TR-semisynthetic (91% Se)	1251 ± 71	0.46 ± 0.09	4.5 x 10 ⁴

^aThe truncated enzyme ends at Gly487 and is missing the C-terminal tripeptide.

^bThe full-length mutant in which cysteine replaces the catalytic selenocysteine residue and is produce recombinantly.

^cThe full-length mutant in which cysteine replaces the catalytic selenocysteine residue and is produce by semisynthesis.

^dData from optimized procedure using a higher ratio of peptide to protein as described under Methods.

Table 3. DTNB reductase activity reported for homodimeric TR in the literature.

Enzyme	k_{cat} (min^{-1})	K_{m} (mM)
Rat TR1 native (109)	2666	
Rat TR1 native (150)	4000	0.66
Rat TR1 recombinant (151)	1726	0.12
Rat TR1 Sec to Cys mutant (109)	126	
Human TR native (149)	4000	0.08
Human TR truncated (149)	92	4.5
Human TR Sec498Cys (149)	34	0.7
<i>Anopheles gambiae</i> (152)	330 ± 36	0.7 ± 0.2
<i>Plasmodium falciparum</i> (15)	1176	0.21

Table 4. Activity of semisynthetic and mutant mTR3 towards thioredoxin.

Enzyme	k_{cat} (min^{-1})	K_{m} (μM)	$k_{\text{cat}} / K_{\text{m}}$ ($\text{s}^{-1} \text{M}^{-1}$)
^a TR-Gly487	No activity	No activity	NA
^b TRSec489Cys	4.1 ± 0.11	49.1 ± 3.2	1.4×10^3
^c TR-semisynthetic Sec489Cys	4.2 ± 0.24	72.5 ± 8.6	1.0×10^3
TR-semisynthetic (63% Se)	1500 ± 81	35 ± 5	7.1×10^5
^d TR-semisynthetic (91% Se)	2220 ± 78	67.6 ± 6	5.4×10^5
^e rat TR1	3000	35	1.4×10^6

^aThe truncated enzyme ends at Gly487 and is missing the C-terminal tripeptide.

^bThe full-length mutant in which cysteine replaces the catalytic selenocysteine residue and is produce recombinantly.

^cThe full-length mutant in which cysteine replaces the catalytic selenocysteine residue and is produce by semisynthesis.

^dData from optimized procedure using a higher ratio of peptide to protein as described under Methods.

^eTaken from (145, 150), purified from rat liver and assayed using *E. coli* Trx.

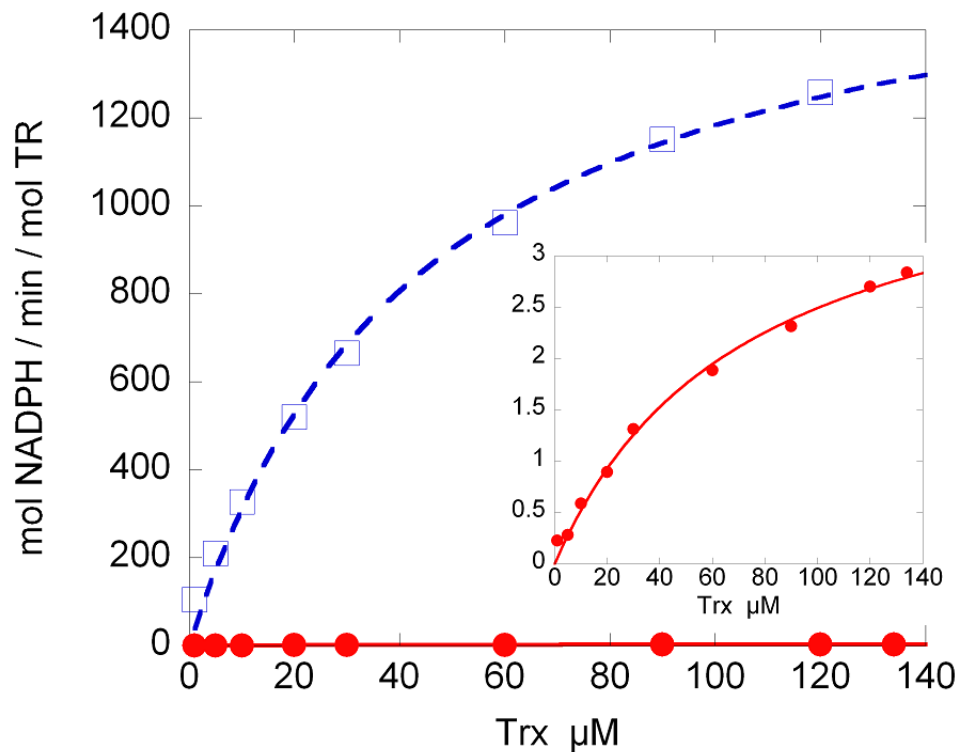


Figure 19. Trx activity plot for semisynthetic mTR3.

Michaelis-Menten plot of V_0/E_T vs thioredoxin concentration for semisynthetic enzyme (\square) and the Sec489Cys mutant (\bullet with insert). Both curves could be fitted to a hyperbolic plot. The semisynthetic data are the average of four replicates per Trx concentration.

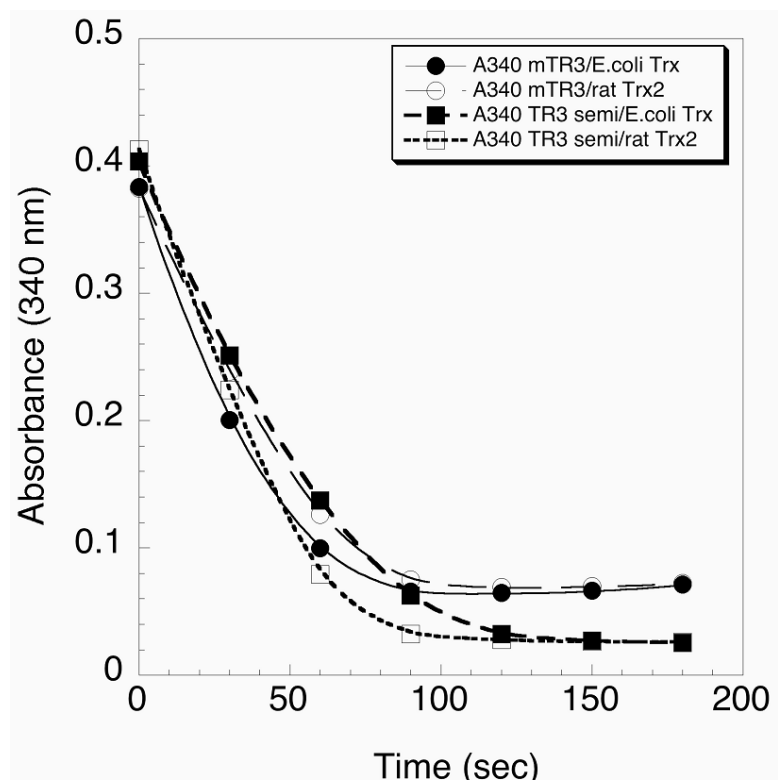


Figure 20. Trx activity of semisynthetic and engineered SECIS produced mTR3.

The activity of the recombinant TR produced in *E. coli* by using an engineered SECIS element (148) is represented by the circles. The activity of the semisynthetic TR is represented by the squares. *E. coli* thioredoxin (closed symbol) and rat thioredoxin-2 (open symbol) were used as substrates.

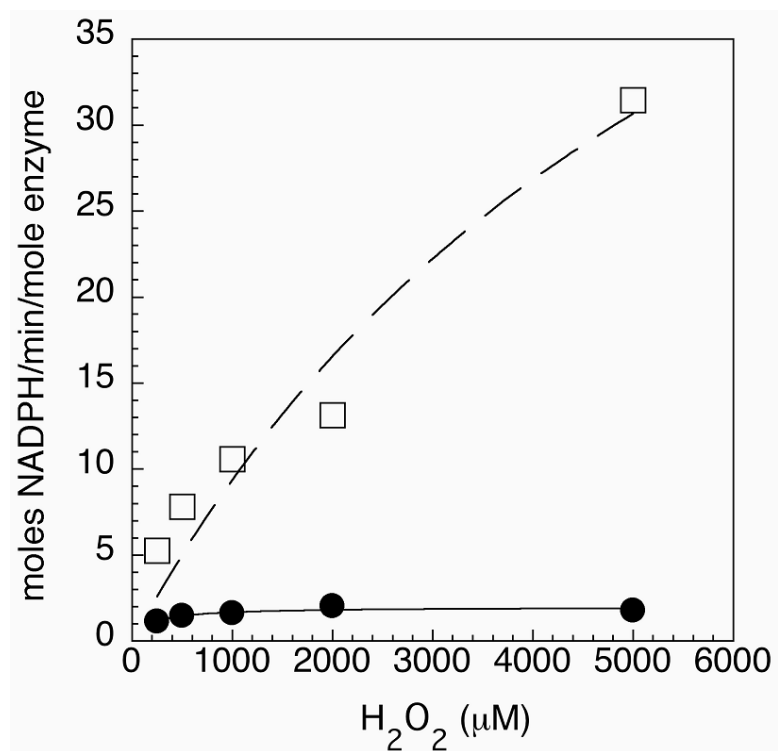


Figure 21. Peroxidase activity plot for semisynthetic mTR3.

Peroxidase activity of semisynthetic enzyme (□) and the Sec489Cys mutant (●). Activity is reported as moles of NADPH oxidized per minute per mole of homodimeric enzyme.

Table 5. Comparison of methods used to construct a semisynthetic TR.

Chitin Resin	Reductant	^a TR concentration in assay [nM]	mol NADPH/min/mol TR
On	NMA	2	1008
Off	NMA	100	48
Off	NADPH	100	27
Off	none	100	8

^aThe enzyme was assayed using 90 μ M thioredoxin as substrate. All other assay conditions were the same as those described in Methods.

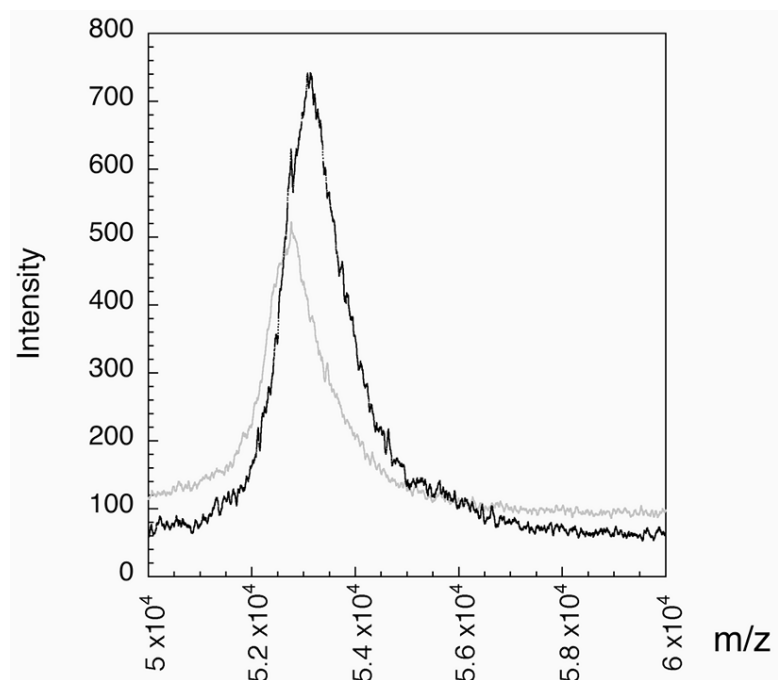


Figure 22. MALDI-MS of semisynthetic and truncated mTR3.

The semisynthetic (theoretical average mass = 53,164) spectrum is in black with an average mass of 53,144, and the truncated (theoretical average mass = 52,857 for carboxylic acid, 52,944 for thioester tagged) spectrum is in light gray with an average mass of 52,787. The difference in mass is clearly observable. The semisynthetic spectrum has a shoulder, which lines up with the peak of the truncated spectrum. The peak width of the semisynthetic enzyme shows that it is a mixture of the two forms.

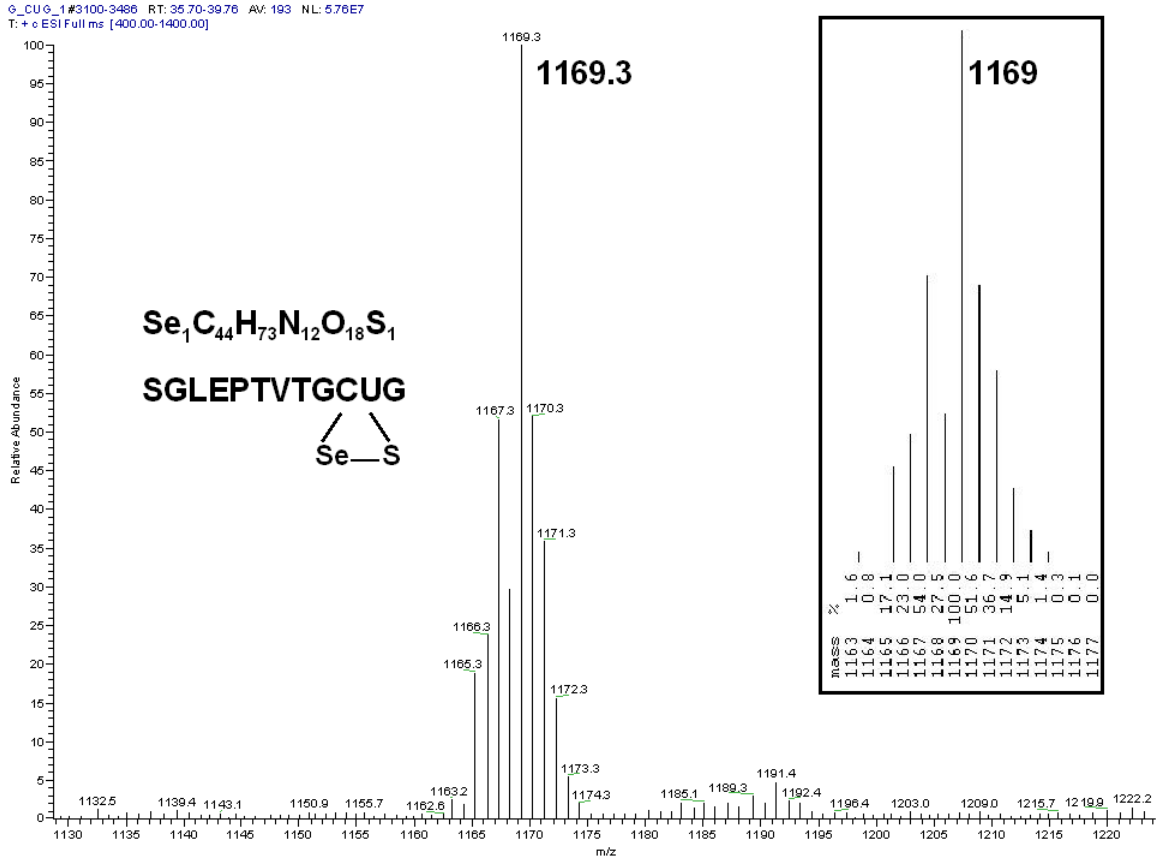


Figure 23. ESI-MS of semisynthetic mTR3 C-terminal tryptic fragment.

ESI-MS of the C-terminal tryptic fragment of mTR3, peptide sequence SGLEPTVTGCUG. The peptide corresponds to the C-terminal peptide of mTR-3 containing the ligated tripeptide CUG. The inset at the right is the predicted isotope pattern for this peptide containing selenium. The mass of the peptide corresponds to the oxidized form as would be expected for a peptide containing selenocysteine.

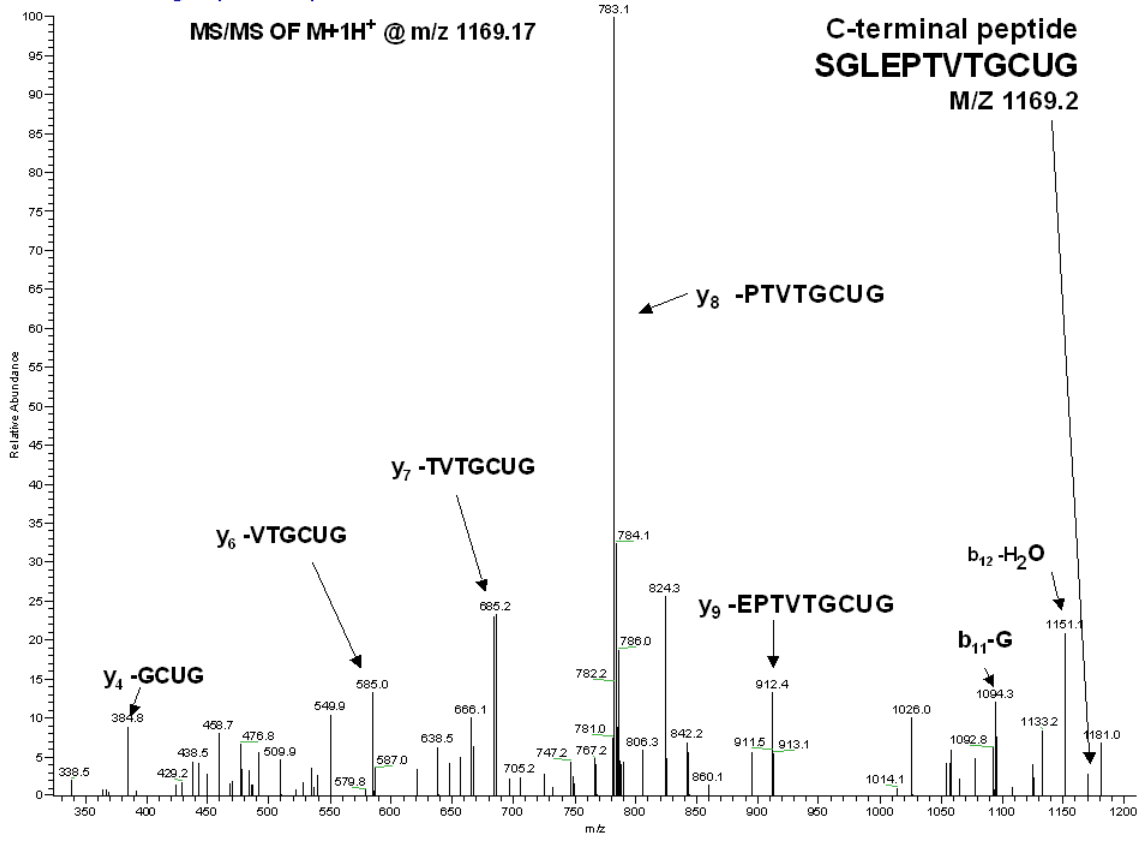


Figure 24. ESI-MS-MS of semisynthetic mTR3 C-terminal tryptic fragment.

ESI-MS-MS of the C-terminal tryptic fragment of mTR3, peptide sequence SGLEPTVTGCUG. The peptide was fragmented by Collision-Induced Dissociation. Ions produced by fragmentation are labeled in the figure with the corresponding peptide sequence.

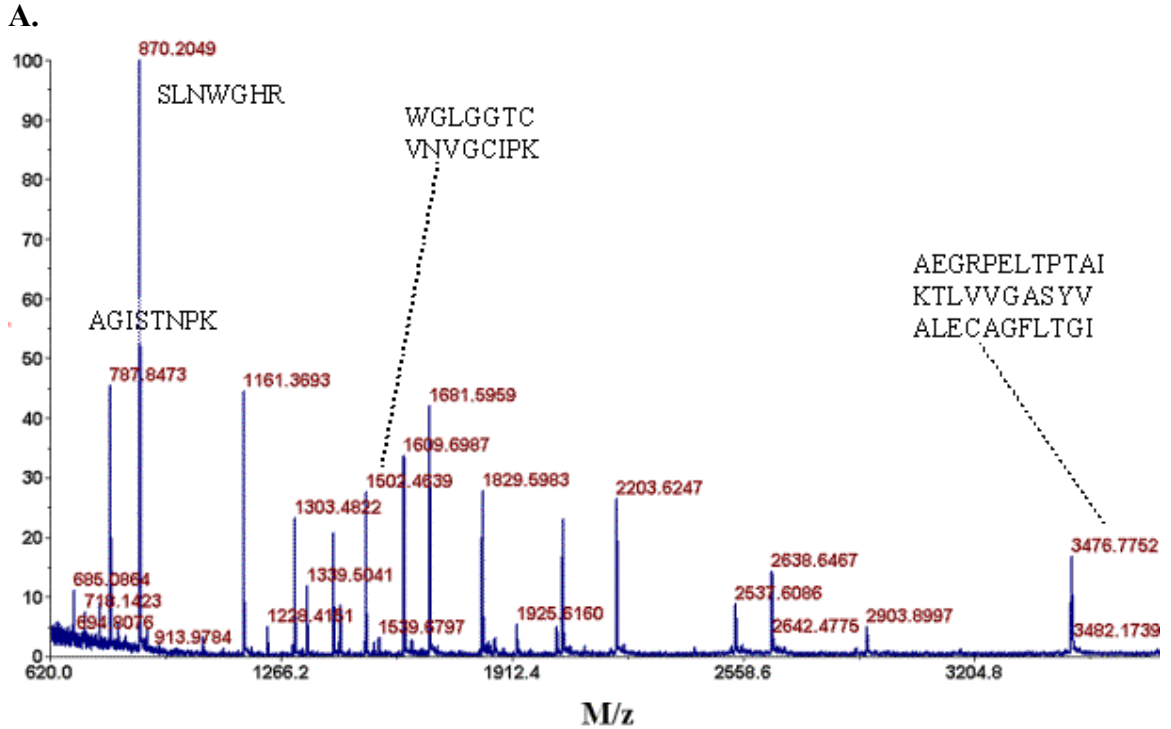


Figure 25. MALDI-TOF of semisynthetic mTR3 digested with trypsin.

(A) MALDI-TOF average mass spectrum for trypsin digest of semisynthetic mTR3. A few peptides are indicated for orientation. (B) Sequence coverage for the trypsin digest of semisynthetic mTR3 using MALDI-TOF (**AA**) with additional fragments identified by ESI-MS (**AA**).

Residues	Thioredoxin Reductase 2	M+H ⁺	Semi-synthetic		Truncated	
		Predicted	MALDI	ESI	MALDI	ESI
353-416	SSTLMDYSNVPTTVFTPLEY GCVGLSEEEAVALHGQEHVE VYHAYYKPLEFTVADRDAQ CYIK	7200.4				
308-340	IIVDAQEATSVPHIYAIGDV AEGRPELTPTAIK	3474.8	3475.0	3476.9	3474.7	3476.9
188-216	TLVVGASYVALECAAGFLTGI GLDTTVMMR	2988.5				
422-449	EPPQLVLGLHFLGPNAGEVT QGFALGIK	2902.6	2902.5	2904.3		2904.3
222-244	GFDQQMSSLVTEHMESHGTQ FLK	2637.2	2637.3	2638.9	2637.1	2638.9
450-473	CGASYAQVMQTVGIHPTCSE EVVK	2537.2	2535.3		2535.1	
76-93	DAHHYGWEVAQPVQHNWK	2202.0	2202.1	2203.3	2201.9	2203.3
1-23	MGGQQSFDLLVIGGGSGGLA CAK	2166.1				
253-270	KLPTNQLQVTWEDHASGK	2052.0	2052.0	2053.2	2051.9	2053.2
143-160	ATLLSAEHIVATGGRPR	1862.1	1862.0	1863.1	1862	1863.1
167-182	GALEYGITSDIFWLK	1827.9	1827.9	1829	1827.8	1829
271-285	EDTGTFDTVLWAIGR	1680.8	1680.8	1681.8	1680.8	1681.8
47-61	WGLGGTCVNVGCIPIK	1503.7	1503.7	1504.8	1501.6	
63-75	LMHQAALLGGMIR	1410.8	1410.7	1411.7	1410.7	1411.8
32-43	VAVADYVEPSPR	1302.7	1302.6	1303.4	1302.6	1303.4
94-104	TMAEAVQNHVK	1227.6	1227.6	1228.4	1227.5	1228.4
480-491	SGLEPTVTGCUG (full length)	1169.4		1169.3		
126-135	ASFVDEHTVR	1160.6	1160.5	1161.2	1160.5	1161.2
479-488	RSGLEPTVTG (truncated)	1016.5				1017.1
105-111	SLNWGHR	869.4	869.3	869.9	869.3	869.9
480-488	SGLEPTVTG (truncated)	860.4				860.3
245-252	GCVPSHIK	840.4	840.4	841.0		
297-304	AGISTNPK	787.4	787.1	787.9		
112-117	VQLQDR	758.4	758.3		758.3	
161-166	YPTQVK	735.4	735.3	735.8	735.3	
291-296	TLNLEK	717.4		717.8		717.8
24-30	EAAQLGK	716.4				
121-125	YFNIK	684.4	684.2	684.8	684.3	
417-421	MVCMR	639.3	639.2		639.2	
286-290	VPETR	601.3				
344-348	LLAQR	600.4				
474-478	LHISK	597.4		597.7	597.3	
217-221	SIPLR	585.4	585.3		585.3	

Figure 26. Mass spectrometry peptide mapping for trypsin digests of mTR3.

CHAPTER 3.

STRUCTURE-FUNCTION STUDIES OF THE C-TERMINAL TETRAPEPTIDE MOTIF OF THIOREDOXIN REDUCTASE USING SEMISYNTHESIS

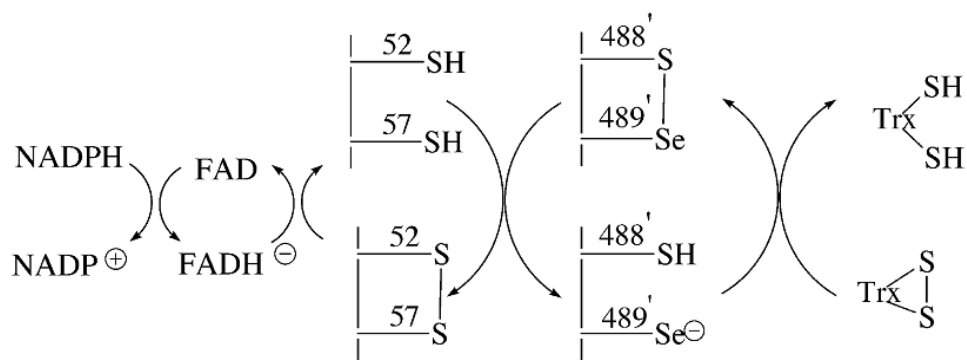


Figure 27. The pathway for transfer of electrons to Trx by mTR3.

The catalytic cycle for mammalian thioredoxin reductase. This Chapter investigates structural details of the C-terminal vicinal selenylsulfide between Cys488' and Cys489'.

Biochemistry 2007, Submitted

Investigation of the C-terminal Redox Center of High M_r Thioredoxin Reductase by Protein Engineering and Semisynthesis [†]

Brian E. Eckenroth[‡], Katharine M. Harris[‡], Brian M. Lacey[‡], Adam P. Lothrop[‡], and Robert J. Hondal^{*‡}

[‡]Department of Biochemistry, 89 Beaumont Ave, Given Laboratory, Room B413, Burlington, VT 05405

[†]These studies were supported by National Institutes of Health Grants GM070742 to RJH.

*To whom correspondence should be addressed. Department of Biochemistry, University of Vermont, College of Medicine. 89 Beaumont Ave, Given Laboratory, Room B413, Burlington, VT 05405. Tel: 802-656-8282. FAX: 802-862-8339. E-mail: Robert.Hondal@uvm.edu.

In the study presented here, we have used semisynthetic production of mouse mitochondrial thioredoxin reductase (mTR3) to investigate the enzymatic dependence on the C-terminal structure of the Sec-containing TR compared to the Cys-containing TR from *Drosophila melanogaster* (DmTR). These enzymes can be divided chemically: those containing Sec and those containing Cys, and they can also be divided structurally: those whose active site contains a vicinal disulfide and that which does not, *Plasmodium falciparum* (PfTR). Here we have investigated two forms of the vicinal disulfide group. The vicinal disulfide forms an eight-membered ring that must be a) opened by the FAD associated dithiol and b) closed after reduction of the substrate thioredoxin (Trx). Each of the steps in the catalytic will have structural implications in two forms. Firstly is the inherent energy strain of the ring. For each intervening residue the size of the ring increases by three atoms and likely reducing the strain. The second is proper orientation of the catalytic residues involved in each step. The results show that insertion of Ala residues between the cysteines in DmTR results 100 fold or greater decrease in Trx activity whereas the equivalent insertions between the Cys and Sec residues of mTR3 results in only a 4 fold decrease.

We have also investigated the role of the C-terminal carboxylate charge. In the structure of rat TR1 (36) it was suggested that the conserved position, Lys29, would form a salt bridge with the C-terminal carboxylate to correctly position the C-terminus for thiol-disulfide exchange with the N-terminal active site. A similar role was suggested for Arg351 from a TR-Trx complex modeling study (100). In neither case is biochemical evidence provided. As either Lys29 or Arg351 could serve different functions, simple

mutagenesis would be unable to distinguish a specific interaction. Therefore, we have used semisynthesis to modify the C-terminal carboxylate to a neutral carboxamide. This mutant shows a significant increase in catalytic activity indicating that the proposed salt bridge is likely not involved in catalysis.

Finally, we have investigated the dependence on the relative position of Sec in the Cys-Sec dyad for mTR3. We have produced the mutant Gly-Sec-Cys-Gly (GUCG) that shows poor activity similar to Sec489Cys. This indicates the Sec incorporation is for a specific function and that the residue must be the C-terminal moiety of the dyad. This relates directly to the results for the Ala insertion mutants and suggests that the role of Sec is not in nucleophilic attack on Trx but possibly as the leaving group during thiol-disulfide exchange with the N-terminal active site.

METHODS

Peptide Synthesis.

Selenocysteine containing peptides were produced by Fmoc solid phase synthesis as previously described (143). Peptide were purified by preparative HPLC from the Shimadzu Corporation (Kyoto, Japan) and verified by Matrix Assisted Laser Desorption Time of Flight Mass Spectrometry on a Voyager DE PRO Workstation from Applied Biosystems (Framingham, MA). Synthesis of the CUG peptide with C-terminal carboxamide utilized a similar protocol with the exception of substitution of Fmoc-PAL

resin from PE Biosystems (Hamburg, Germany) to yield the carboxamide upon cleavage from the resin.

Cloning and Expression of mTR3.

The expression, purification and semisynthesis for mutants in this section are as described in the previous chapter. An additional mutant of mTR3 with the C-terminal sequence of Ser-Cys-Cys-Ser (SCCS) was produced by mutagenesis (via PCR amplification). Reaction conditions and methods were as described for the GCCG mutant in Chapter 2. To help the reader distinguish the mTR3 mutants from the *DmTR* mutants in this study, the abbreviation mTR3 will precede the C-terminal sequence (mTR3-GCUG for example).

Cloning and Expression of DmTR.

The *Drosophila melanogaster* TR clone (accession number AF301144), was a generous gift from Stephan Gromer. For production of *DmTR* in *E. coli*, we subcloned the coding region of *DmTR* (via PCR amplification) into plasmid pTYB1 of the Impact System from New England Biolabs, to generate the TR-intein-fusion protein. Primers were purchased from Integrated DNA Technologies Inc. (Coralville, IA). Primers were designed for production of the full length TR containing the C-terminal tetrapeptide Ser-Cys-Cys-Ser (SCCS⁴⁸⁸⁻⁴⁹¹), a truncated TR, removing the C-terminal tripeptide CCS⁴⁸⁹⁻⁴⁹¹, the full-length mutants Ser-Cys-Ala-Cys-Ser (SCACS⁴⁸⁸⁻⁴⁹²) and Ser-Cys-Ala-Ala-Cys-Ser (SCAACS⁴⁸⁸⁻⁴⁹³).

The PCR reaction mixtures contained 100 pg template DNA, 50 pmol of each primer, 2 units of Vent DNA Polymerase, 2-3 mM magnesium chloride, in a volume of 100 μ L. Each PCR was performed on a GeneAmp PCR System 2400 from Perkin Elmer Life Sciences, Inc. (Boston, MA) using 25 cycles with the following parameters: 96 $^{\circ}$ C for 45 sec, 50 $^{\circ}$ C for 30 sec, and 72 $^{\circ}$ C for 180 sec. The product was analyzed by analytical agarose gel electrophoresis and then purified using the QIAquick Purification Kit from Qiagen (Valencia, CA). The PCR product and plasmid pTYB1 were each incubated with Kpn I and Nde I for 2 h at 37 $^{\circ}$ C, purified using the QIAquick kit, then ligated at 16 $^{\circ}$ C for 16 h using T4 DNA ligase at 37 $^{\circ}$ C. To enhance the amount of positive clones, the ligation was digested Sal I, a unique restriction site removed upon product insertion. *E. coli* DH5 α cells were made competent via the Inoue method (153) and then transformed with 50 ng of purified DNA. The culture was plated onto LB agar containing 200 μ g/mL ampicillin and incubated at 37 $^{\circ}$ C. Individual colonies were used to inoculate 100 mL of LB containing 200 μ g/mL ampicillin and allowed to shake at 37 $^{\circ}$ C overnight. Plasmids were purified using the QIAfilter Plasmid Prep Midi from Qiagen, screened by 1% analytical agarose gel electrophoresis, and verified by sequencing at the University of Vermont DNA Sequencing Facility using an ABI 3100-Avant Genetic Analyzer.

Production of C-terminal Mutants of DmTR.

Each of the TR mutants from *Drosophila* are expressed as the TR-intein-chitin binding domain fusion protein and are affinity purified from chitin agarose as described for the mTR3 (Chapter 2). *Escherichia coli* ER2566 cells were used for production of

recombinant wild-type (WT) and mutant *DmTR*. The cells were transformed with 50 ng of plasmid, plated on LB-ampicillin plates containing 200 µg/mL ampicillin, and incubated at 37 °C overnight. A single colony was used to grow a 100 mL inoculum culture of LB (200 µg/mL ampicillin). This culture was incubated overnight at 37 °C with shaking. Ten milliliters of inoculum culture was added to a 1 L baffled Pyrex Fernbach flask containing TB media at pH 7.0 containing 200 µg/mL ampicillin. The cells were incubated at 37 °C with shaking (100 rpm) until the O.D. 600 nm reached 1.0. The cells were then chilled on ice until the temperature decreases to 20 °C and induced by adding IPTG to a final concentration of 0.5 mM followed by incubation at 20 °C overnight with shaking (100 rpm). The cells were harvested by centrifugation in a Beckman J21B centrifuge (JA-14 rotor) at 7000 X g at 4 °C for 10 min and then stored at -20 °C. Cells are thawed on ice and homogenized in MOPS buffer, and lysed by sonication with a Branson 350 Sonifier (Danbury, CT). The wild type enzyme, C-terminal sequence SCCS, as well as the C-terminal sequence mutants SCACS and SCAACS were released from the intein by the addition of NMA.

Thioredoxin Activity pH Optima.

Activity towards Trx was tested as a function of pH for each construct. Due to the insolubility of insulin below pH 7.0, each assay utilized 500 µM Trx, which is approximately ten times greater than the calculated K_m . To avoid differences in ionic strength, each assay contained buffer with a final concentration of 30 mM citrate/ 30 mM Tris/ 30 mM phosphate adjusted from pH 5.5 to 9.5 with the exception of the GUUG mutant which required the profile to be extended to pH 10.5. The concentration of TR in

the assay was that which was used for the Trx Michaelis-Menten profile: 2nM for wild type mTR3 and 25 nM for wild type *DmTR*. The concentration for each mutant was adjusted to get signal similar to that of the respective wild type. Each assay contained 0.15 mM NADPH and 1 mM EDTA. The activity was measured at 340nm and background corrected. The data in duplicate were normalized to the percent of maximal activity for each given mutant and plotted as Activity % vs. pH.

RESULTS AND DISCUSSION

Production of TR.

The expression and purification methods for *DmTR* are identical to mTR3 with the exception of expression in pTYB1 rather than pTYB3. The reason for this is due to the presence of Nco I and Sap I restriction sites within the *DmTR* sequence. The background digest to increase the number of positive clones was performed with Sal I as there is also a Hind III restriction site in the *DmTR* coding sequence. The expression of *DmTR* was significantly increased in TB media versus LB media. Initial production of the truncated form of *DmTR* yielded approximately 20 mg per 6L of cell culture in LB media. This was also the case for mTR3 in the previous chapter. Expression in TB media yielded 20-30 mg per 1L of media for *DmTR*. Improvement was also shown for mTR3, though not to the same degree (35 mg per 6L culture). Subsequently, the mutants produced for this study were produced in TB media as described in the methods section of this chapter.

A representative SDS-PAGE for expression and chitin cleavage for the wild type *DmTR* can be seen in **Figure 28**. Excellent solubility of the fusion protein is demonstrated by comparison of the lysate supernatant (lane 13) and the lysate pellet (lane 12). For each of the cleavage reagent cocktails, the eluant and chitin retained samples respectively are shown. The cleavage from the intein was significantly slower than observed for truncated mTR3 as can be seen by the fusion protein band still remaining on the resin after a 24-hour incubation with cleavage reagent. Like mTR3, very little elution is observed with buffer not containing a cleavage reagent (lane 9). This experiment yielded 127 mg from 6L of cell culture (21 mg/L), with a significant amount still retained on the resin. Estimation from the SDS-PAGE and NaOH strip of the chitin resin indicates only about 50-70 % is cleaved from the intein. Cleavage of *DmTR* from the intein was also tested from pH 7.5 to 8.5 using NMA with similar results. Yield was only slightly improved by sequential rounds of incubation with fresh cleavage reagent. This indicates that a significant amount of *DmTR* remains as the fusion protein.

The truncated form of *DmTR* shows incomplete cleavage from the intein though yield in this step is not an issue due to the high level expression for *DmTR*. Poor cleavage from the intein was seen with the mTR3-SCCS mutant where the majority of the fusion protein was retained on the resin. The yield for this mutant was only 2.6 mg for 6L of cell culture. This is less than 10 % of a typical yield for mTR3. These results indicate that a Ser residue at the intein cleavage junction is partly inhibitory for our system.

Activity of mTR3 Towards Thioredoxin.

Sufficient activity towards the natural substrate Trx has been shown to be dependent on the incorporation of selenocysteine as the penultimate residue in mammalian thioredoxin reductase. During the TR catalytic cycle the conserved cysteine position is expected to form a disulfide intermediate with Cys52 and the Sec489' being the leaving group. Upon resolution of this disulfide and release of the C-terminus in its reduced form, the Sec residue is then the attacking nucleophile to form a mixed selenylsulfide with the substrate Trx. The re-oxidation of the C-terminus occurs by attack on the mixed selenylsulfide by the resolving cysteine, Cys488', of mTR3 with subsequent release of reduced Trx. As shown in **Table 6**, sequence containing the C-terminal carboxamide was considerably more active (3010 min^{-1}) than the naturally occurring carboxylic acid (2220 min^{-1}). The mTR3-GUCG shows similar activity to the Sec489Cys mutant, 8.3 and 4.1 min^{-1} respectively, while the mTR3-GUUG mutant was even less active. As indicated by the % peptide incorporation, the ligation reaction is less efficient with Sec as the residue attacking the thioester. However, even with correction for the incorporation, the GUCG and GUUG mutants would still have poor activity compared to wild type. Mutation to the SCCS motif of *DmTR* shows similar activity to that of the Sec489Cys mutant. Similar results for the human homologue of TR have recently been reported (154). Interestingly, the insertion mutants mTR3-GCAUG and mTR3-GCAAUG show ~25 % of the wild-type activity.

The TR activity was also evaluated as a function of pH. Both the leaving group and nucleophilic effects of the conserved selenocysteine position would be expected to

contribute to the observed activity dependence on pH. The optimal pH for activity towards Trx was determined for each of the TR mutants from pH 5.5 to 9.5 with the exception of the mTR3-GUUG mutant, which required pH 10.0 to reach maximal activity, **Figure 29**. Both the wild type carboxylic acid and carboxamide achieve optimal activity at a similar pH, approximately 7.0 to 7.2, whereas the Sec489Cys mutant has a pH optimum between pH 8.0 and 8.5. This is as would be expected due to the pK_a of 5.3 for selenocysteine and the pK_a of 8.2 for cysteine where at physiological pH the cyteine is expected to be protonated and therefore less nucleophilic than the selenol.

This is not the observation for the mTR3-GUCG mutant where the interchange position and the resolving position have been reversed. For this mutant, there is only a modest alkaline shift in pH optima to which is still 0.5 units lower than the Sec489Cys mutant **Figure 29**. This mutant has a similar k_{cat} for Trx as the Sec489Cys at pH 7.0. The pH optima measured during the steady state is likely to include a contribution from the resolving position of TR. In the wild-type enzyme with high activity, the low pK_a of the selenol is expected to dominate the reaction profile. In the mutants with lower activity, however, we begin to see the impact of the resolving position. This may explain the lower pH optima for the mTR3-GUCG mutant where the selenocysteine is in the resolving position.

The insertion mutants mTR3-GCAUG and mTR3-GCAAUG have activity towards Trx that is 25 % of wild type and is 100 fold higher than the mTR3-GUCG and mTR3-GCCG mutants yet the pH optima is near 8.0. In these insertion mutants, the relative position of the Sec has been retained. If the Sec position were responsible for interchange with the N-terminal active site, one would expect poor activity for the Ala

insertion mutants. Therefore the insertion is expected to impact: 1) the strain on the ring formed when in the C-terminus exists in the oxidized state and; 2) the potential distance the TR resolving cysteine would be from the mixed selenylsulfide between Sec489' and Cys32 of Trx. It would be expected that both of these difference would affect the rate but a shift in the pH optima higher than that of the mTR3-GUCG mutant is unexpected.

Low Activity TR Trx Assays and Consumption of NADPH.

The proposed general mechanism of a high M_r TR was discussed in Chapter 1 (**Figure 10**) in terms of individual steps. These steps are an extrapolation of the mechanistic investigations of GR where each type of enzyme has two distinct cycles; the reductive half reaction where NADPH is consumed to reduce the enzyme and the oxidative half reaction where the enzyme is re-oxidized by consumption of the cognate substrate GSSG or Trx. GR converts between the oxidized form (E_{ox}) and the 2-electron reduced form (EH_2) to complete both cycles, with consumption of 1 equivalent of NADPH. The addition of the C-terminal active site for TR requires an additional equivalent of NADPH (EH_4) to be consumed before Trx can be reduced. Fully reduced GR (EH_4) or TR (EH_6) form extremely slowly. This means that TR in the steady state will cycle between EH_2 and EH_4 . Therefore, TR mutants that have poor activity towards Trx could still consume 1-2 equivalents of NADPH per subunit in the pre-steady state. And this is what we typically observe in the Trx assay.

Enzymes that have the lowest activity towards Trx require 1-2 μM enzyme in the assay. When performing these assays, it was observed that there was a significant change in absorbance at 340 nm after addition of mutant TR to the cuvette (~5 seconds). This is

due to the high TR concentration resulting in a visible consumption of NADPH at the start of the assay followed by the slow decrease in absorbance during the assay even in the absence of Trx. While this analysis is at best semi-quantitative compared to the established stopped-flow method developed by Arscott, Ballou, and Williams (78, 93), it does provide support in addition to the DTNB reductase activity that the low activity mutants produced are functional enzymes.

Activity for DmTR Towards Thioredoxin.

The Trx activity of the mutants produced for *DmTR* can be seen in **Table 7**. Residue insertions between the Cys residues for *DmTR* results in a loss of activity that is much greater than that observed for mTR3. Both mutants show poor activity towards Trx with a 142 fold and 328 fold decrease from wild type respectively. Nearly identical results are observed for mitochondrial TR from *Caenorhabditis elegans* (*CeTR2*) where Ala insertions result in >100 fold loss in activity (Brian M. Lacey, personal communication). This is in stark contrast to the equivalent mutations for mTR3 which still retain ~20 % of the wild type activity. The only difference is the Sec residue for mTR3.

Modifications of the C-terminal carboxylate of *DmTR* show a gain in activity similar to that of mTR3 (Adam P. Lothrop, personal communication). These modifications are produced by cleavage from the intein using reagents other than thiol. The neutral hydroxamic acid produced by cleavage with hydroxylamine shows a 70 % increase in activity, which is in agreement with that observed for the mTR3 carboxamide mutant. The thiocarboxylate produced by cleavage with ammonium sulfide also shows

this increase in activity along with a 3 fold decrease in K_m . The pH optima for the wild type enzyme is ~ 8.0 with no change observed with either of the carboxyl variants. An alkaline shift is observed for the Ala insertions mutants (**Figure 30**) as it is for the equivalent mutants from *Ce*TR2. These trends are identical to that observed for mTR3.

Comparison of DTNB Reductase Activities.

The small molecule disulfide DTNB has long since been used for quantification of free thiols in proteins (155) as well as to evaluate thiol-disulfide exchange reactions (156), as is the process catalyzed by TR. The DTNB can therefore be a substrate for the C-terminal selenylsulfide (or disulfide) and the N-terminal disulfide as discussed in the previous chapter. Each TR in this study displays significant DTNB reductase activity. We also observe product inhibition with very high concentrations of DTNB near 5-10 times K_m . In both mTR3 and *Dm*TR, the presence of the C-terminus imparts an increase in DTNB reductase catalytic efficiency (k_{cat}/K_m) compared to the truncated forms of TR. This is consistent with that observed for *Dm*TR (78) as well as *Pf*TR (55).

For our truncated form of the mTR3 (**Table 8**), we observe a k_{cat} of $856 \pm 43 \text{ min}^{-1}$ whereas the semisynthetic wild-type enzyme has a k_{cat} of $1251 \pm 71 \text{ min}^{-1}$. The increase in k_{cat} for the wild type represents the activity of the selenylsulfide relative to the N-terminal disulfide towards DTNB. The truncated enzyme also exhibits a 6-fold increase in K_m compared to wild type. This increase in K_m is also seen in full length Sec489cys mutant as well as the semisynthetic mTR3-GUCG and mTR3-GUUG forms. The semisynthetic variants mTR3-GCAUG and mTR3-GCAAUG do not display a significant difference in k_{cat} compared to the truncated yet have K_m values similar to that of the wild

type. The DTNB reductase data can therefore be divided into three groups on the basis of catalytic efficiencies (k_{cat}/K_m) that correlate to Trx activities. The mutants with poor Trx activity have the lowest DTNB efficiency and are similar to truncated mTR3. This is attributed to the increase in K_m , as has been reported for mutants of *DmTR* (78) and *PfTR* (55). The mTR3 low efficiency group ($5000\text{-}20,000\text{ s}^{-1}\text{ M}^{-1}$) includes the truncated, SCCS, GCCG, GUCG, and GUUG mutants. The wild-type efficiency group ($\sim 5 \times 10^4\text{ s}^{-1}\text{ M}^{-1}$) includes both Ala insertion mutants where the single Ala shows an increase in efficiency while the double Ala shows a decrease. The C-terminal carboxamide mutant is distinguished as a high efficiency group at 10^5 . This is >10 fold higher than the wild-type group when the 28 % lower selenium content of this mutant is taken into consideration.

The non-selenium containing *DmTR* also show excellent activity towards DTNB with results that very similar to the mTR3. The respective wild type enzyme has a k_{cat} of 178 min^{-1} for truncated *DmTR* (**Table 9**), and 157 min^{-1} for the wild type. This is ~12 % the activity seen in the wild-type mTR3. The *DmTR* also shows the decrease with the double Ala insertion seen with the mTR3. There are much smaller differences in both k_{cat} and k_{cat}/K_m for *DmTR*. For mTR3 there is a 10 fold increase in k_{cat}/K_m while it is only 3 fold for *DmTR*. The k_{cat}/K_m for *DmTR* fall into the low efficiency group for mTR3. The C-terminal hydroxamic acid of *DmTR* shows a significant increase in efficiency (2.3 fold). The thiocarboxylate does show an increase in activity but has identical efficiency when compared to wild type. These results are in agreement with what is observed in the mTR carboxamide mutant where neutralization of the negative charge at the C-terminus results in an increase in catalytic efficiency.

Peroxidase Activity of Semisynthetic mTR3.

Peroxidase activity is characteristic of the selenium incorporation in mammalian TR. Like DTNB, it also has been reported to have a low millimolar K_m and is likely not a physiologically relevant activity for the enzyme. Peroxidase activity plots for thioredoxin reductase previously reported show poor saturation, but have been limited to concentrations less than 5 mM (109, 157). In performing this study, we have expanded the profile to 70 mM peroxide. The results demonstrate poor saturation for wild type carboxylic acid and carboxamide forms, **Figure 31A**, as well as the Sec489Cys mutant. We previously reported an activity of $71 \pm 7 \text{ min}^{-1}$ with a K_m of $6.6 \pm 0.5 \text{ mM}$ when limiting the analysis to substrate concentrations equivalent to that reported in the literature (5 mM). After repeated extended analysis of the wild type carboxylic acid enzyme we observe an activity of $1753 \pm 257 \text{ min}^{-1}$ with a K_m of $259 \pm 33 \text{ mM}$ using 50 nM enzyme while the carboxamide has an activity of $3204 \pm 351 \text{ min}^{-1}$ with a K_m of $167 \pm 17 \text{ mM}$ using 20 nM enzyme. A result of this is the extremely low k_{cat}/K_m which are >100 fold lower than DTNB (**Table 10**).

As shown in **Figure 31B**, the profiles of the mTR3-GCAUG, mTR3-GCAAUG, and mTR3-GUCG mutants display a different property, however. The mTR3-GUCG required 500 nM enzyme and shows only about 10-15 % of the activity of the mTR3-GCAUG and mTR3-GCAAUG yet each of these three mutants shows saturation with estimated K_m values of 14 mM, 6.8 mM, and 9.5 mM respectively. These values are in better agreement with previous estimations. The interpretation of this data is that, while the wild type enzyme displays significant peroxidase activity, a definitive estimation of

kinetic parameters is not applicable, as it does not represent a reasonable binding event. We have, however, produced three mutants with mM K_m values are more indicative of a potential binding event. A complete summary of the data is shown in **Table 10**.

We also tested the impact of the concentration of the co-substrate NADPH on the saturation profile. **Figure 32A** shows the wild-type enzyme while **Figure 32B** shows the mTR3-GCAUG mutant. With each enzyme the saturation curve remains the same from 25 μ M to 500 μ M NADPH. In each case, progress curves remained linear over the 2-minute time frame of the assay with the exception of the 25 μ M NADPH at the 70 mM peroxide concentration where linearity was maintained to 90 seconds due to eventual depletion of NADPH. A characteristic of the DTNB assay is the observation of product inhibition at very high concentrations of substrate. This effect is not observed with H₂O₂ as substrate.

Interpretation of Structure-Function Study.

We have determined that the Cys containing enzymes are far more dependent on vicinal residues to reduce the natural substrate Trx than the Sec containing enzyme from mouse. The mTR3 mutant GCAUG retains 16 % k_{cat} while the GCAAUG mutant has 22 % k_{cat} when compared to the wild type sequence GCUG. This is in stark contrast to that which is observed for *Dm*TR and *Ce*TR2. The SCACS mutant for *Dm*TR shows a 142 fold reduction in k_{cat} while the GCACG mutant for *Ce*TR2 shows a 145 fold reduction in k_{cat} . For the double insertion, the SCAACS mutant for *Dm*TR shows a 328 fold reduction in k_{cat} while the GCACG mutant for *Ce*TR2 shows a 90 fold reduction in k_{cat} .

Insertion of each Ala is expected to progressively reduce the ring strain. In a strictly chemical sense, the larger ring is expected to be more stable and therefore less reactive in the ring opening step. In contrast there should be a corresponding decreased energy barrier to closing the ring. Therefore, the combined impact of ring strain on the enzymatic cycle is currently unknown and cannot be eliminated as a contributing factor in each of these enzymes. This is demonstrated by the partial loss of activity for the GCAUG and GCAAUG mTR3 mutants. However, simply replacing a single selenium atom in the ring with a sulfur atom, as is the case for both *Dm*TR and *Ce*TR, results in a far greater loss of activity.

The pH optima determined for wild type mTR3 is 7.0-7.2 while the Ala insertions both shift to pH 8 (**Figure 29**). Similarly, the wild type *Dm*TR has an optimal pH of 7.5 - 8.0 while the Ala insertions shift to pH 8.5 (**Figure 30**). The kinetic parameters are determined at pH 7.0 where wild type mTR3 activity is at maximum. At this pH, the mTR3 Ala insertions still retain 70-80 %, the wild type *Dm*TR 80%, and the *Dm*TR Ala insertion 50 %, of their respective maximal activities. However, the shift in the pH optima is only responsible for ~20 % of the loss in activity for the Ala insertions and adjusting solution pH will not recover the 100 fold loss in activity observed in *Dm*TR and *Ce*TR2. The identical shift in pH optima indicates an alteration in the same chemical step, but one that is compensated for by the presence of selenium in mTR3.

We have also investigated the impact of the negative charge of the C-terminal carboxylate in catalysis. It was suggested from the crystal structure of the rat enzyme that the conserved Lys26 could serve as an anchor to position the C-terminus for electron transfer from the FAD associated disulfide by salt bridge formation during the catalytic

cycle (36). If this were a critical interaction, alteration of the C-terminus would be expected to decrease activity. A second possibility is that the proximity of the negative charge to electron and proton transfer during the enzymatic cycle would be inhibitory to the enzyme in which case neutralization should result in an increase in activity. Our results indicate that a specific interaction with, or charge contribution from, the C-terminal carboxylate does not appear critical to catalysis.

Neutralization of the carboxylate charge by conversion to the carboxamide for mTR3 results in a 2-fold increase in activity towards Trx and peroxide. The carboxamide mutant also shows a greater than 3 fold increase in activity with a 10 fold increase in k_{cat}/K_m with the negatively charged substrate DTNB. These results are similar to what is observed for small peptide thiol-disulfide exchange reactions investigated by Zhang and Snyder (158) where the 5-fold decrease in thiol disulfide exchange for the peptide Cys-Cys compared to Cys-Cys-Ala was hypothesized to be due to the proximity of the carboxylate to the thiol. Substitution to a hydroxamic acid for *Dm*TR also shows the same behavior as the mTR3 carboxamide with both Trx and DTNB as substrate. The lack of a change in pH optima indicates a chemical step has likely not been altered in these variants but possibly involves product release.

From interpretation to hypothesis.

Under Michaelis-Menten conditions we are looking at the impact on the overall rate of catalysis. Therefore, the effect we see reflects the combination of the ring opening step, where the C-terminus becomes reduced, and the ring closing step, where the C-terminus is re-oxidizes after electron transfer to Trx. Each step is broken into two coupled

reactions (**Figure33**); 1a) formation of a mixed disulfide with 1b) the first leaving group, and 2a) resolution of the mixed disulfide with 2b) a second leaving group. If these mutants perturb the structural position for formation of either mixed disulfide, one would expect equivalent results. Since this is not what is observed for the Ala insertions, we can eliminate 1a from each step as the critical point for mTR3. However, this assumption must be made cautiously due to the low activity for the *Dm*TR and *Ce*TR Ala mutants as there is no biochemical data that defines which Cys forms the interchange with the FAD associated active site.

Once the mixed disulfide is formed, the structural position should be fixed and therefore its role as the second leaving group should also be retained, eliminating 2b from each step. Resolution of the mixed disulfide in the ring opening step is performed by the FAD-associated resolving cysteine Cys62 and is conserved, therefore 2a for the ring opening can also be eliminated.

Even after elimination of several reactions for mTR3 we are still left with the first leaving group (1b) of the ring-opening step and the TR-Trx mixed disulfide resolution (2a) of the ring closing step. The ring closing step is governed by two opposing forces. For example, insertion of residues will favor ring formation by reducing the energy barrier of ring strain but becomes less favorable due to the increase in conformational entropy. Again, these forces should impart the same effect for each of the equivalent TR mutants in the absence of an altered chemical step. Therefore it is the hypothesis here that disruption of the vicinal disulfide results in the alteration of an enzymatic chemical step, likely during ring opening, that is more critical in the non-selenium containing TRs. This is supported by the alkaline shift in pH optima observed for each TR by increasing the

size of the ring. With such the dramatic loss of activity of mTR3 with Trx for the GUCG, GCCG, and SCCS mutants in comparison to the GCAUG and GCAAUG mutants, we conclude that maintaining the Sec C-terminal to the Cys is essential but the vicinal nature is not.

Each of the mTR3 mutants produced in this study that display poor Trx and H₂O₂ activity fall into the DTNB efficiency category (due to increased K_m) characteristic of the truncated enzyme. This is important, as it is likely that the DTNB reductase activity of these mutants is attributed to the FAD-associated active site. We suspect that the loss of activity for these mutants is due to the poor reduction of the C-terminal motif by the FAD-associated active site (the ring opening step). This is best demonstrated by the mutant mTR3-GUCG. This mutant also has significantly lower Trx and H₂O₂ activity with DTNB efficiency similar to that of the truncated enzyme. The peroxidase activity profile of the WT is characteristic of a chemical reaction and not enzymatic. Therefore, one would expect the peroxidase reaction to be independent of the Sec position once the C-terminal motif is reduced. Since a significant loss in activity is observed experimentally, this further supports our interpretation that the C-terminal motif is not efficiently reduced in the ring opening step. Combining the results from all three substrates (Trx, DTNB, and H₂O₂) we hypothesize that the Sec is required for mTR3 in the ring opening step, likely functioning as the leaving group (LG₁ in **Figure 33**). We will address this hypothesis experimentally in the next Chapter.

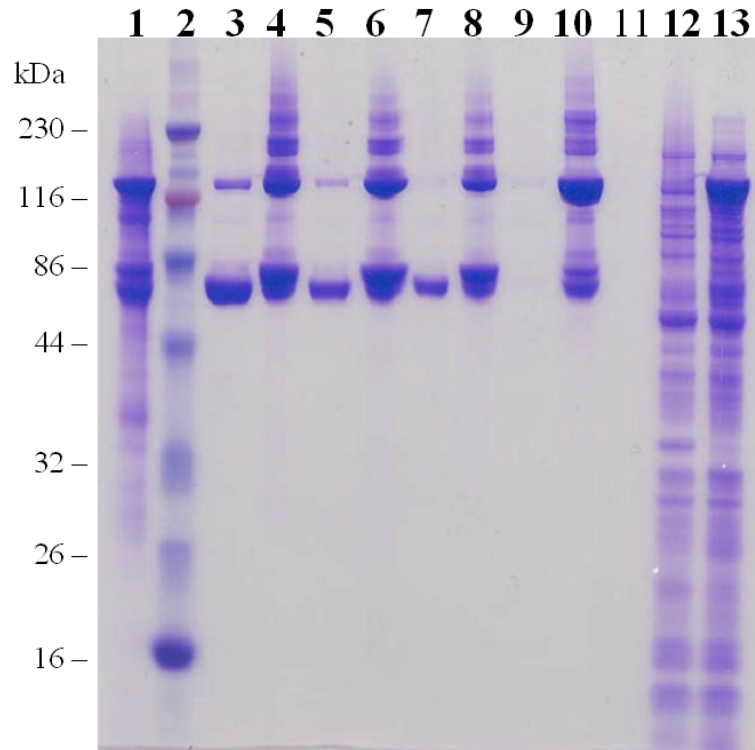


Figure 28. SDS-PAGE of *DmTR* cleavage from the intein.

Evaluation of *DmTR* cleavage from the intein with alternative reagents by 10 % SDS-PAGE. Lane 1, loaded chitin resin; lane 2, markers; lane 3, NMA eluted; lane 4, resin after NMA elution; lane 5, ammonium sulfide eluted; lane 6, resin after ammonium sulfide elution; lane 7, hydroxylamine eluted; lane 8, resin after hydroxylamine elution; lane 9, buffer only eluted; lane 10, resin after buffer elution; lane 11, blank; lane 12, pre induction; lane 13, cell lysate supernatant. Resin-bound samples are evaluated by stripping with 1% SDS. Eluant lanes represent equivalent loads, as do the lanes containing the resin strip.

Table 6. Semisynthetic mTR3 thioredoxin reductase activity.

Enzyme	k_{cat} (min^{-1})	K_{m} (μM)	% Peptide Incorporation	$k_{\text{cat}} / K_{\text{m}}$ ($\text{s}^{-1} \text{M}^{-1}$)
^a mTR3-G- <i>COO</i> ⁻	No activity	No activity	NA	NA
^b mTR3-G CCG - <i>COO</i> ⁻	4.1 ± 0.11	49.1 ± 3.2	NA	1.4 x 10 ³
mTR3- SCCS - <i>COO</i> ⁻	5.0 ± 0.06	32.0 ± 8.8	NA	2.6 x 10 ³
^c mTR3-G- CUG - <i>COO</i> ⁻	2220 ± 78	67.6 ± 6	91	5.5 x 10 ⁵
^d mTR3-G- CUG - <i>CONH</i> ₂	3010 ± 351	41.6 ± 5.0	63	1.2 x 10 ⁶
mTR3-G- UCG - <i>COO</i> ⁻	8.3 ± 0.1	36.1 ± 1.3	32	3.8 x 10 ³
mTR3-G- UUG - <i>COO</i> ⁻	1.2 ± 0.1	64.8 ± 16.1	10	3.1 x 10 ²
mTR3-G- CAUG - <i>COO</i> ⁻	350 ± 14	20.8 ± 3.5	100	2.8 x 10 ⁵
mTR3-G- CAAUG - <i>COO</i> ⁻	501 ± 41	34.9 ± 10.0	100	2.4 x 10 ⁵
^e rat TR1	3000	35	NA	1.4 x 10 ⁶

^aThe truncated form of the enzyme missing the C-terminal tripeptide Cys-Sec-Gly.

^bThe full length mutant Sec489Cys.

^cThe wild type enzyme, the hyphen between Gly and Cys (or Sec) indicates production by semisynthesis.

^dThe wild type enzyme produced by semisynthesis with a C-terminal carboxamide.

^eTaken from (145, 150), purified from rat liver and assayed using *E. coli* Trx.

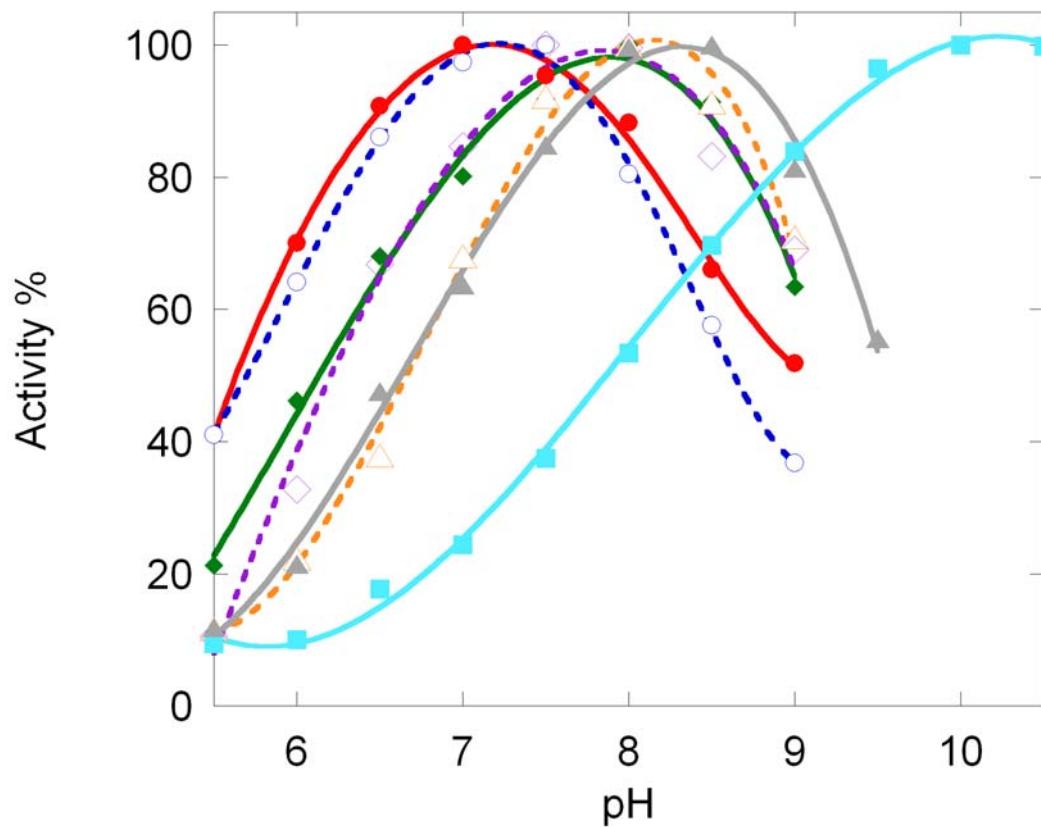


Figure 29. Trx activity as a function of pH for mTR3.

Activity towards thioredoxin as a function of pH for semisynthetic mutants of mTR3. The key indicates the C-terminal sequence following mTR3-G; -GCUG-COO⁻ (●), -GCUG-CONH₂ (○), -GCAUG (◆) -GCAAUG (△), -GUCG (◇), -GUUG (■), -GCCG (▲).

Table 7. *Dm*TR thioredoxin reductase activity.

Enzyme	k_{cat} (min^{-1})	K_{m} (μM)	$k_{\text{cat}} / K_{\text{m}}$ ($\text{s}^{-1} \text{M}^{-1}$)
^a TR-S- <i>COO</i> ⁻	No activity	No activity	NA
^b TR-S CCS - <i>COO</i> ⁻	299.4 ± 7.4	173.3 ± 8.1	2.9×10^4
^c TR-S CCS - <i>CONHOH</i>	513.3 ± 33.3	172.5 ± 21.7	5.0×10^4
^d TR-S CCS - <i>COS</i> ⁻	491.9 ± 19.6	67.8 ± 7.3	1.2×10^5
TR-S CACS - <i>COO</i> ⁻	2.12 ± 0.3	298.3 ± 58.0	118
TR-S CAACS - <i>COO</i> ⁻	0.91 ± 0.2	166 ± 58.0	91

^aThe truncated form of the enzyme missing the C-terminal tripeptide Cys-Cys-Ser.

^bThe wild type enzyme.

^cThe wild type enzyme produced as the C-terminal hydroxamic acid (Adam P. Lothrop).

^dThe wild type enzyme produced as the C-terminal thiocarboxylate (Adam P. Lothrop).

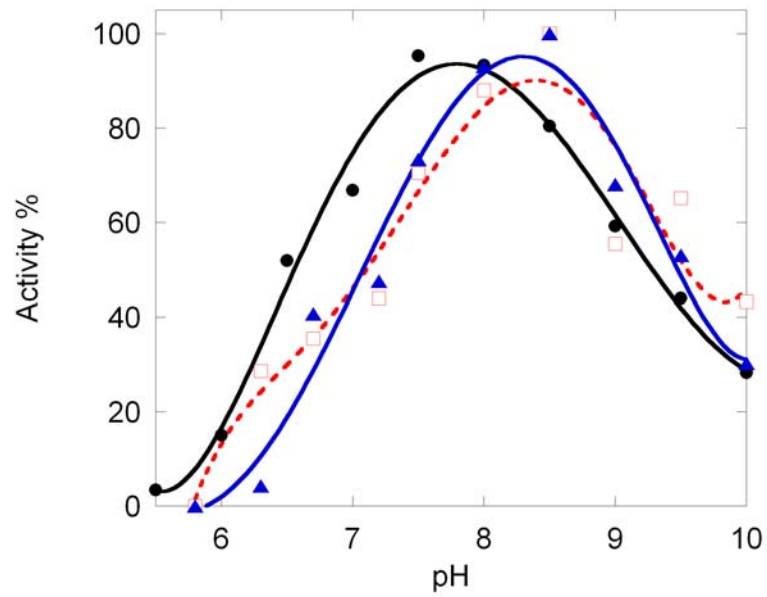


Figure 30. Trx activity as a function of pH for *DmTR*.

Activity towards thioredoxin as a function of pH for the *DmTR* mutants SCCS (●), SCACS (□), SCAACS (▲).

Table 8. DTNB reductase activity for semisynthetic mTR3.

Enzyme	k_{cat} (min^{-1})	K_{m} (mM)	$k_{\text{cat}} / K_{\text{m}}$ ($\text{s}^{-1} \text{M}^{-1}$)
^a mTR3-G-COO ⁻	856 ± 43	2.72 ± 0.43	5.2 x 10 ³
^b mTR3-GCCG- COO ⁻	794 ± 78	1.75 ± 0.41	7.6 x 10 ³
mTR3-SCCS- COO ⁻	627 ± 18	0.53 ± 0.19	2.0 x 10 ⁴
^c mTR3-G-CUG- COO ⁻	1251 ± 71	0.46 ± 0.09	4.5 x 10 ⁴
^d mTR3-G-CUG-CONH ₂	3284 ± 133	0.13 ± 0.02	4.2 x 10 ⁵
mTR3-G-UCG- COO ⁻	751 ± 51	1.61 ± 0.34	7.8 x 10 ³
mTR3-G-UUG- COO ⁻	914 ± 18	1.84 ± 0.12	8.3 x 10 ³
mTR3-G-CAUG- COO ⁻	1010 ± 26	0.26 ± 0.03	6.5 x 10 ⁴
mTR3-G-CAAUG- COO ⁻	999 ± 44	0.43 ± 0.08	5.6 x 10 ⁴

^aThe truncated form of the enzyme missing the C-terminal tripeptide Cys-Sec-Gly.

^bThe full length mutant Sec489Cys.

^cThe wild type enzyme, the hyphen between Gly and Cys (or Sec) indicates production by semisynthesis.

^dThe wild type enzyme produced by semisynthesis with a C-terminal carboxamide.

Table 9. DTNB reductase activity for *Dm*TR.

Enzyme	k_{cat} (min^{-1})	K_{m} (mM)	$k_{\text{cat}} / K_{\text{m}}$ ($\text{s}^{-1} \text{M}^{-1}$)
^a TR-S-COO ⁻	178.0 ± 7.0	0.75 ± 0.09	4.0 x 10 ³
^b TR-SCCS-COO ⁻	157.0 ± 12.4	0.22 ± 0.07	1.2 x 10 ⁴
TR-SCACS-COO ⁻	187.5 ± 17	0.20 ± 0.06	1.7 x 10 ⁴
TR-SCAACS-COO ⁻	94.9 ± 4.1	0.25 ± 0.03	6.3 x 10 ³

^aThe truncated form of the enzyme missing the C-terminal tripeptide Cys-Cys-Ser.

^bThe wild type enzyme.

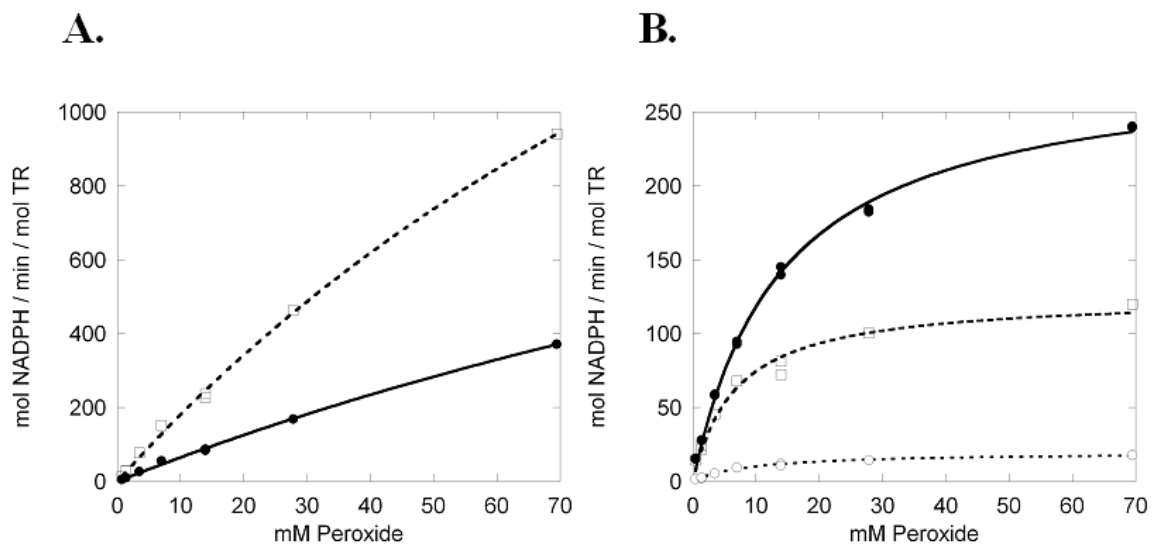


Figure 31. Peroxidase activity for mTR3 mutants.

Michaelis-Menten plots in the form of V_0/E_T vs. hydrogen peroxide concentration for mammalian thioredoxin reductase C-terminal mutants. Panel A shows the wild-type enzyme with the naturally occurring carboxylic acid (●) and wild-type peptide sequence produced as a C-terminal carboxamide (□). Panel B shows the GCAUG (●), GCAAUG (□), and GUCG (○) mutants.

Table 10. Peroxidase activity of semisynthetic mTR3.

Enzyme	k_{cat} (min^{-1})	K_{m} (mM)	$k_{\text{cat}} / K_{\text{m}}$ ($\text{s}^{-1} \text{M}^{-1}$)
^a mTR3-G- COO ⁻	2.1 ± 0.04	65 ± 17	0.5
^b mTR3-GCCG- COO ⁻	19.6 ± 1.9	233 ± 36	1.4
^c mTR3-G-CUG- COO ⁻	1753 ± 257	259 ± 46	113
^d mTR3-G-CUG-CONH ₂	3204 ± 351	167 ± 24	320
mTR3-G-UCG- COO ⁻	19.7 ± 0.8	9.5 ± 1.2	35
mTR3-G-UUG- COO ⁻	6.0 ± 0.7	47 ± 10	2.1
mTR3-G-CAUG- COO ⁻	284 ± 3.9	14 ± 0.7	338
mTR3-G-CAAUG- COO ⁻	125 ± 6.4	6.8 ± 1.2	306

^aThe truncated form of the enzyme missing the C-terminal tripeptide Cys-Sec-Gly.

^bThe full length mutant Sec489Cys.

^cThe wild type enzyme, the hyphen between Gly and Cys (or Sec) indicates production by semisynthesis.

^dThe wild type enzyme produced by semisynthesis with a C-terminal carboxamide.

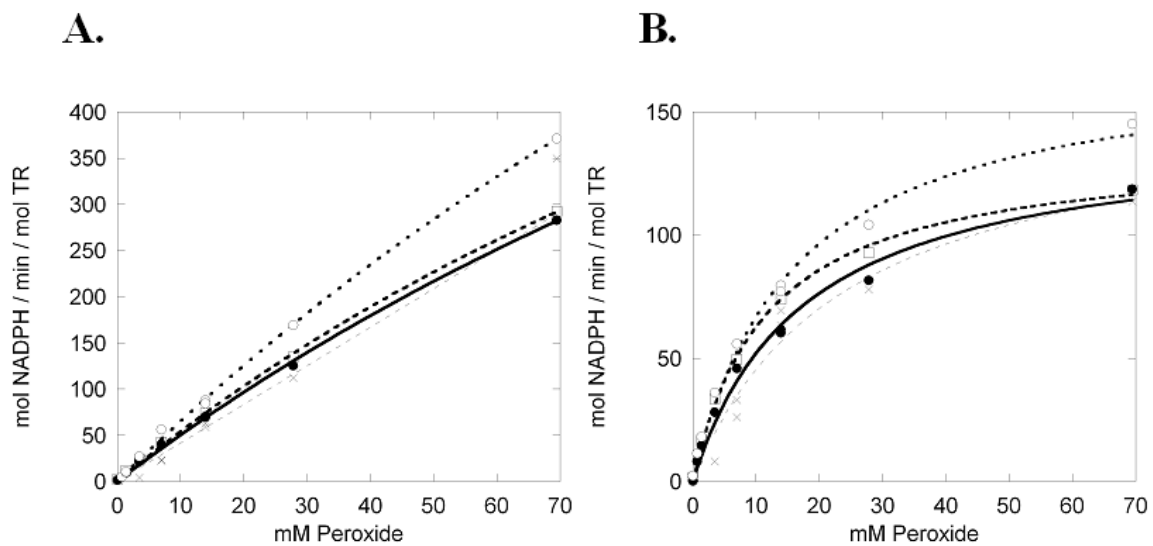


Figure 32. Peroxidase activity as a function of NADPH concentration.

Hydrogen peroxidase activity for semisynthetic mTR3 with NADPH concentrations at 25 μM (●), 100 μM (□), 200 μM (○), and 500 μM (×). Panel A is wild type, B is the C-terminal mutant GCAUG.

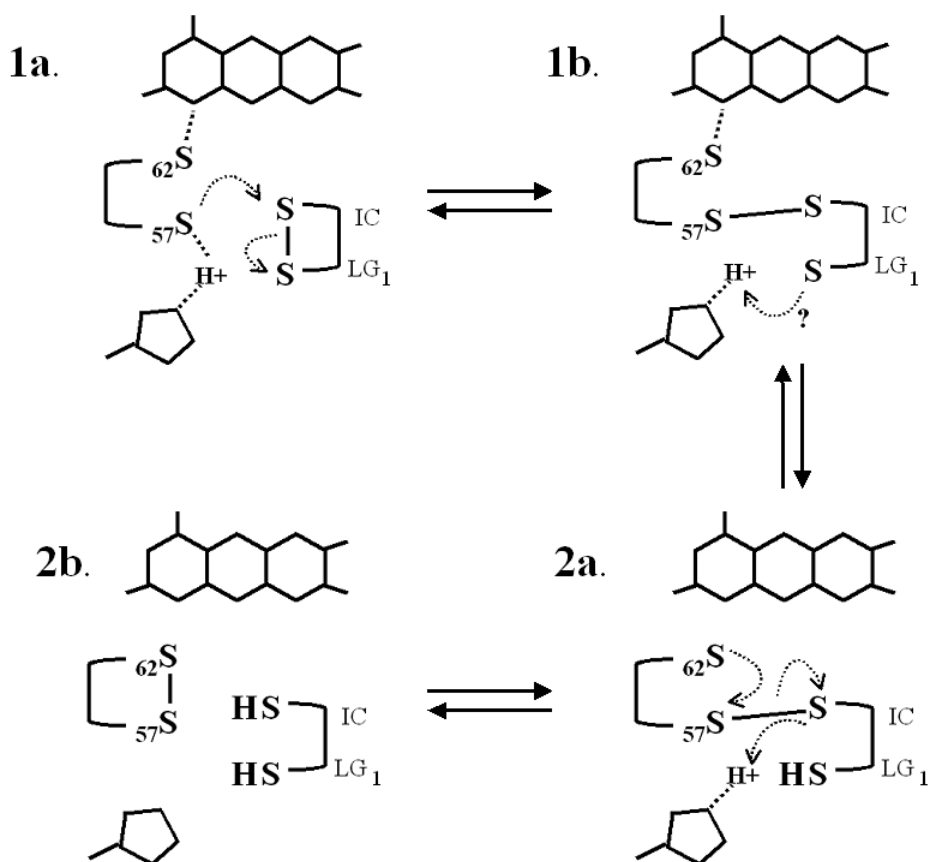


Figure 33. Steps of thiol-disulfide exchange for TR.

The steps for thiol-disulfide for thioredoxin reductase that occurs between the FAD-associated active site (Cys57, Cys62) and the C-terminus, the ring opening step. 1a) Upon reduction of the FAD-associated disulfide, Cys57 will form the interchange (IC) with a Cys from the C-terminus with the other Cys being the first leaving group (LG₁) which would need to be protonated (1b) if Cys but would not be if Sec. The resolution step, 2a and 2b, should proceed as in the GR cycle. The same general cycle subsequently occurs between the C-terminus or TR in the reduced state and the oxidized disulfide of Trx and would be the ring closing step.

CHAPTER 4.

TRUNCATED THIOREDOXIN REDUCTASE AS A DISULFIDE OXIDOREDUCTASE INVESTIGATED BY PEPTIDE COMPLEMENTATION

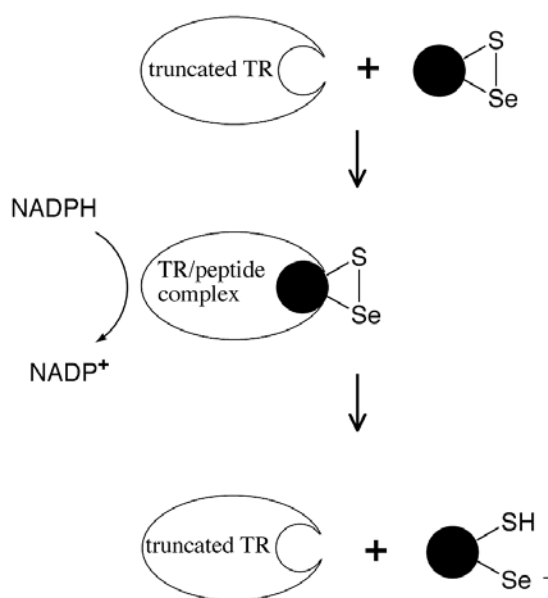


Figure 34. Peptide complementation of TR.

Peptide Complementation of thioredoxin reductase (TR). Oxidized tetrapeptides corresponding to the C-terminal active site motif of TR are substrates for the truncated form of the enzyme in a manner similar to glutathione reductase and its cognate substrate oxidized glutathione.

In the course of developing the semisynthetic method, we also attempted to produce a non-covalent semisynthetic TR by using a technique called peptide complementation. In such a system, a truncated enzyme missing part of its active site can be restored to full or partial activity by exogenous addition of a synthetic peptide that complements the active site with the missing amino acids. The most prominent example of peptide complementation is the S-protein/S-peptide system developed by Richards (134). In our peptide complementation system, we demonstrate that tetrapeptides in the oxidized form equivalent to the C-terminal active sites of both mTR3 and *Dm*TR, only weakly complement thioredoxin reductase activity but behave more like substrates for the truncated enzymes. This is reasonable because as part of the enzyme, the oxidized form of the C-terminal tetrapeptide must be reduced by the N-terminal redox-active dithiol during the enzymatic cycle. A disulfide bond formed between vicinal Cys-Cys (or Cys-Sec) residues results in the formation of an eight-membered ring and this assay examines the kinetics of the ring opening step that occurs during the enzymatic cycle of TR. The observation that oxidized tetrapeptides can serve as substrate for the truncated forms of TR demonstrate that TR, like GR, may be considered a disulfide oxidoreductase where its own C-terminus is the cognate substrate (**Figure 35**). Using this assay we can isolate the ring-opening step for TR in a manner analogous to the GSSG reduction by GR (**Figure 33** of Chapter 3). We observe that for each of the peptides assayed, *Dm*TR showed higher activity than mTR3. There is also a dramatic dependence for Sec in the second position demonstrated by mTR3 but not *Dm*TR.

METHODS

Activity of truncated TR towards C-terminal Tetrapeptide Substrates.

Tetrapeptides Ac-GCUG(ox), Ac-GCCG(ox), Ac-SCUS(ox), and Ac-SCCS(ox) were prepared by Fmoc solid-phase peptide synthesis and oxidized to the monomeric form using a newly described procedure for making disulfide bonds on-resin (143). The peptides were purified by preparative HPLC and verified as intramolecular disulfides by MALDI-TOF mass spectrometry using a Voyager-DE PRO from Applied Biosystems (Framingham, MA). The peptides were treated as substrates for the truncated *Dm*TR and mTR3 using conditions similar to the DTNB assay and enzyme concentrations were adjusted to get a signal at 340 nm as is seen in the thioredoxin (Trx) assay. Activity was measured by the decrease in absorbance at 340 nm for the consumption of NADPH, corrected for background in the absence of enzyme as well as in the absence of substrate, and plotted as mole of NADPH consumed per minute per mole of homodimeric TR. Due to the uniqueness of this system, we have reported the activity values for each peptide as the slopes of the plot of V_o/E_T vs. peptide concentration. Each peptide assayed is then evaluated as a fold difference in slope when compared to another peptide.

RESULTS AND DISCUSSION

A peptide complementation approach was tested in comparison with the ligated semisynthetic mTR3 as only three amino acids out of a total of 490 are missing from the

intact enzyme. Peptide Ac-GCUG was synthesized and tested for its ability to “complement” the truncated enzyme missing tripeptide CUG. This tetrapeptide is *N*-acylated and begins with a glycine residue and *as such, cannot ligate to the thioester-tagged enzyme produced from the intein fusion*. Variations of the Trx assay were performed in which Trx, insulin, or both were missing from the assay. The results of these experiments are summarized in **Table 11** and demonstrate that the selenium-containing peptide was required for NADPH consumption. The function of the insulin in the assay is to provide a source of oxidant for Trx so that the concentration of the oxidized Trx remains high during the course of the assay. When Trx was absent, the oxidized form of the peptide was reduced by the truncated form of the enzyme, resulting in the consumption of NADPH. The results in Table 1 show that more NADPH is consumed when both Trx and insulin are present in the assay mixture. The transiently formed enzyme/peptide complex may reduce Trx, or the resulting reduced peptide may reduce Trx. These results indicate that the peptide is *primarily acting as a substrate for the truncated enzyme, rather than forming a reconstituted enzyme as in the S-protein/S-peptide complex (134)*.

Truncated TR as a Disulfide Reductase.

Preliminary results demonstrated that the oxidized tripeptide Cys-Sec-Gly-OH(ox) is a substrate for mTR3 when added to the assay mixture containing NADPH and truncated TR (**Figure 36**) with an activity of 260 min^{-1} . The low affinity observed for the peptide by the enzyme, is likely the result of minimal binding contacts in this complementation system. When the selenium atom is replaced with a sulfur atom in the

homologous peptide CCG(ox), the activity is reduced to 0.81 min^{-1} , indicating that the ring opening step is greatly affected by the replacement of a selenium atom with a sulfur atom.

We subsequently tested oxidized tetrapeptides as substrates for both *DmTR* and mTR3 so that we could fully examine the effect of flanking residues on either side of the Cys-Cys or Cys-Sec dyad. We tested the tetrapeptides: Ac-GCUG(ox), Ac-GCCG(ox), Ac-SCCS(ox), and Ac-SCUS(ox) (all as the oxidized, monomeric-cyclic peptides) as substrates for the truncated enzymes. A summary of the kinetic data for ring opening is given in **Table 12** with the plots shown in **Figure 37**. Comparing Ac-GCUG(ox) to Ac-GCCG(ox) demonstrates that there is a 308 fold decline in activity in mTR3 and only a 36.2 fold decrease for *DmTR*. The ratio of ring-opening rates for the peptides Ac-SCUS(ox) and Ac-SCCS(ox) with mTR3 is 511 fold while the equivalent comparison is only 5.65 fold with *DmTR*, **Table 13**. Since the assays do not reach saturation, differences in K_m must still be taken in consideration when comparing Ser and Gly containing peptides. However, it is reasonable to assume that the equivalent peptide pairs (SCCS/SCUS and GCCG/GCUG) would not have a significant difference in K_m as a result of the substitution of a selenium atom for a sulfur atom. The data demonstrates a dramatic difference in the rate of peptide turnover in this step of the reaction mechanism between the two enzymes. There is a 10 to 100 fold greater dependence on the Sec residue for mTR3 compared to *DmTR* for these peptide pairs.

Prior to the cloning of *DmTR*, the peptide Ac-GCAUG(ox) was assayed in comparison to Ac-GCUG(ox) for truncated mTR3 (**Figure 38**). For this peptide, the Sec is retained C-terminal relative to Cys but separated by a single Ala residue. The fold

difference for this pair GCUG/GCAUG was only 8.4 fold, which is minor in comparison to the 308 fold for GCUG/GCCG with mTR3. Preliminary results were also obtained for the peptide Ac-GUCG(ox). The peptide was not completely purified therefore a value for direct comparison to the other peptides is not possible. However, the crude peptide was assayed with both mTR and *Dm*TR with no difference in activity observed between the two enzymes. Neither mTR nor *Dm*TR showed activity to the disulfide substrates cystine, homocystine, or GSSG.

Finally, we also assayed peptides containing the non-protein *D*-isomer of cysteine substituted individually for the two positions. There was no activity observed for Ac-GC_DC_LG(ox) or Ac-GC_LC_DG(ox) for mTR3. *Dm*TR (**Figure 39**) showed a 3 fold decrease in activity for Ac-GC_DC_LG(ox) compared to Ac-GCCG(ox) and no activity for Ac-GC_LC_DG(ox). This difference in activity observed by a stereo-isomer substitution indicates there is an additional structural component impacting the ring opening step.

Indication of a Critical Leaving Group Effect for mTR3.

The data in Chapter 3 demonstrates that the truncated forms of both enzymes can catalyze the reduction of the disulfide DTNB. An explanation of why DTNB is a substrate for TR but cystine is not has been partially addressed by Ascott and coworkers (94) in applications with the mixed disulfide R-S-S-TNB (TNB-S is 5-thio-2-nitrobenzoate). In this example, TNB-S⁻ will be the leaving group because of the strong electron withdrawing properties of the 2-nitrobenzoate group. Such mixed disulfides are also easier to break than a typical disulfide bond because they are highly polarized. This property has been used in investigating the mechanism of GR. The mixed disulfide

between glutathione and TNB-S⁻ (G-S-S-TNB) is a substrate for GR with kinetic isotope effects indicating a single proton transfer step as rate limiting (95). The interpretation of this data is that the departing GSH would require protonation but the TNB-S⁻ would not. Therefore, we posit that DTNB is a substrate for TR due to the very low pK_a (4.75) of the leaving group thiol that is formed upon reduction of this disulfide (159).

The exact same situation exists in the peptide Ac-GCUG(ox), which has a low pK_a leaving group (Se) and the S-Se bond is also much weaker than a typical disulfide bond due to the polarization in the bond conferred by the Se atom. By comparing the rate of reduction of peptide Ac-GCUG(ox) vs. peptide Ac-GCCG(ox) by the truncated mTR3, this large difference in the rate of ring opening between these two peptides can be understood in terms of leaving group pK_as. This is further supported by the 8.4 fold decrease in ring opening for the GCUG/GCAUG pair compared to the 308 fold decrease for the GCUG/GCCG pair for mTR3. In the Ac-GCAUG(ox) peptide, the Sec position relative to Cys (C-terminal) is retained. It can therefore be hypothesized that the necessity for Sec in mTR3 is its function as the leaving group in the ring opening step.

Correlation to C-terminal Structure-Function Results.

A comparison of full-length TR activities determined by the steady-state Trx activity and the data for the ring opening step assayed with the truncated TR is shown in **Table 14**. Taking into consideration that the data from the two methods are derived rather differently, there is a remarkable level of agreement between the two methods. For *DmTR*, the GCUG/GCCG and SCUS/SCCS pairs correlate 20% and 30% of the loss in Trx activity to the ring opening step while the GCUG/SCCS are within 50%. In each pair,

there a greater fold difference in ring opening than observed in Trx activity. For mTR3, the fold difference in activity for the GCUG/GCCG pair for Trx is 292 and ring opening is 308. This near identical result is also observed for the GCUG/GCAUG pair with 6.3 and 8.4 fold difference in activity observed by the methods respectively. From this analysis, we hypothesize that the loss in Trx activity upon mutation of the Sec to Cys in mTR can be attributed to the reduction in the rate of ring opening.

While these results from the two methods are in agreement, and peptide complementation data lead us to a leaving group effect hypothesis, the question of **why** still remains. Why would Sec be required as a leaving group if the catalytic base is conserved in TR? A simplified interpretation would be that *DmTR* has a functional catalytic base but mTR3 does not. However, the well-established model based on mechanistic studies with GR and recently with TR from *Plasmodium falciparum* (93), indicate that the catalytic His is essential for multiple steps in the reaction cycle (see **Figure 10 of Chapter 1**). Therefore, if mTR3 did not have a functional base it should have little or no activity regardless of whether it contains Sec or not.

A second possibility is that the reaction cycle requires a second catalytic base which is functional in *DmTR* but non-functional or absent in mTR3. For example, one base would be required for protonation of the first leaving group and another for protonation of the second leaving group that is generated upon resolution of the interchange mixed-disulfide. Based on sequence alignments, this residue was proposed to be His106 in *DmTR* (65). However, this residue is also conserved in mammalian TRs, and mutation of His106 to Phe in *DmTR* results in only a 3 fold reduction in activity (121). Finally there is no explanation as to why cystine is not a substrate for *DmTR*

considering its activity towards the Cys-Cys cyclic peptides. The same conundrum exists for GR where GSSG is a substrate but cystine activity is poor (160) even though both molecules are intermolecular cysteine disulfides.

There is also an interesting observation when considering the Ser and Gly containing sequences for the two enzymes. *DmTR* shows no preference for SCCS or GCUG with either assay method yet mTR3 does. Based on the proposed function of Ser acting as a general acid/base in the *DmTR* motif (65), there should be better agreement between the two enzymes. The peptide complementation data shows minor rate enhancement by replacing Gly with Ser in a Cys-Cys or Cys-Sec peptide indicating some potential functionality of the Ser residues. However, there is still no explanation as to why the SCCS motif cannot replace the GCUG motif in mTR3, as they appear interchangeable for *DmTR*. It also does not explain why the effect Sec has with both methods for mTR3 and why it is muted in *DmTR*. Our conclusion is that there is a structural difference between mTR3 and *DmTR*, other than the C-terminal tetrapeptide motif, responsible for the requirement for Sec in mTR3. Chapter 5 will examine this question and correlate the enzymatic data to structural differences between these two enzymes.

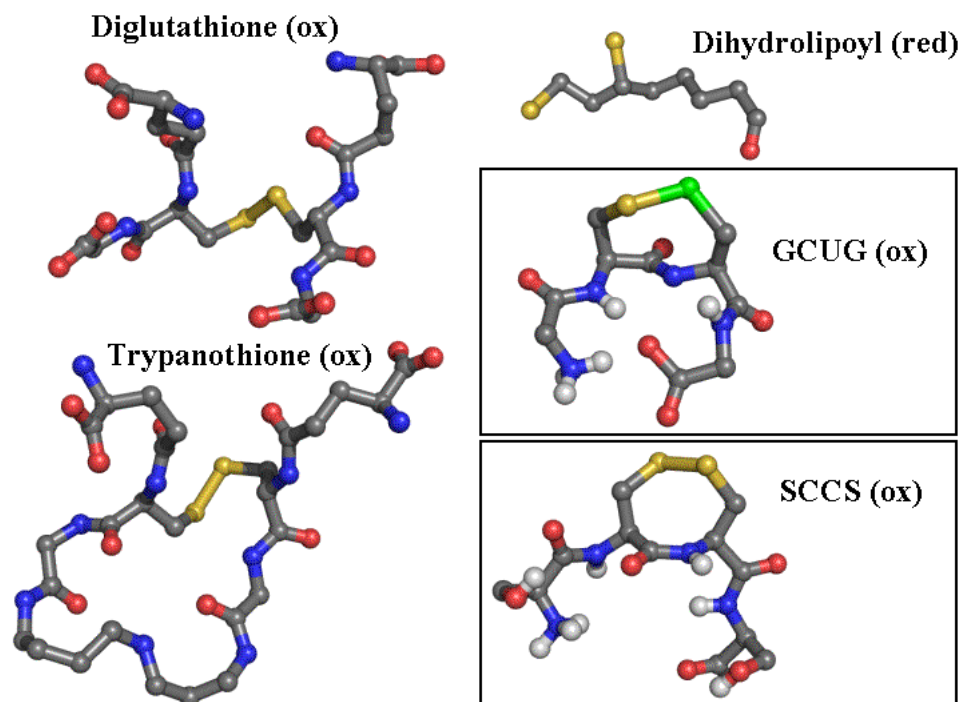


Figure 35. Cognate substrates revisited for truncated TR.

Using oxidized tetrapeptides equivalent to the C-terminal motif of TR as substrates for the truncated enzyme we are able to look at steps in the catalytic cycle in a manner equivalent to GR, TryR or LipDH and their cognate substrates (34, 37, 130). The tetrapeptides are the cognate substrate in the peptide complementation assay.

Table 11. Summary of TR/Ac-GCUG peptide ^acomplementation kinetics.

^b Enzyme	100 μ M peptide	160 μ M insulin	3 μ M Trx	^c Rate (nmoles NADPH/min)
TR _{Gly487}	+	+	+	4.20 \pm 0.60
TR _{Gly487}	+	-	-	2.25 \pm 0.21
TR _{Gly487}	+	-	+	1.96 \pm 0.086
TR _{Gly487}	+	+	-	2.60 \pm 0.062

^aEnzyme assays were performed in a volume of 600 μ L containing 100 mM potassium phosphate buffer, pH 7.0, 1 mM EDTA, with 8.4 μ M enzyme. Other assay components are as indicated in the table.

^bIndicates that the truncated form of the enzyme ends at residue 487.

^cThe rate is calculated by monitoring the loss of NADPH at 340 nm.

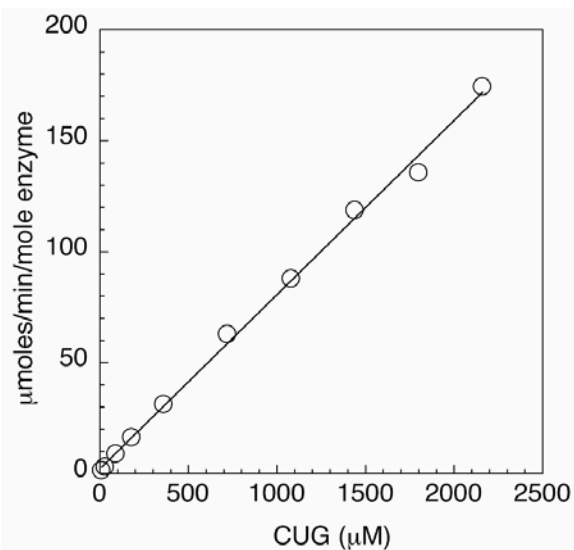


Figure 36. Peptide complementation of mTR3 with CUG(ox).

Rate of reduction (ring opening) of oxidized tripeptide CUG(ox) with truncated mTR3. A linear increase in activity is observed as the concentration of tripeptide increases in the assay. The truncated enzyme could not be saturated with tripeptide due to solubility limits of the peptide under the assay conditions. The rates of peptide turnover were calculated by measuring the slope of a plot of NADPH consumption (in min^{-1}) vs peptide concentration (in mM).

Table 12. Summary of activities toward tetrapeptides for the truncated TRs.

Enzyme	^a Peptide (turnover rate in min ⁻¹ /mM)			
	Ac-SCCS(ox)	Ac-SCUS(ox)	Ac-GCCG(ox)	Ac-GCUG(ox)
^b mTR3-G	0.21	107.3	0.06	18.5
^c <i>Dm</i> TR-S	57.0 (271) ^d	322.6 (3)	2.4 (40)	87.0 (4.7)

^aThe rate of peptide turnover was determined at pH 7.0 in potassium phosphate buffer as described in the methods. The relative activities for the individual peptides are the slopes from the titration curve in min⁻¹/mM.

^bMouse mitochondrial TR missing the C-terminal tripeptide Cys-Sec-Gly.

^c*Drosophila melanogaster* TR missing the C-terminal tripeptide Cys-Cys-Ser.

^dThe ratio of rates (fold difference) between *Dm*TR-S and mTR3-G are given in parentheses in bold.

Table 13. Ratio of peptide turnover rates for the truncated TRs.

Enzyme	SCUS/SCCS (Se/S)	GCUG/GCCG (Se/S)	GCUG/SCCS (Se/S)	SCCS/GCCG (S/S)	SCUS/GCUG (Se/Se)
^a mTR3-G	^c 511	308	88.1	3.5	5.8
^b DmTR-S	5.65	36.2	1.5	23.7	3.7

^aMouse mitochondrial TR missing the C-terminal tripeptide Cys-Sec-Gly.

^b*Drosophila melanogaster* TR missing the C-terminal tripeptide Cys-Cys-Ser.

^cThe ratio of rates (fold difference) between the peptide pair.

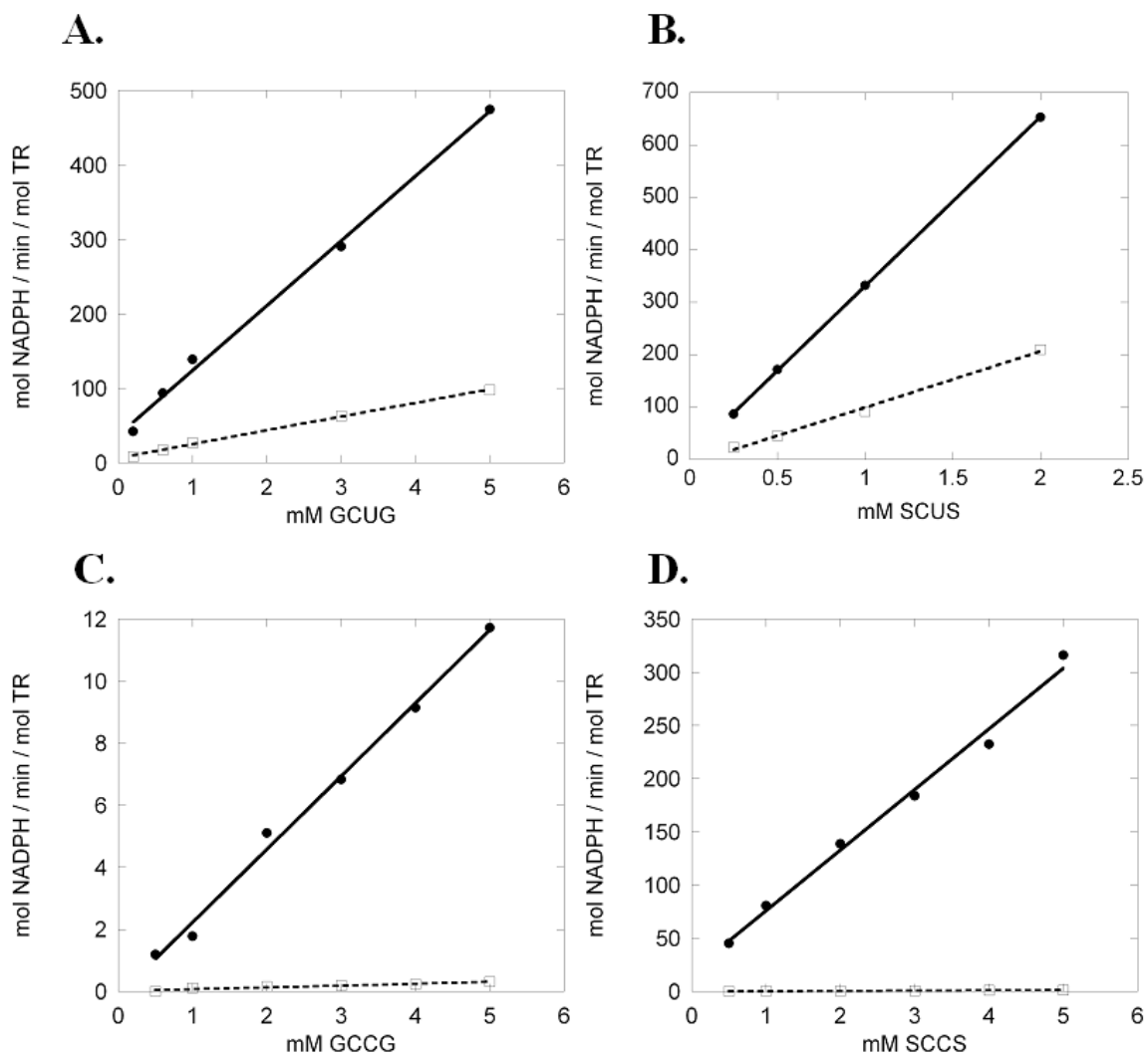


Figure 37. Rate of ring opening for tetrapeptides(ox).

Rate of reduction (ring opening) using oxidized tetrapeptides as substrates for truncated enzymes DmTR (solid) and mTR3 (dashed). (A) Peptide Ac-GCUG(ox) as substrate; (B) Peptide Ac-SCUS(ox) as substrate; (C) Peptide Ac-GCCG(ox) as substrate; and (D) Peptide Ac-SCCS(ox) as substrate.

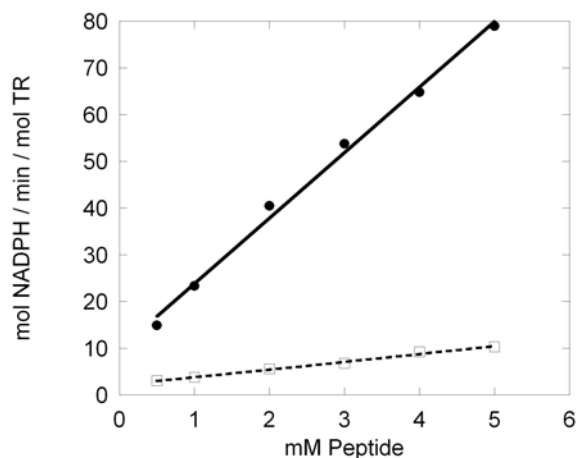


Figure 38. Rate of ring opening Ac-GCAUG(ox) for mTR3.

Rate of reduction (ring opening) using the oxidized tetrapeptides Ac-GCUG(ox) (solid) and Ac-GCAUG(ox) (dashed) as substrates for truncated mTR3. The Activity for the Ac-GCUG(ox) was 14.0 while the Ac-GCAUG(ox) activity was 1.66. This results in an 8.4 fold activity ratio.

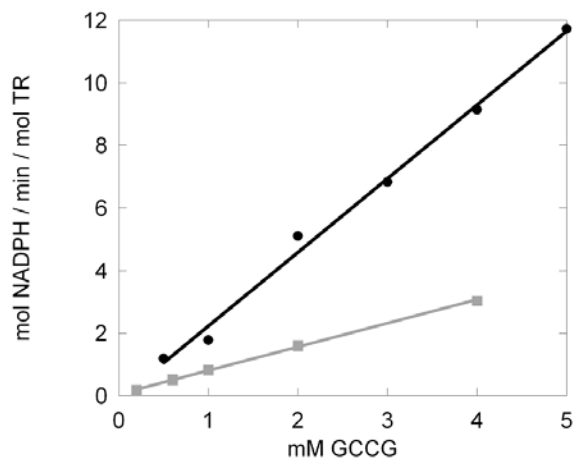


Figure 39. Rate of ring opening for Ac-GC_DC_LG(ox) with *Dm*TR.

Rate of reduction (ring opening) using oxidized tetrapeptides as substrates for truncated *Dm*TR. The peptide Ac-GCCG(ox) as substrate is shown in black. The peptide Ac-GC_DC_LG(ox) as substrate is shown in grey.

Table 14. Rates of ring opening step compared to full-length TR activities.

Peptide pair	<i>Dm</i> TR	^e <i>Dm</i> TR-S	mTR3	^f mTR3-G
	^b Full length	Ring Opening	Full Length	Ring Opening.
GCUG/GCCG ^a	^c 7.5	36.2	292	308
SCCS/GCCG	7.5	23.7	0.7	3.5
GCUG/SCCS	1	1.5	435	88.1
GCUG/GCAUG	N.D. ^d	N.D.	6.3	8.4

^aThe *Dm*TR full length data is taken from (65).

^bActivities from thioredoxin assay.

^cThe numbers represent the ratio of each pair.

^dNot determined.

^eMouse mitochondrial TR missing the C-terminal tripeptide Cys-Sec-Gly.

^f*Drosophila melanogaster* TR missing the C-terminal tripeptide Cys-Cys-Ser.

CHAPTER 5.

THE CRYSTAL STRUCTURE OF THIOREDOXIN REDUCTASE FROM *DROSOPHILA* *MELANOGASTER* WITH TETRAPEPTIDE MODELING FOR COMPARISON WITH MAMMALIAN THIOREDOXIN REDUCTASE

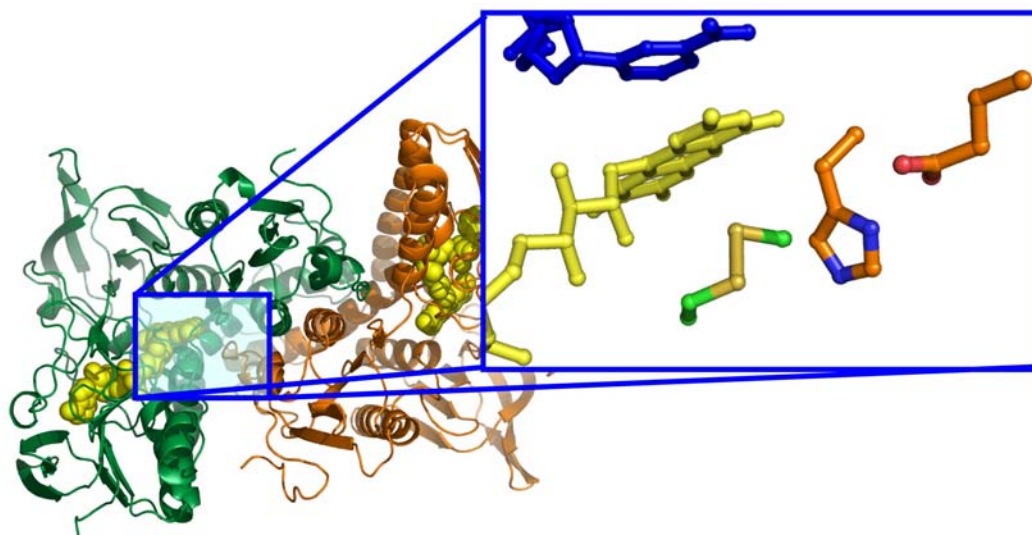


Figure 40. The crystal structure of mTR3.

The homodimeric structure of the mTR3 with a zoom of the key conserved catalytic components NADPH (blue), FAD (yellow), and N-terminal disulfide from chain A (green backbone). The Glu-His pair from chain B (orange backbone) is also shown. The structure is mTR3 from this Chapter. The NADPH is from (35).

Biochemistry 2007, Apr 24; 46(16): 4694-4705

Structural and Biochemical Studies Reveal Differences in the Catalytic Mechanisms of Mammalian and *Drosophila melanogaster* Thioredoxin Reductases

Brian E. Eckenroth[‡], Mark A. Rould[§], Robert J. Hondal^{†*} and Stephen J. Everse^{‡*}

[†]These studies were supported by National Institutes of Health grant GM070742 to RJH and by a Department of Energy EPSCoR grant DE-FG02-00ER45828 to RJH and SJE administered by Susan S. Wallace, Chair, Department of Microbiology and Molecular Genetics, University of Vermont.

[‡]Department of Biochemistry, 89 Beaumont Ave, Given Building, Room C401, Burlington, VT 05405

[§]Department of Molecular Physiology and Biophysics, 312 Health Sciences Research Facility, Burlington, VT 05405

*To whom correspondence should be addressed. Department of Biochemistry, University of Vermont, College of Medicine. 89 Beaumont Ave, Given Building, Room B413, Burlington, VT 05405. Tel: 802-656-8282. FAX: 802-656-8220. E-mail: Robert.Hondal@uvm.edu

*To whom correspondence should be addressed. Department of Biochemistry, University of Vermont, College of Medicine. 89 Beaumont Ave, Given Building, Room B418, Burlington, VT 05405. Tel: 802-656-8271. FAX: 802-656-8220. E-mail: Stephen.Everse@uvm.edu

In order to explain why mammalian thioredoxin reductase (TR) requires Sec but TR from *Drosophila melanogaster* (*DmTR*) can utilize Cys, we have solved the X-ray crystal structure of *DmTR* in the truncated form (missing the C-terminal tripeptide sequence Cys-Cys-Ser) at 2.4 Å resolution. We have also solved the X-ray crystal structure of mouse mitochondrial TR (mTR3) in the truncated form (missing the C-terminal tripeptide Cys-Sec-Gly) at 2.25 Å resolution, though refinement is not complete. The NMR structures of the oxidized tetrapeptides used in the peptide complementation studies were oriented in the active site of both mTR3 and *DmTR* using oxidized diglutathione bound to GR as a template. *DmTR* has a more open tetrapeptide binding pocket than the mouse enzyme and accommodates peptide Ser-Cys-Cys-Ser(ox) in a *cis* conformation that allows for protonation of the leaving group Cys by His464'. In contrast, mTR3 shows a more narrow tetrapeptide binding pocket, which restricts the mammalian redox-active tetrapeptide Gly-Cys-Sec-Gly to a *trans* conformation. This places the Sec residue further away from the conserved catalytic histidine residue into a position unsuitable for protonation. The analysis here explains why *DmTR* can function with Cys but mTR3 requires Sec as a low pK_a leaving group.

METHODS

Crystallization of TR from Drosophila.

Purified *Dm*TR was dialyzed against 10 mM potassium phosphate pH 7.4 with 300 mM NaCl and 1 mM EDTA then concentrated to 26 mg/mL. Crystals were grown at 20 °C using the hanging drop diffusion method with a reservoir solution containing 200 mM succinate pH 5.5 and 22 % PEG 6000. Hanging drops were 10 µL in volume containing 6 µL protein, 3 µL reservoir, and 1 µL of 10 mM NADP. Crystals (280 x 100 x 100 µm) were fully grown in 5 to 7 days. Cryoprotection was achieved by dipping the crystal in reservoir solution containing 4 % increments of ethylene glycol for 4 min per step until a final concentration of 20 % was achieved.

Crystallization of TR from Mouse.

Purified mTR3 was dialyzed against 10 mM potassium phosphate pH 7.4 with 300 mM NaCl and 1 mM EDTA then concentrated to 25 mg/mL. Crystals were grown at 20 °C using the hanging drop diffusion method with a reservoir solution containing 150 mM MES pH 5.5, 2 % ethylene glycol, and 23 % PEG 6000. Hanging drops were 8 µL in size with 5 µL of protein, 2 µL of reservoir, and 1 µL of 10 mM NADP. Crystals (1000 x 240 x 240 µm) were fully grown in 1 to 3 days. Cryoprotection was achieved by dipping the crystal in reservoir solution containing either a final concentration of 36 % PEG 6000 or 25 % ethylene glycol for 5 minutes.

Data Collection, Structure Determination and Refinement for DmTR.

Data was collected at $-169\text{ }^{\circ}\text{C}$ using a Rigaku RU-H3R generator with a copper rotating anode on a Mar345 image plate detector. The data was indexed using DENZO and scaled and merged using SCALEPACK (161). The structure of rat TR1 (PDB 1H6V) was used for molecular replacement routines with CNS (v 1.1)(162). The cross-rotation search yielded a single peak 2.8σ above the mean and the translational search found a peak 2.1σ above the mean. Rigid-body refinement reduced the R-factor to 0.46 for data from 15 to 2.4 \AA . Data were processed using space group R32. Model building was based upon simulated-annealing omit map interpretation with the graphics program O (163). Successive rounds of refinement were performed by simulated annealing, occupancy, and B-factor refinement using CNS and CCP4 (164). In the later stages of refinement, the position of the FAD as well as the NADP (minus the nicotinamide moiety) was determined by fitting omit maps. Final refinement was performed using REFMAC5 (165) in CCP4, version 5.0.2, with the entire model as a single TLS group. Electrostatic surface maps were computed using GRASP (166). All electrostatic maps are in units of kT/e where k is the Boltzmann's constant, T is the absolute temperature, and e is the proton charge. The scale is -11 (red), 0 (white), and $+11$ (blue). Images were generated using PyMOL (167).

C-terminal Peptide Structure and Docking.

The oxidized tetrapeptides Ac-GCUG, Ac-GCCG, and Ac-SCCS were examined by NMR spectroscopy and found to exist as a population of four major conformers

(Deker and Hondal, unpublished) as has been previously described for a similar peptide with a vicinal disulfide bridge (58). Each of the four conformers was placed at the reaction interface proximal to the conserved flavin-associated active site sequence CVNVGC of both *Dm*TR and mTR3 (PDB 1ZKQ) (35). Because of the high similarity between the reaction mechanisms of GR and TR, we used the orientation of oxidized glutathione (GSSG) in the active site of GR (PDB 1GRA, (34)) to orient the structures of our oxidized peptides in the active site of TR. The disulfide bond of the oxidized peptides was placed in an orientation similar to that of the disulfide bond of GSSG and evaluated for the potential to form the interchange mixed-disulfide as well as for positioning of the leaving group in relation to the catalytic histidine of GR and TR. Additional restrictions on the placement of the peptide were imposed by the covalent interchange mixed-disulfide structure of GR (PDB 1GRE (34)). Using the two GR structures, priority was given in the peptide modeling to the first step (interchange) of the GR GSSG-dependent oxidative half-reaction by super-positioning of the C β and sulfur (or selenium) atoms to the interchange cysteine of glutathione I (GSH I).

Independent fits for each peptide were performed for both cysteines in peptide SCCS(ox), or the Cys and Sec in peptide GCUG(ox), as the interchange residue. Alignments were performed using the graphics program O (163). Each aligned conformation was evaluated for steric and electrostatic interactions. (Note: In the analysis below we have used the residue numbering for mTR3 as deposited for the structure 1ZKQ (35) to make it easier for the reader should they wish to view the PDB file. The authors of this deposited structure retained the mitochondrial leader sequence in their numbering system. For reference, this places Sec as residue 523 rather than residue 489.)

RESULTS AND DISCUSSION

Crystallization of TR.

In the methods section of this Chapter are the optimized conditions for crystallization of mTR3 and *Dm*TR. Both enzymes went through extensive screening to achieve these conditions and throughout the optimization process, some key trends and observations were made. The optimized conditions for mTR3 generated amazing crystal formation that could be observed in real time and resulted in extremely large crystals (**Figure 41**). It is expected that these crystals could be used for high-resolution studies in the future. The current space group is $I4_122$ and the data is 95 % complete at 2.25 Å with the current R_{free} at 31.7 % (**Table 15**). However, the mouse structure refinement was not completed, as it was published by another group (35). Therefore, this published structure was used for the analysis within this Chapter. The crystallization process for mTR3 did provide the groundwork to crystallize *Dm*TR in a much shorter time frame.

Both enzymes have several observations in common. The primary challenge was hypernucleation, usually in the form of long thin needles. An example of this effect is shown in **Figure 42**. Both enzymes preferred PEG 6000 as the precipitant with lower molecular weight PEGs resulting in either increased hypernucleation or no development and higher molecular weight PEGs typically resulting in precipitation of the protein rather than crystal formation. This effect could also be reduced by the addition of a small molecular weight PEG such as 1000 or the addition of ethylene glycol. These additives

were effective in the 1 % – 5 % range with the ethylene glycol being the most effective. The concentration of PEG 6000 could range from 18 % to 25 % with protein concentrations in the 20 – 30 mg/mL range. This high concentration could be achieved by increasing the NaCl to 300 mM in the protein dialysis buffer prior to concentrating. Lower protein concentrations resulted in hypernucleation.

An increase in buffer concentration was also a contributor to producing fewer and larger crystals. Most commercial screens begin with 100 mM buffer, but 150 – 200 mM buffer was most effective for these proteins. Both proteins preferred pH 5.5 and could form crystals with MES (preferred by mTR3), succinate (preferred by *DmTR*), or citrate as buffer. A decrease in pH inhibited crystal formation while an increase in pH increased the hypernucleation. Screens with pH > 7.0 most commonly resulted in either precipitation of the protein or conversion of the needles to clusters of a thin, hair-like morphology. Phosphate buffers were to be avoided as they often formed salt crystals, especially when screening with metal salts (often zinc or calcium) as the precipitant. As a result of this experience, the protein storage buffer was reduced to 10 mM phosphate buffer for crystallization samples. The final key to crystallization of these enzymes was a modified droplet ratio. It is typical to use equal volumes of reservoir solution and protein. The best crystal conditions for TR used reservoir solution at half the volume of the protein.

Cryoprotection was deemed necessary for diffraction of both proteins as room temperature capillary mounts were not suitably stable for the time to collect a data set, and as crystals of equal size were 1 – 2 Å higher in resolution when cryoprotected. The means of cryoprotection, however, was usually trial and error. Four different data sets

were collected for mTR3 and three were collected for *Dm*TR with each having different conditions. Each *Dm*TR condition contained ethylene glycol but the method varied from a single concentration soak for 5 or 10 minutes to the 2 % incremental additions used for the data set resulting in the final structure. The mTR3 conditions were a) increasing to 36 % PEG 6000, b) 30 % glycerol, c) 14 % ethylene glycol and d) 25 % ethylene glycol. This inconsistency in conditions resulted in the consumption of large numbers of crystals. Fortunately, crystals were not a limiting factor due to their rapid growth for both enzymes. However, for *Dm*TR especially, individual droplets had a limited lifespan once we began removing crystals. Upon accessing a droplet, precipitation of non-crystallized protein began to develop and the remaining crystals mottled. An individual drop could be used for 1 – 2 hours before the crystals became unusable.

Crystal Structure of TR from Drosophila.

A representative crystal used to collect the data is shown in **Figure 43**. The crystal belongs to the space group *R*32, has a single monomer in the asymmetric unit, and the physiological dimer is generated by the two-fold symmetry axis. The final model has an R_{free} of 24.7 % at a resolution of 2.4 Å (**Table 16**). Truncated *Dm*TR has 488 residues of which 8-488 were observed in the electron density and deposited in the final model (PDB 2NVK). Residues 487 and 488 showed weak density (**Figure 44**) and high B factors, which agrees with previous results where the electron density of the C-terminal tail containing the second redox active disulfide of the enzyme was either very weak or absent in the crystal structures of rat TR1 (36) and mTR3 (35). The overall fold is as expected for a GR family member with an N-terminal FAD-binding domain, a NAD(P)-

binding central domain, and C-terminal dimerization domain (**Figure 45**). The position of the FAD and NADP were verified during refinement by multiple iterations of annealing while omitting the cofactors. The enzyme has low affinity for the oxidized form of the NADP cofactor, which is evident in the crystal structure by the absence of clear density for the nicotinamide moiety and high B factors for the remaining atoms of the cofactor. The physiological dimer is generated by the crystallographic two-fold symmetry and is shown in **Figure 46**.

The *Dm*TR model has a RMS residual of 0.84 Å upon least squares superposition of the C α atoms to those of mTR3 (PDB 1ZKQ), 1.15 Å to rat TR1 (PDB 1H6V) (36), and 1.16 Å to human GR (PDB 1GRA) **Table 17**. A structural overlay of *Dm*TR and GR displaying the essential catalytic components of GR is shown in **Figure 47**. *Dm*TR shares 55 % sequence identity with mTR3 and the majority of sequence deviations are found on external loops, primarily in the NADP-binding domain. A distinct difference in the structures is observed at the interface where thiol-disulfide exchange takes place between the FAD-associated disulfide and the C-terminal disulfide motif of the adjacent monomer of TR. Helix 1 (residues 19-29), helix 3 (residues 97-121) and helix 6 (residues 335-347) compose the Rossmann fold helical face of the FAD-domain. Helix 1 contains the conserved Lys26, previously suggested as a potential anchor for the carboxyl terminus (36), while helix 2 contains the conserved active site sequence CVNVGC.

Helix 3 is of particular interest as the residues projecting toward the interface are each smaller compared to the mammalian enzymes containing Sec (**Figure 48A**). For *Dm*TR the residues are Val110, Thr114, and Asp117 as is the case for *A. gambiae* and *A. mellifera*, which have C-terminal sequences similar to that of *Dm*TR (TCCS and SCCS,

respectively). While valine occupies position 110 in *DmTR*, bulkier amino acids Leu or Ile are found at the equivalent position in mammalian TRs. Threonine114 of *DmTR* is replaced by either His or Tyr at this position in the mammalian enzyme (**Figure 48B**). The amino acid at position 117 is most variable when comparing sequences, Asp in *DmTR*, but is the bulkier Gln (numbered 146) in mTR3. Additionally in both mammalian TR structures (rat TR1 (36) and mTR3 (35)), these residues also project towards the interface.

In addition to residue substitutions in helix 3, the widening of the substrate-binding site is contributed to by the rotation of helix 3 away from the active site and towards the dimer interface. This is analogous to the rotation observed for the equivalent helix, **Figure 49**, in trypanothione reductase (TryR) when compared to GR for accommodation of the larger trypanothione substrate (37, 168). The movement is limited to turns 2-5 of the 6-turn helix from Asn105 to Leu118 (this is Asn134 to Leu147 in 1ZKQ) with a maximum shift of 1.68 Å at Val110. The source of this shift does not appear to be a function of residue substitutions at the packing between helix 2 and 3 but rather a packing interaction between His 106 in helix 3 and Phe404'. This residue is within the helix between strands 3 and 4 of the dimerization domain of the second molecule and follows a conserved bulky hydrophobic residue, which packs within the dimerization domain. While His106 is conserved in TR there is a Thr substituted for Phe 404' for the mammalian enzymes (Thr437' in 1ZKQ). His 106 was previously suggested to be a base catalyst for *DmTR* (36) however results from recent mutagenesis studies indicate a structural role instead (121).

Electrostatic Surface Potential of DmTR.

The electrostatic surface potential calculated for *DmTR* was compared to that of mTR3, rat TR1, and GR (**Figure 50**). The most electropositive was GR and the most electronegative was rat TR1 in the general ranking (+++) GR, mTR3, (-) *DmTR*, (---) rat TR1. While the three TRs show significant differences, neither shows significant electropositive potential at the GR substrate-binding pocket. This is significant in three areas. The first is in the lack of activity for TRs toward GSSG. The GSSG molecule contains four acidic groups that must be stabilized in the substrate-binding pocket for GR. The unsuccessful attempt in the literature to convert human TR1 to a GR by a 16 amino acid C-terminal truncation and mutagenesis concluded the failure to do so was due to the negative electrostatic potential of TR (149). This conclusion is consistent with the equivalent observation in *DmTR*.

The second point is in reference to the loss in activity reported upon mutation of the serines in the *DmTR* motif to aspartic acids (65). Each of the mutants, DCCG, GCCD, and DCCD showed less activity than the GCCG mutant. Firstly, increasing the local negative charge surrounding and electron transfer step is expected to be unfavorable. Second, this introduction of local charge at an already electronegative active site would be less favorable as well.

The final area of significance is the difference in DTNB reductase activity observed for truncated forms of TR. Truncated mTR3 shows very high DTNB reductase activity (856 min^{-1}), which is 60 % of the wild type activity. The truncated *DmTR* shows good activity (178 min^{-1}), which is nearly identical to the wild type activity. These results

are in stark contrast to that reported for truncated forms of human TR1 (149) and mutant rat TR1 (109) which show very low DTNB reductase activity (33 min^{-1} and 63 min^{-1} respectively) that are $<5 \%$ of the respective wild types. DTNB, like GSSG, is a negatively charged substrate with a carboxylic acid group on each TNB-. Upon reduction of the DTNB disulfide, the low pK_a of the TNB thiolate means it will be unprotonated. This results in a significant generation of local negative charge during the reaction. The activity trends for DTNB with the truncated TRs follow the electronegativity trends where mTR3 is the least electronegative and has the highest activity while rat TR1 is the most electronegative and has the least activity. Similar results have been recently reported for the reactivity of a reversible disulfide on the surface of yellow fluorescent protein with GSSG (169). Engineering of a more positive electrostatic surface by mutagenesis of three local surface residues to Arg resulted in a 13-fold increase in the rate of thiol-disulfide exchange for the negatively charged GSSG but very little change in the reactivity towards the neutral substrate HED (2-mercaptoethanol in disulfide form) or the positively charged substrate cysteamine disulfide (169). Therefore, the increase in K_m for DTNB as well as the difference in activities between mutant forms of different TRs could be explained by comparing differences in the active site surface electrostatic potentials. This is further supported by the observed increase in DTNB efficiency upon neutralization of the C-terminal carboxylate in mTR3.

Alignment of Tetrapeptides with GSSG.

One of the key questions in the TR mechanism is how the C-terminal redox dyad is reduced by the N-terminal redox center on the opposite subunit. The C-terminal redox

center is either a Cys-Cys or Cys-Sec dyad as we have introduced earlier. Our analysis begins with the known conformations of a Cys-Cys(ox) dyad (which are rare in protein structures) that have been reported previously. For example, the solution structure of Ac-Cys-Cys-NH₂(ox) has been examined by NMR spectroscopy and found to exist as a mixture of four different conformers (58, 170). These conformers are designated as C⁺, C⁻, T⁻, and T'⁻. The designations “C” and “T” represent the geometry of the peptide bond as either *cis* or *trans*, whereas the designations “+” and “-” refer to the helicity of the disulfide bond. It was found that peptide Ac-Cys-Cys-NH₂(ox) also had a second T-conformer that is defined by a larger separation of C α atoms and this peptide was designated as T'⁻. Our NMR solution studies of peptides Ac-SCCS(ox), Ac-GCCG(ox), and Ac-GCUG(ox) also show that the same four major conformers described by Reitz and coworkers are also the major conformers of these three peptides which are summarized in **Table 18** (Deker and Hondal, unpublished).

The observation that oxidized tetrapeptides can serve as substrate for the truncated forms of TR demonstrate that TR, like GR, may be considered a disulfide oxidoreductase where its own C-terminus is the cognate substrate. Using this relationship and the available structures for GR, we started by asking the question: which of the four known conformers of Cys-Cys(ox) aligns with GSSG in the GR structure? We therefore aligned the four known conformations of peptide Ac-SCCS(ox) to the thiol-disulfide interchange step observed in GR (34). The formation of the mixed-disulfide between Cys57 and a Cys from the C-terminus of the second molecule of TR in the *Drosophila* homodimer would represent the binding of GSSG in GR (PDB 1GRA) and the formation of the subsequent mixed-disulfide intermediate (PDB 1GRE). We

hypothesize that this step, interchange, is to be structurally and biochemically conserved between GR and TR. The comparison of these two GR structures shows the primary difference is the movement toward each other of the interchange Cys (Cys58 of GR) side chain and the Cys side chain from GSH I. Using GSH I of GSSG as a reference (**Figure 47**), each tetrapeptide was fit such that the position and angle of the cysteines involved in the interchange step were equivalent.

Altogether, we evaluated eight possible orientations for a given tetrapeptide in the active site of TR because each of the four conformations can be overlaid with the sulfur atoms of GSSG in two different orientations (by rotation of 180°), which would either place the N-terminal Cys in the interchange position or the C-terminal Cys in the interchange position. To form the interaction between the C-terminal carboxylate and Lys29 in rat TR1 (Lys26 in *Dm*TR or Lys56 in 1ZKQ) proposed by Sandalova (36), the C-terminal Cys or Sec must be in the interchange position. For each of the alignments, no additional electrostatic interactions or hydrogen bonds are predicted without requiring significant changes of the peptide positioning such that the chemistry is unlikely to occur. This is not unexpected as: 1) the C-terminal tail is quite mobile, 2) is normally covalently attached to the protein and likely does not require binding contacts (demonstrated by the peptide assays), and 3) even in GR, most of the contacts with the GSSG substrate are water mediated (see Chapter 1) only a few interactions are direct contacts.

Upon alignment of the sulfur atoms of peptide SCCS(ox) with the sulfur atoms of GSSG, it is clear that peptides in the C⁺ conformation place the leaving group Cys (C-terminal Cys) in a favorable position for protonation from His464' (His467' in GR, His497' in mTR3, see **Figure 51A**). This histidine has been shown to be essential for GR

(88) and proposed as a conserved acid/base catalyst throughout the protein family (97, 168) including TR (93, 99). Maintaining the interchange position and angle for the *trans* (T- and T'-) peptides, however, results in a rotation of the leaving group Cys by approximately 90° (**Figure 51B**) as is also observed for the C- conformation. This moves it away from His464' by increasing the distance from 3.5 Å to 5.1 Å and to an angle not reasonable for protonation. In order to align the C-terminal sulfhydryl of peptide SCCS(ox) in the T- conformation with the GSH II Cys so that it would be in a favorable position for protonation from His464', the interchange cysteine (N-terminal Cys of SCCS(ox)) must be rotated away from the interchange residue (Cys57). **Therefore, for protonation of the first leaving group by His464', the ring must be in the C+ conformation.**

Figure 52 models the interface between subunits where the oxidized tetrapeptide would be reduced by the N-terminal redox center in *Dm*TR and mTR3, respectively. As can be seen in the Figure, the binding pocket for the oxidized tetrapeptide is significantly larger in the case of *Dm*TR (**Figure 52A**) compared to that of mTR3 (**Figure 52B**). This larger binding pocket in *Dm*TR can accommodate the larger size of the C+ conformer of the SCCS(ox) tetrapeptide. The distance from the NH of the N-terminal Cys to the CO of the C-terminal Cys is larger in the C+ conformer than in the T- conformer. In addition, the larger binding pocket of *Dm*TR can also more easily fit the bulkier side chains of Ser. The T- conformer is much more compact and forms a tight turn structure that is better accommodated in the binding pocket of mTR3.

Using this same analysis with the mTR3 structure published by Biterova *et al.* (35) (PDB 1ZKQ) using our NMR structures of GCUG(ox) (Deker and Hondal,

unpublished), we find that GCUG(ox) in the T- conformation with Cys in the interchange position appears to be the most favorable conformation for interchange with Cys86 from chain A. *With Sec oriented in the interchange position*, an unfavorable interaction with the carbonyl from the adjacent Cys residue occurs with His497', but we would like to emphasize that we cannot rule out the T- orientation with Sec in the interchange position. The fit of the GCUG(ox) tetrapeptide in the binding pocket of mTR3 is shown in **Figure 52D**. A surface representation of tetrapeptide SCCS(ox) in the C+ conformation docked in the binding pocket of *DmTR* is shown in **Figure 52C** for comparison. A stereo diagram of tetrapeptide GCUG(ox) in the C+ conformation positioned in the binding pocket of mTR3 is shown in **Figure 53**. This stereodiagram clearly shows the steric clashes from the residues of helix 3 that makes this a poor fit in the binding pocket.

The peptides $GC_D C_L G$ and $GC_L C_D G$ fall into structural classifications different than the other peptides. Introduction of the *D*-form amino acid in either position results in a rigid structure that is 100% in a single conformation. Placing *D*-Cys in the first position results in a T- like conformation while placing it in the second position results in a T+ like position. As seen in **Figure 54A**, the *D-L* peptide is more compact and fits at the reaction interface while the *L-D* peptide shown in **Figure 54B** is very elongated and is not well fit to the reaction interface.

Structural Explanation for the Peptide Complementation Data.

In the mammalian enzyme, replacement of Sec with Cys greatly impairs this ring opening step as can be seen in **Table 12 Chapter 4**. For example, the ratio of turnover rates for peptides Ac-SCUS(ox) and Ac-SCCS(ox) is 511 fold, which is similar to the

308 fold difference between peptides Ac-GCUG(ox) and Ac-GCCG(ox). These data strongly support our hypothesis that the ability of mTR3 to protonate the leaving group in the ring opening step of the catalytic cycle is greatly impaired compared to *DmTR*. Our interpretation that proton transfer to the leaving group is partially rate limiting is in agreement with conclusions made about the GR mechanism, where proton transfer from His467' to the thiol of GSH II has also been shown to be partially rate limiting (94, 95).

In *DmTR*, the presence of a Sec residue does not radically alter the rate of ring opening as it does for mTR3. For example, if we compare the ratio of turnover rates for peptides Ac-SCUS(ox) and Ac-SCCS(ox) we see only a 5.65 fold difference. This ratio is increased to 36 fold when comparing peptides Ac-GCUG(ox) and Ac-GCCG(ox). A 24 fold increase is observed for *DmTR* when the effect of flanking residues of the tetrapeptide motif is examined by comparing the ratio of turnover for peptides Ac-SCCS(ox) and Ac-GCCG(ox). In the mammalian enzyme, the presence of flanking serine residues on either side of the Cys-Cys or Cys-Sec dyad only slightly (3-6 fold) improves the activity (**Table 13 Chapter 4**). These data indicate that the ability of *DmTR* to protonate the leaving group is not impaired, *as is the case for the mammalian enzyme*, since it allows for the C⁺ conformation. This interpretation provides a better answer to the question as to why DTNB is a substrate for TR and cystine is not. Since *DmTR* can utilize cysteine in the SCCS or GCCG motif, the final piece of the answer is the structure. Both DTNB and cystine are linear intermolecular disulfides. A linear molecule is not likely to be able to adopt the C⁺ type conformation conferred by the intramolecular vicinal disulfide ring, which is why DTNB with its low pK_a is a substrate but cystine is not.

When this data is put in context with the structural data, we can explain the loss of activity when Sec is replaced with Cys in the mammalian enzyme and why Cys-containing TRs (such as *Dm*TR) can function with high activity. *Dm*TR has a more open, interfacial active site than the mammalian enzyme. The residues from helix 3 proximal to the FAD-associated active site are less bulky to more freely accommodate the hydroxyls of the adjacent serines (SCCS). The increase in the available space is also likely to make the enzyme more amenable to the conformational switching of the SCCS(ox) peptide from T- (*trans*) to C+ (*cis*) necessary to protonate the leaving group cysteine during interchange. The GC_DCLG(ox) peptide, due to its rigid nature, is likely to require extra space for rearrangement rather than a simple ring flip to receive the proton from His464'. This would account for the lower activity in *Dm*TR compared to Ac-GCCG(ox) and lack of activity with mTR3. In contrast to *Dm*TR, the mammalian TRs have evolved a more restricted active site by incorporating bulkier residues on helix 3. This smaller active site shows a steric preference for Gly compared to Ser and was unable to accommodate either peptide in the C+ conformation without requiring significant rearrangement of the active site. Exclusion of the C+ conformation would make Sec essential as the first leaving group in the ring opening step for mTR3.

Other crystallization trials.

Several other crystallographic approaches to study TR were investigated but are currently without success. The structure reported in this Chapter is of the truncated form of *Dm*TR used in the peptide complementation studies, as was the case for the mTR3 structure. As indicated previously, the available TR structure from rat (1H6V) (36) and

mouse (1ZKQ) (35) do not have structural information for the C-terminus. Crystallization of the semisynthetic mTR and the wild type *Dm*TR was attempted but have yet to produce diffraction quality crystals. In the case of mTR3, clusters of thin, hair-like quasi-crystals developed. Attempts to further evaluate these were limited by material.

With *Dm*TR, the starting material is not limiting but issues with hypernucleation and rapid needle formation are currently hampering diffraction quality crystal development. Variations in buffer, PEG, pH, additives, and protein concentration that were successful with the truncated forms have not been useful with the full length enzyme. The addition of reducing agent or NADPH has also been explored and did partially reduce the hypernucleation, but this is counter to the aims of this project as it is the oxidized form of the C-terminus that we are interested in.

Co-crystallization and soaking-in experiments have been explored with mTR and the peptide CUG(ox). Data sets were collected and difference Fourier did not reveal any bound peptide. These experiments are hampered by the low solubility of the mammalian motif and the low affinity the enzyme shows for the small peptide, as discussed in the previous Chapter. Not only are high concentrations of peptide required to saturate the enzyme, but the low affinity also means it is likely to be displaced by the cryoprotectant. The results from these experiments and absence of the C-terminus from the previously published TR structures demonstrates the significance of using the peptide complementation approach to establish a GR-like system for TR. Establishing this GR – truncated TR relationship demonstrates the relevance of the peptide modeling.

As indicated in the Introduction, there is no structural or biochemical information on the interaction between TR and Trx. Co-crystallization of mTR3 with Trx was briefly

investigated. The crystals and a SDS-PAGE gel are shown in **Figure 55**. Addition of Trx to the droplet resulted in beautiful crystals (**Figure 55A**) but the Trx remained in the droplet (**Figure 55B**). Formation of a covalent complex was also investigated, as was done for TR from *E. coli* (49, 171). Following this previous work, we cloned the Trx active site mutant Cys32-Gly-Pro-Ser (wild type is Cys32-Gly-Pro-Cys) and the C-terminal mTR mutant Gly-Ser-Cys-Gly. The Cys32 in Trx is reacted with DTNB to form a Trx-TNB mixed disulfide, which can be attacked by the C-terminal Cys in the mTR3 mutant to form the complex. After many variations of this experiment, only Trx dimer and no complex was observed. It was concluded that several side reactions could be occurring. We first demonstrated that the truncated mTR3 reduced the Trx-TNB disulfide via the N-terminal active site. Secondly, depending on the redox state of mTR3 several other mixed disulfides could form to prevent the desired complex.

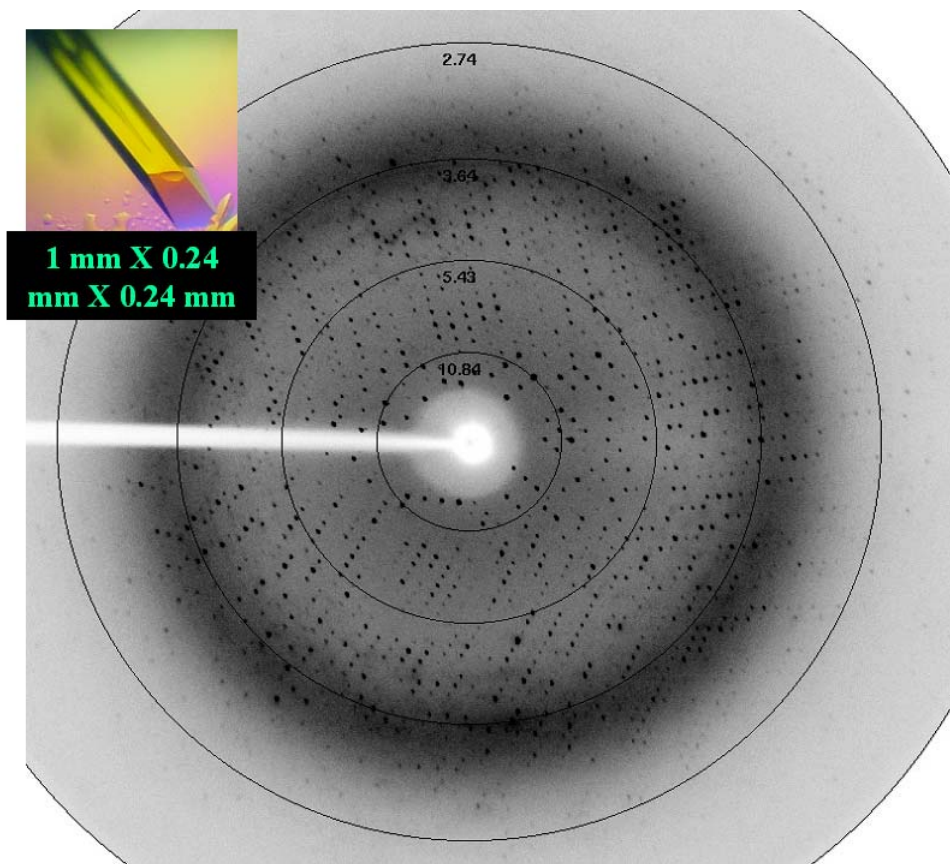


Figure 41. Crystal of mTR3 with x-ray diffraction pattern.

The space group currently used in refinement is $I4_122$. The data processed to >95 % complete at the limit of the range collected, 2.25 Å.

Table 15. Crystallographic statistics for ^amTR3-G.

Cell Parameters	
space group	I4 ₁ 22
a, b, c (Å)	110.509 110.509 208.025
Data Collection Statistics	
resolution range (Å)	15 – 2.25
unique reflections	29,494
completeness (%)	95.6 (95.4)
redundancy	5.23
R_{merge}^b (%)	8.1
I/σ	21.3 (6.6)
Model Statistics	
R_{work}^c	28.3
R_{free}^d	31.7
# Atoms, non-hydrogen	
Protein	3679
Ligand	53
r.m.s. deviation, bonds (Å)	0.008
r.m.s. deviation, angles (°)	1.08
Ramachandran plot (%)	
most favored regions	86.3
additionally allowed	12.7
generously allowed	1.0
disallowed regions	0.0

^aMouse mitochondrial TR missing the C-terminal tripeptide Cys-Sec-Gly.

^b $R_{\text{merge}} = \frac{\sum \sum |I(h)_j - \langle I(h) \rangle|}{\sum I(h)}$, where $I_{(h)j}$ is the j th measurement of diffraction intensity of reflection h and $\langle I(h) \rangle$ is the average intensity of reflection h for all j measurements.

^c $R_{\text{work}} = \frac{\sum (|F_o| - |F_c|)}{\sum |F_o|}$.

^d R_{free} is calculated using a test set of 10% of the reflection excluded from refinement

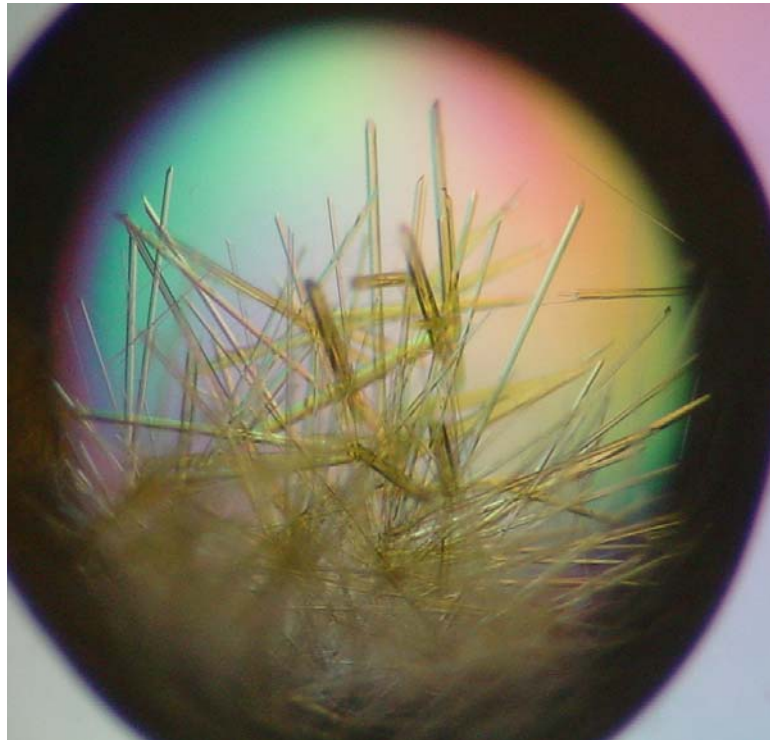


Figure 42. Hypernucleation of TR crystals.

Example of the hypernucleation in the needle form seen for mTR3 (shown) and *Dm*TR.

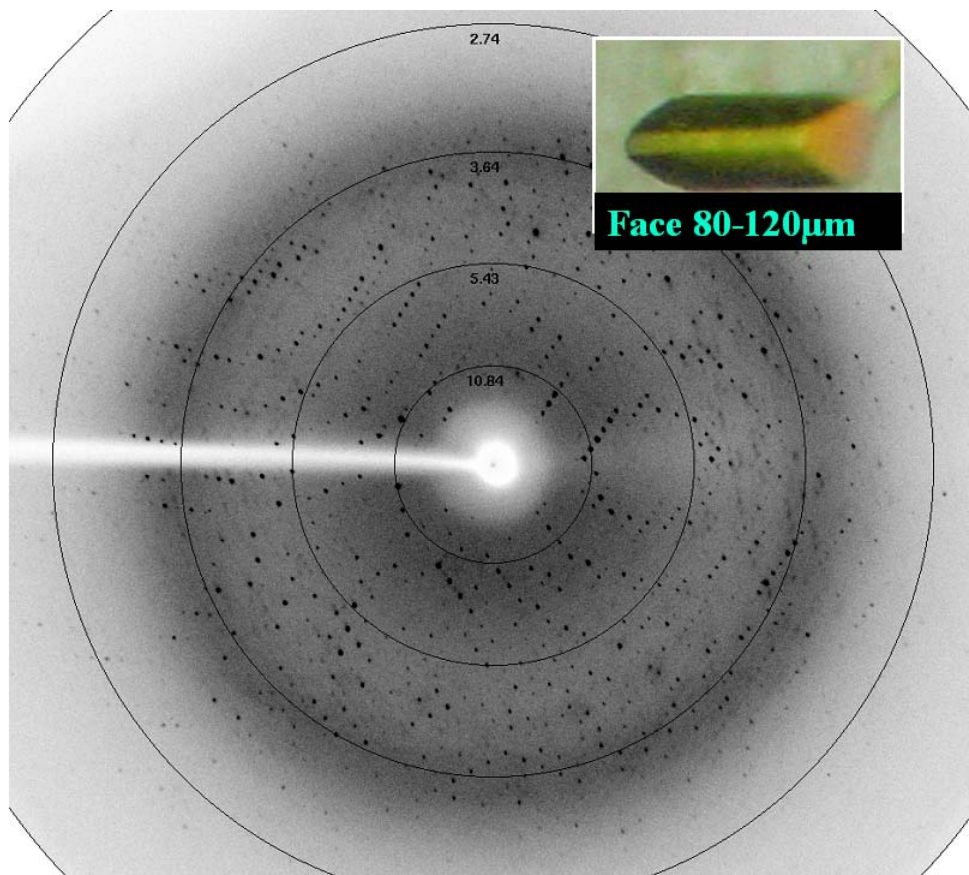


Figure 43. Crystal of *DmTR* with x-ray diffraction pattern.

The crystal and diffraction pattern for the structure of *DmTR* solved at 2.4 Å resolution ($R_{work} = 19.8\%$, $R_{free} = 24.7\%$).

Table 16. Crystallographic statistics for ^a*Dm*TR-S.

Cell parameters	
space group	<i>R</i> 32
	151.487
a, b, c (Å)	151.487
	134.259
Data collection statistics	
wavelength (Å)	1.5418
resolution range (Å)	15 – 2.4
unique reflections	22,987
completeness (%)	98.7 (90.3)
redundancy	7.85
R_{merge} (%) ^b	5.9
I/σ	36.8 (2.8)
Molecular replacement search models	1H6V
Model statistics	
Resolution (Å)	15 – 2.4
R_{work} ^c	19.8
R_{free}	24.7
Refined model	
# amino acid residues	480
# FAD molecules	1
# NADP molecules	1
# Water molecules	121
# Atoms, non-hydrogen	
protein	3684
ligand	92
r.m.s. deviation, bonds (Å)	0.011
r.m.s. deviation, angles (°)	1.359
Ramachandran plot (%)	
most favored regions	89.0
additionally allowed	9.6
generously allowed	0.7
disallowed regions	0.7
Average B-factor (Å ²)	49.14
Range of B-factors (Å ²)	39.6 – 95.7

^a*Drosophila melanogaster* TR missing the C-terminal tripeptide Cys-Cys-Ser.

^b $R_{\text{merge}} = \frac{\sum \sum |I(h)_j - \langle I(h) \rangle|}{\sum I(h)}$, where $I_{(h)j}$ is the j th measurement of diffraction intensity of reflection h and $\langle I(h) \rangle$ is the average intensity of reflection h for all j measurements.

^c $R_{\text{work}} = \frac{\sum (|F_o| - |F_c|)}{\sum |F_o|}$.

^d R_{free} is calculated using a test set of 10% of the reflection excluded from refinement

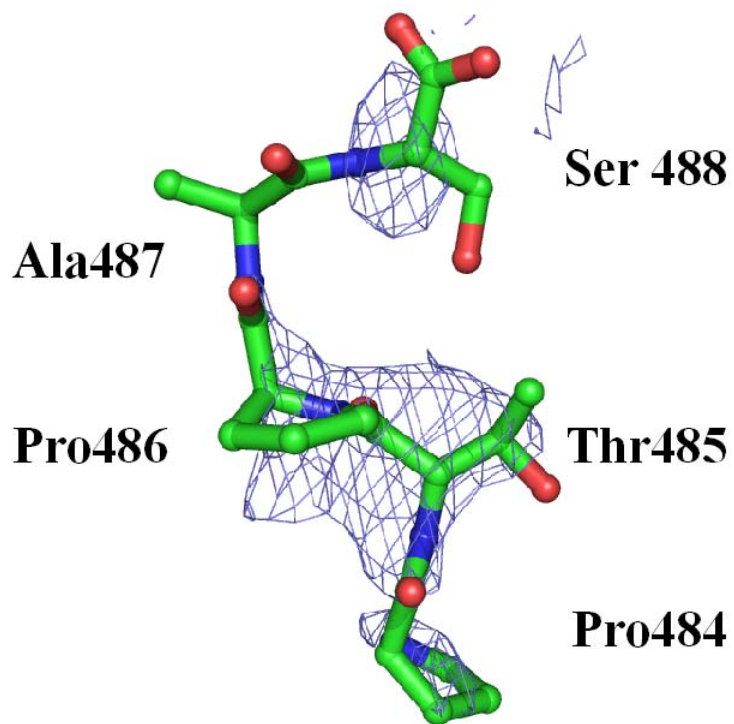


Figure 44. Omit density map for *DmTR* C-terminus.

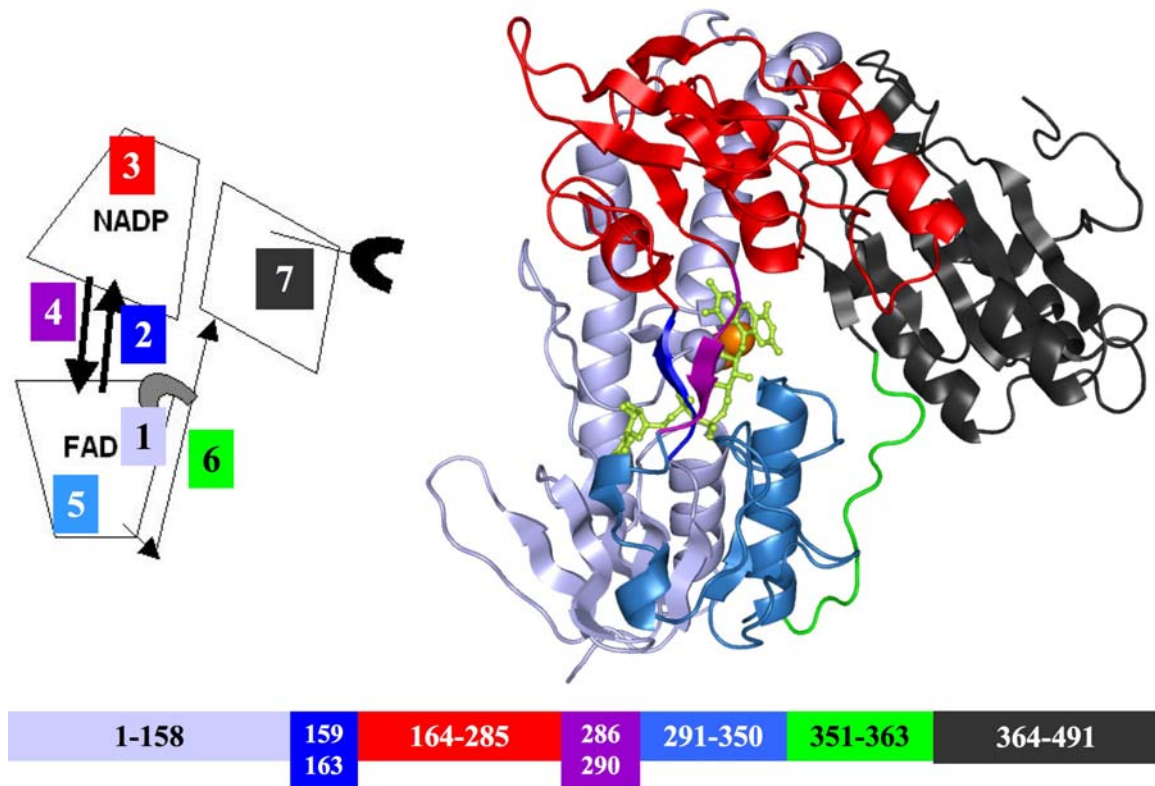


Figure 45. The crystal structure of *DmTR*.

The figure shows a cartoon representation of TR (left), the structure of *DmTR* (right), and the protein sequence (bottom). The color-coding correlates the linear sequence to segments in the structure. The description of TR is simplified three-domain architecture. The dimerization domain (black) is continuous with the sequence while the FAD binding domain and NADP binding domain are not. For example, segment 1 extends beyond the NADP binding domain and contributes to the dimerization interface and segment 5 is within the FAD binding domain but is C-terminal to the NADP binding domain.

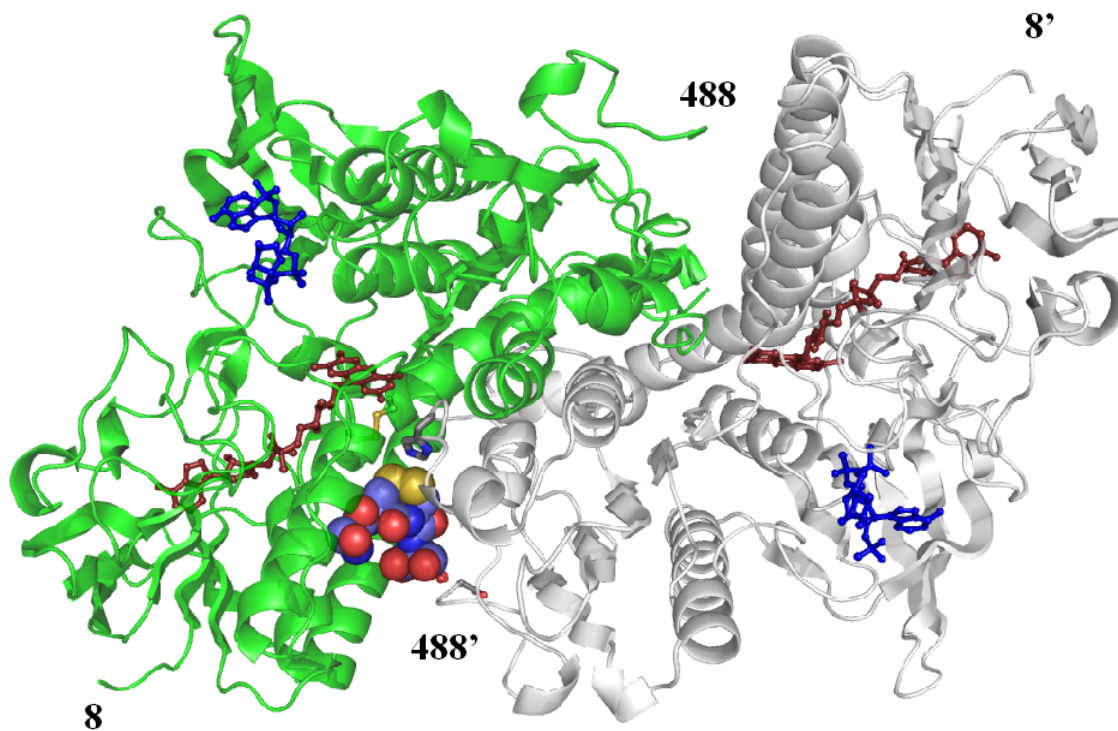


Figure 46. The homodimeric model of *DmTR*.

The homodimeric model of *DmTR* with chain A in green and chain B in gray. The SCCS(ox) tetrapeptide in the C+ is oriented with Cys489' as the interchange and shown in space-filling model. The NADP without the nicotinamide moiety is indicated in blue, the FAD in dark red. The prime designation for residue numbers indicates the B chain of the TR homodimer.

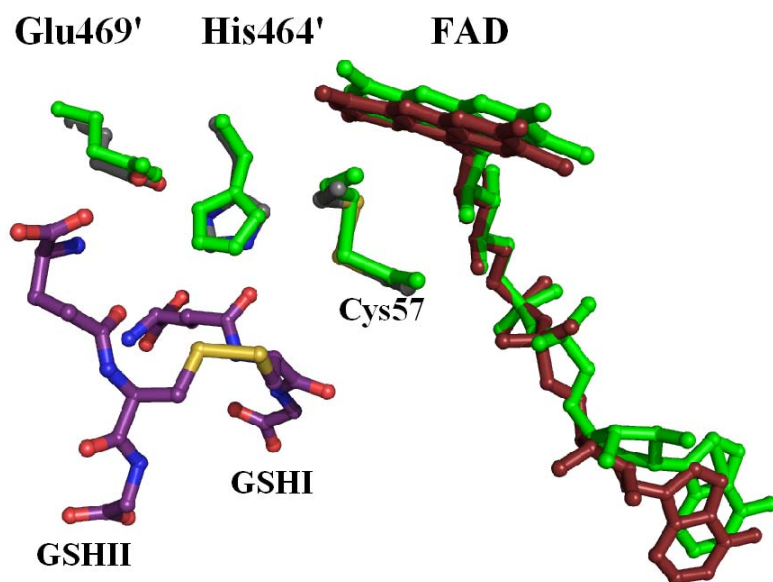


Figure 47. Structural alignment of *DmTR* and GR.

Structural alignment of Glutathione Reductase (1GRA) (34) and *DmTR* (Green). The residue numbers are for *DmTR*. Essential catalytic components are shown along with GSSG in purple

Table 17. Least squares structural comparison of the ^aGR family.

Structure 1	Structure 2	^b R.M.S.D. Å
^c <i>Dm</i> TR	^d mTR3 (1ZKQ)	0.84
<i>Dm</i> TR	^e Rat TR1 (1H6V)	1.15
<i>Dm</i> TR	GR (1GRA)	1.16
<i>Dm</i> TR	^f TryR (1BZL)	1.23
GR	TryR	1.09

^aGlutathione Reductase (34).

^bC-alpha deviation.

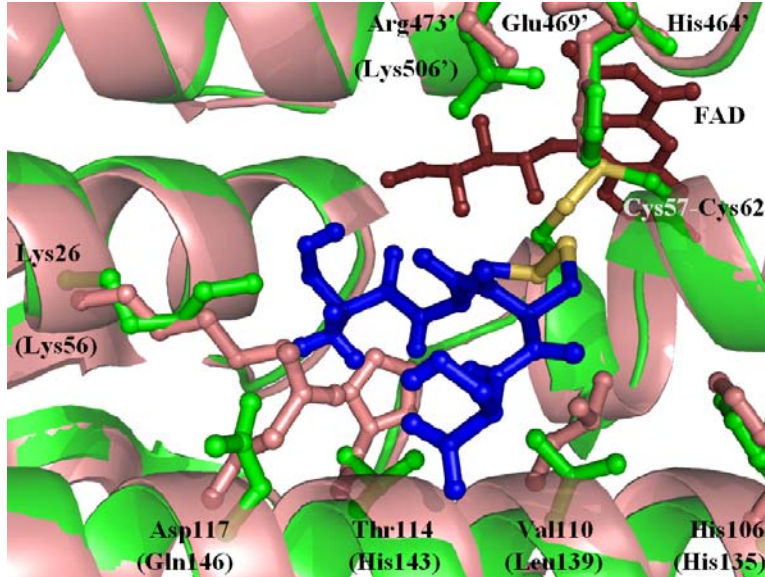
^c*Drosophila melanogaster* TR.

^dMouse mitochondrial TR (35).

^eRat cytosolic TR (36).

^fTrypanothione reductase (37).

A.



B.

	106	110	114	117	404	
<i>Dm</i> TR1	HKL	VQSVQ	NHIKSV	NWVTRV	DLRDK	PTEFFIP
<i>Am</i> TR	EAL	RtavQ	NHVKS	VNwvtr	VELRTK	PTEFFIP
<i>Ag</i> TR	ATL	TESVQ	NHIKSV	NWVTRV	DLRDQ	PTEFFIP
<i>Mm</i> TR3	KTMAE	AVQN	NHVKS	SLNWG	HRVQLQDR	PLEFTVA
<i>Hs</i> TR2	RKMAE	AVQN	NHVKS	SLNWG	HRVQLQDR	PLEFTVA
<i>Rn</i> TR1	EKMTE	SVQN	NHIGSL	NWGYR	VALREK	PLEWTVP
<i>Ce</i> TR1	NHLRDS	VQDHI	ASLNW	GYRVQL	REK	PLEYTIS

Figure 48. Tetrapeptide binding pocket ribbon overlay.

Panel A is a close-up view of the SCCS(ox) tetrapeptide (blue) in the C+ conformation with Cys 489' as the interchange residue positioned in the *Dm*TR structure (green) with an overlay of the mTR3 (PDB 1ZKQ) (35) colored in salmon. The residues for mTR3 are indicated in parentheses. **Panel B** is a multiple sequence alignment generated with ClustalW (131) with either the PDB ID or accession number in parentheses. The sequences are TR1 from *D. melanogaster* (AF301144_1), TR from *A. mellifera linguistica* (AAP93583.1), TR from *A. gambiae* (CAD30858.1), TR3 from *M. musculus* (PDB 1ZKQ), TR2 from *H. sapiens* (Q9NNW7), TR1 from *R. norvegicus* (PDB 1H6V), and TR1 from *C. elegans* (AF148217_1). The alignment shows helix 3 from Chain A along with the loop from the dimerization domain of Chain B. The numbering is in accordance with the TR from *Drosophila*.

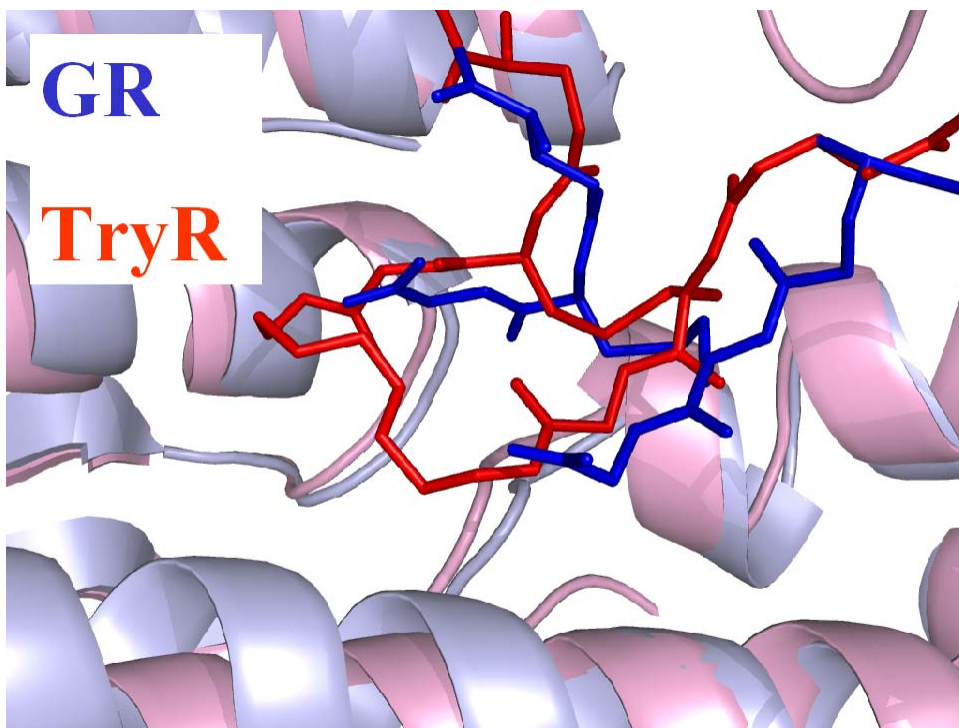


Figure 49. GR, TryR structural overlay.

Structural overlay of glutathione reductase in blue/light blue (1GRA) (34) and trypanothine reductase (1BZL) (37) red/pink. The view is identical to the previous figure demonstrating the equivalent helical shift to accommodate the larger trypanothine substrate vs. GSSG.

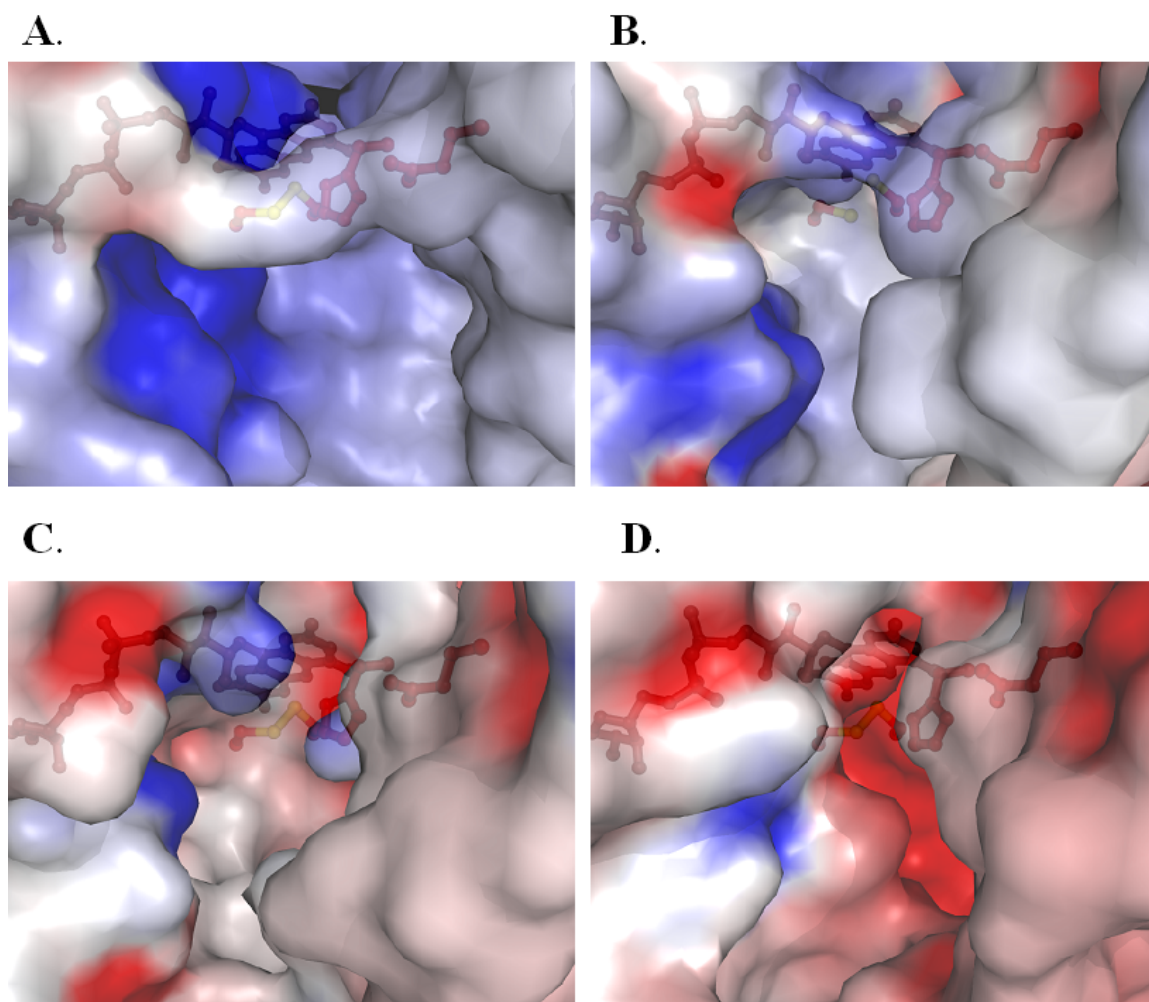


Figure 50. Electrostatic surface potentials.

Electrostatic surface potential showing a close-up of the reaction interface where thiol-disulfide exchange occurs between the conserved N-terminal dithiol and the C-terminal tetrapeptide of TR or the GSSG substrate for GR. A) GR (1GRA) (34); B) mTR3 (1ZKQ) (35); C) *Dm*TR; D) rat TR1 (1H6V) (36).

Table 18. Tetrapeptide conformer distribution.

Conformer distributions (%) determined by NMR for oxidized tetrapeptides (Deker and Hondal unpublished results).

^a Conformer	Ac-GCUG	Ac-GCCG	Ac-SCCS
C+ ^b	9	33	47
C-	0	6	5
T-	70	47	40
T- ^c	21	14	8

^aThe orientation of the peptide bond between the Cys-Cys or Cys-Sec dyad can be *cis* (C) or *trans* (T).

^bThe helicity (+ or -) of the disulfide bond.

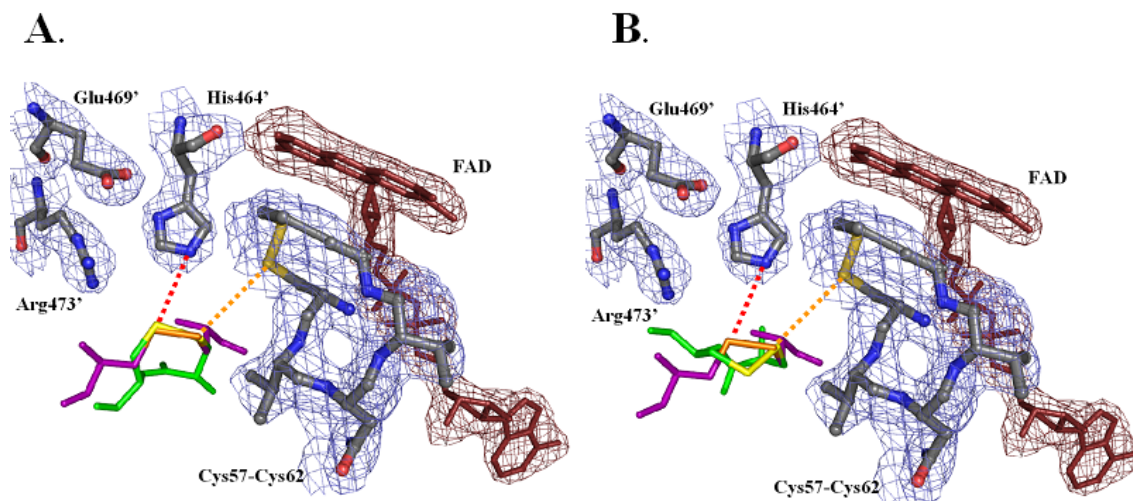


Figure 51. SCCS(ox) aligned with GSSG.

Alignment of the tetrapeptide SCCS(ox) in the structure of TR from *Drosophila*. The tetrapeptide structures were determined by NMR spectroscopy and placed in the active site of TR in accordance to the position of GSH I (the interchange position) in the GR structure (PDB 1GRA). Shown is the FAD cofactor (dark red) and the helical loop of the conserved active site sequence CVNVGC, which are components of chain A. Also shown is Arg473' from the B chain as well as His464' and Glu469', which are analogous to His467' and Glu472' in GR. The oxidized C-terminal disulfide of the B chain is reduced by the FAD-associated disulfide of the A chain during the enzymatic cycle. The residues from TR are in gray, oxidized glutathione is in purple, the tetrapeptide is in green, and omit electron density for the 2.4 Å structure is shown. Cys57 of *Dm*TR is in position for interchange with GSH I and the Cys489 of the SCCS(ox) tetrapeptide, which is indicated by the orange dashed line. Glutathione II is in position from protonation from His464' as is Cys490' of the SCCS(ox) tetrapeptide when in the C⁺ conformation (**Panel A**), but not when in the T- conformation (**Panel B**) as indicated by the red dashed line. Only the cysteines for the SCCS(ox) peptide and GSSG are shown for simplicity.

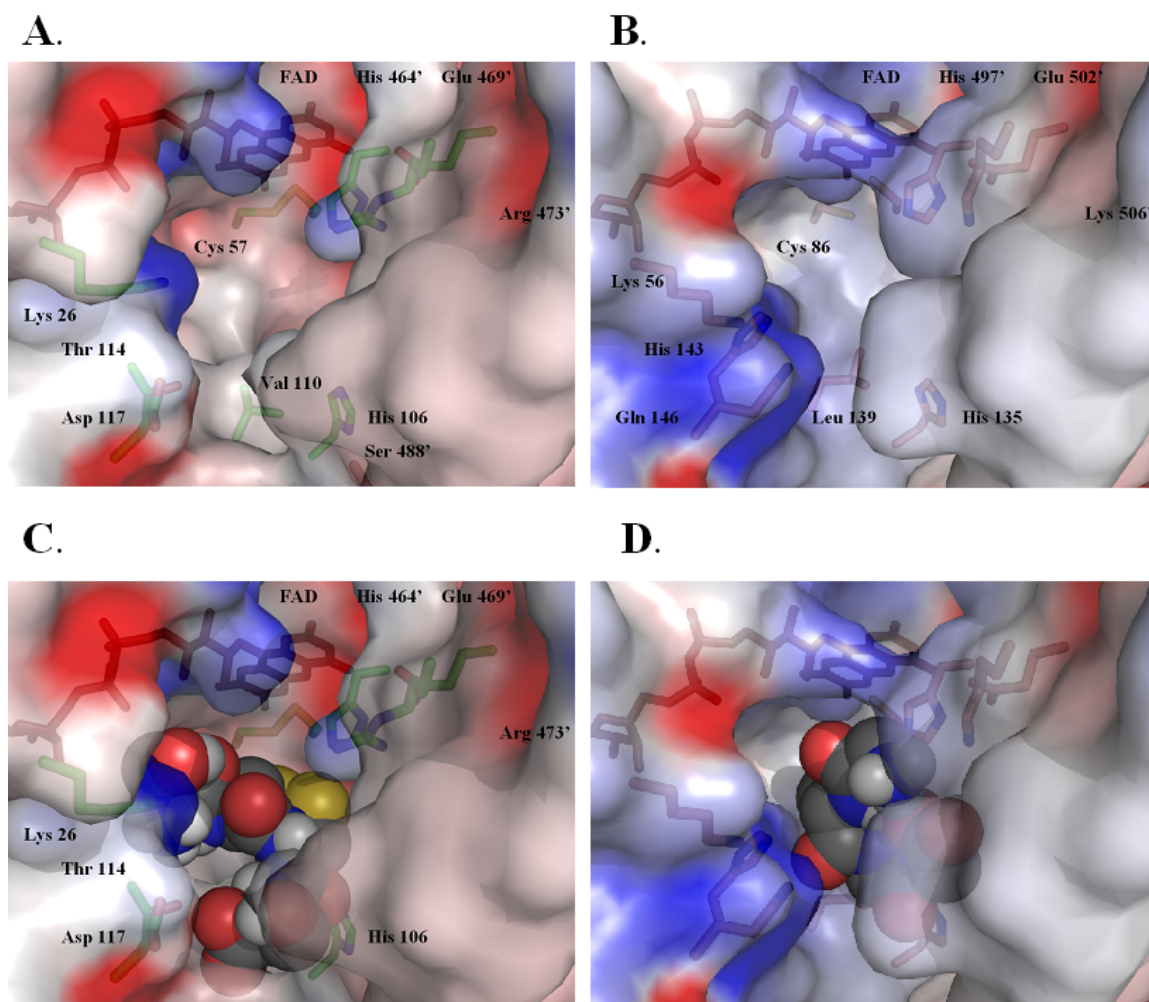


Figure 52. *DmTR* and mTR3 surface potentials with peptide fits.

Electrostatic surface potential calculated using for TR showing a close-up of the reaction interface where thiol-disulfide exchange occurs between the conserved N-terminal dithiol and the C-terminal tetrapeptide of the adjacent subunit containing the 8-membered ring that must be opened during redox cycling. (A) Interface for *DmTR*; (B) Interface for mTR3 (PDB 1ZKQ) (35); (C) The tetrapeptide SCCS(ox) in the C⁺ conformation with Cys489' in the interchange position for *DmTR*; (D) The tetrapeptide GCUG(ox) in the T-conformation with Cys522' in the interchange position for mTR3.

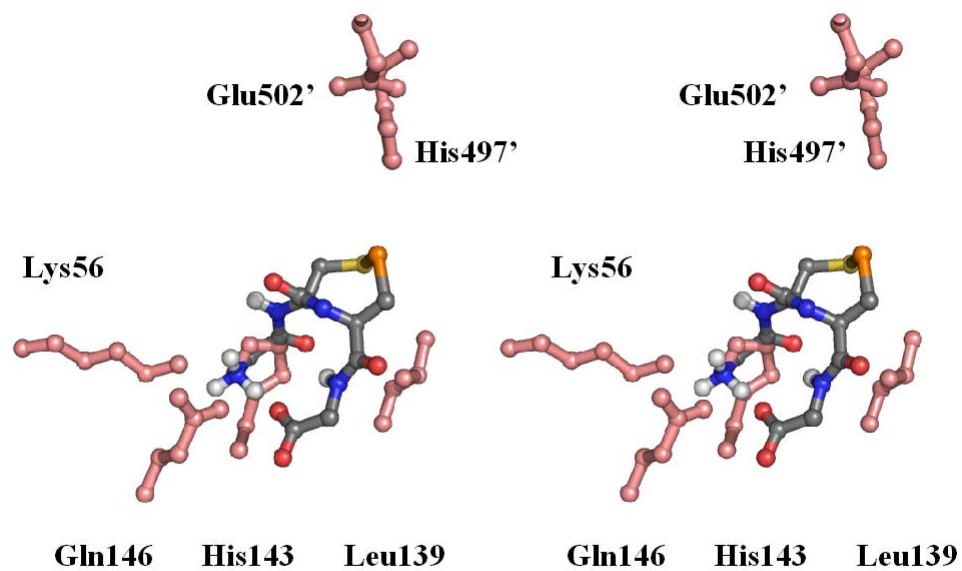


Figure 53. Stereo-view of mTR3 with GCUG(ox) C+.

Stereo diagram for mTR3 (PDB 1ZKQ) (35) showing residues from helix 3 along with the tetrapeptide GCUG(ox) in the C+ conformation with Cys522' (sulfur in yellow) in the interchange position and Sec523' (selenium in orange) in the leaving group position..

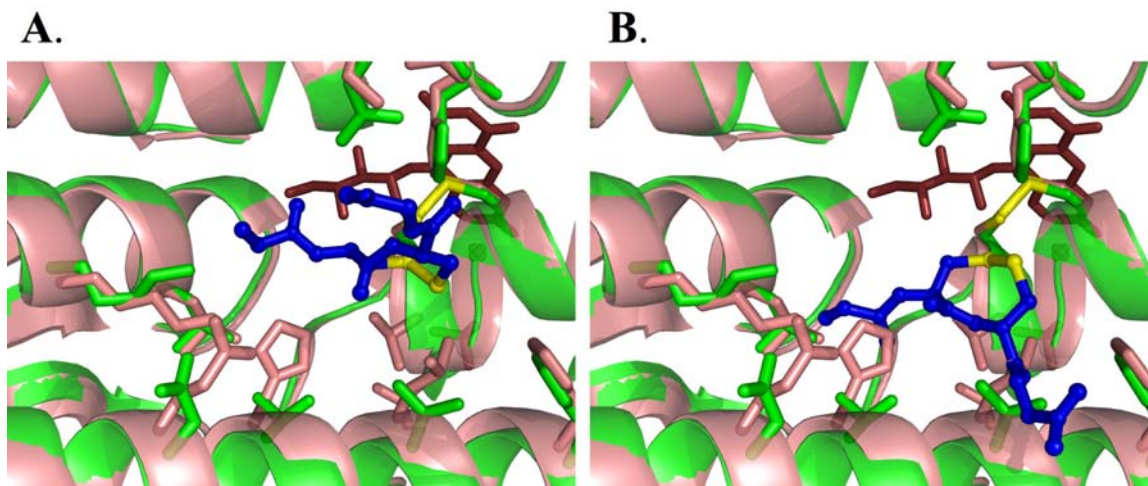


Figure 54. Ribbon view of GC_DC_LG(ox) and G C_LC_DG(ox) fits.

Alignment of the tetrapeptides GC_DC_LG(ox) (A) and G C_LC_DG(ox) (B) in the active site of mTR3 (Salmon) (35) and *Dm*TR (green).

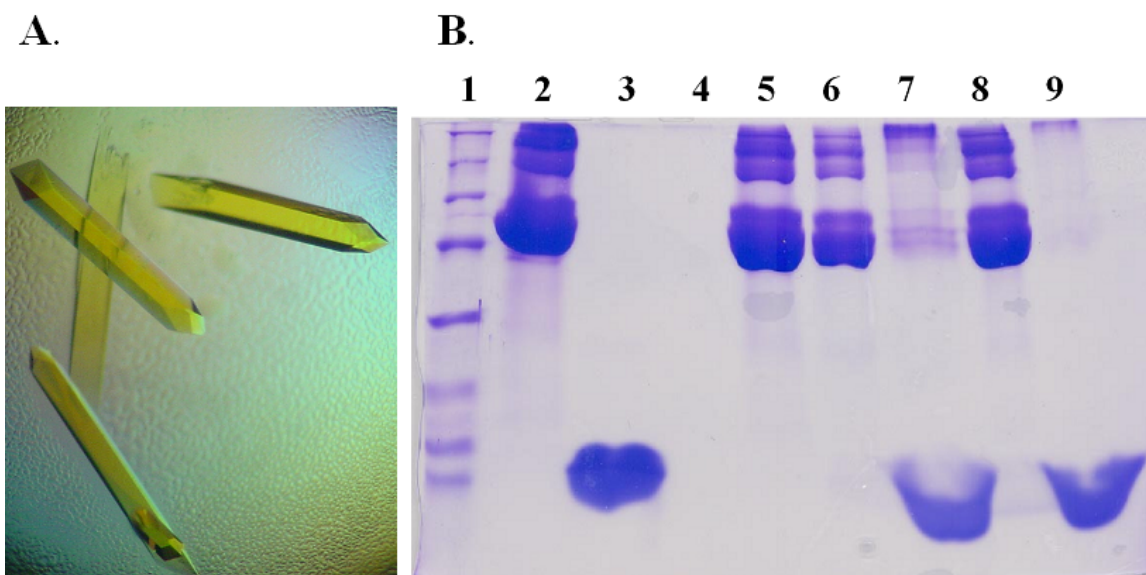


Figure 55. Co-crystallization trial of mTR3 and Trx.

A) Crystals (length 1.5 mm) with the oily background the thioredoxin. B) 12% SDS-PAGE of the crystal drop. Lane 1, Markers; lane 2, purified mTR3; lane 3, purified Trx, lane 4, blank, lane 5; mTR3 crystal from condition without Trx; lane 6 and 8, mTR3 crystal from co-crystallization trials; lanes 7 and 9, droplet solution from co-crystallization trials after crystal formation.

CHAPTER 6.

CONCLUSION AND MODEL

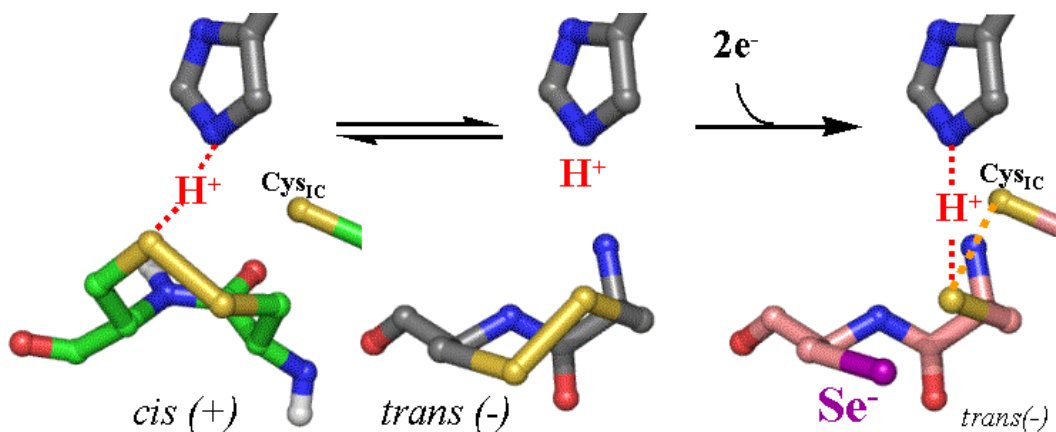


Figure 56. Model for the requirement of Sec in mammalian TR.

Prior to the formation of the interchange mixed disulfide, the Cys-containing TR from *Drosophila melanogaster* undergoes conformational change to the *cis* (+) conformation for protonation of the first leaving group (left). The structure of *Dm*TR accommodates the flanking Ser residues as well as the peptide in the *cis* (+) conformation. The structure of the mammalian enzyme restricts the peptide to the *trans* (-) conformation (right) preventing protonation of the first leaving group. The low p*K*_a of the selenol (Se⁻) of Sec obviates the need for protonation during the ring opening step.

The dissertation presented here has completed three specific aims: 1) development of a semisynthetic technique (Chapter 2) to produce mTR3 for structure-function studies (Chapter 3), 2) development of a new technique, peptide complementation (Chapter 4), to investigate the mechanism of TR, and 3) determination of the crystal structure of *Dm*TR (Chapter 5) for comparison with mammalian TR. The results from these aims represent a significant contribution to our field. The structural comparison of mammalian and *Drosophila melanogaster* TRs, in combination with biochemical evidence from full length and truncated enzymes has generated the first hypothesis (**Figure 56**) for the requirement of Sec in mammalian TR in the 10 years since Sec was first identified in the enzyme.

We have shown that maintaining Sec in the C-terminal position of the dyad is essential to mTR3 function but that the vicinal motif is not. The data from the peptide complementation assays show that the loss in activity by mutation of Sec in mTR3 is attributed to a loss in activity in the ring opening step. The structural positioning of the oxidized tetrapeptides in accordance with the interchange step of GR with GSSG explains why the low pK_a of Sec is required for the mammalian enzyme but not *Dm*TR even though the catalytic acid base, the His-Glu dyad, is conserved throughout the protein family. Our hypothesis that protonation of the first leaving group is partially rate limiting in the catalytic cycle of TR is complete agreement with the current understanding of the mechanism of GR (88, 94, 95).

KEEPING MECHANISMS IN PERSPECTIVE

The GR protein family is an ideal module for the merger of a structural biology and biochemical analysis to understand how evolution selects for a common approach to an essential process. That process is thiol-disulfide exchange. Each enzyme then adapts to a specific need on the basis of a target or a cognate substrate. For example GR, TR and TryR function to reduce their cognate disulfides by consumption of NADPH whereas LipDH functions to generate NADH by consumption of the cognate dithiol. So, not only does a common architecture evolve for compensation of a different cognate substrate, but also allows for shifting of equilibrium to reverse the direction of the reaction.

Understanding the **common** elements of a general mechanism is as important as understanding the *unique* elements of a specific mechanism within a protein family. Taking both sets of elements into consideration is essential for structure-based design of therapeutics to be effective (6, 14). TR is *unique* within the protein family in that its own C-terminus is the cognate disulfide substrate for the conserved active site. This adds an additional thiol-disulfide exchange reaction prior to reduction of its true cognate substrate Trx. We expect that the **common** element is the interchange step resulting in the mixed disulfide with the conserved FAD-associated active site. We hypothesize that this step is structurally and biochemically conserved between GR and TR.

MODEL FOR THE REQUIREMENT OF SEC IN MAMMALIAN TR

Selenocysteine has been shown to account for the broad substrate range unique to mammalian TRs, including its ability to reduce peroxides (114) and ascorbate (115, 172). It has been assumed that the incorporation of the selenium atom in mammalian TR for the lower pK_a expected for Sec compared to Cys (109), however, one must distinguish a selective advantage (broad substrate range) from a necessary function (reduction of Trx). The low pK_a of Sec does not account for the requirement of Sec demonstrated by the dramatic loss in Trx activity upon mutation of the Sec to Cys if the base-catalyzed mechanism of the GR family is conserved. The structural analysis here could account for the necessity for the selenium atom in the mammalian TR.

Both the Ac-GCUG(ox) and Ac-GCCG(ox) peptides show an equilibrium shift towards the *trans* peptide conformation while Ac-SCCS(ox) shows an equilibrium favoring the *cis* conformation.. Alignment of these peptides in the active site of mTR3 according to the interchange step of GR also shows a preference for the peptides in the *trans* conformation. In our model, the more restricted tetrapeptide binding pocket of mammalian TR resulting from incorporation of bulkier residues and a shift of helix 3 restricts the peptide to the *trans* conformation and does not accommodate the flanking serines of the *Drosophila* motif. In the *trans* conformation, the low pK_a of the Sec would become essential due its inability to be protonated by His 497' (PDB 1ZKQ). The *trans* conformation also shows an intramolecular hydrogen bond between the C-terminal carboxylate and the amide hydrogen of the penultimate cysteine in the NMR structures of the peptides containing a terminal Gly. This would contribute to the stability of the *trans*

conformer and result in the shift in equilibrium to *trans* and decreasing the rate of switching to the *cis* conformation. This could contribute to the decrease in activity reported for the mutation of the terminal Ser to Gly (Ser491') for the *Drosophila* TR that is not observed for the equivalent mutation for Ser488' (65).

The TR from *Drosophila* has evolved a different tetrapeptide binding pocket than that of the mammalian form of the enzyme. The residues from helix 3 proximal to the FAD-associated active site are less bulky to accommodate the hydroxyls of the flanking serines of the SCCS motif and allow the peptide to adopt the *cis* conformation. The increase in the available space is likely to make the enzyme more amenable for the conformational switching of the GCCG peptide from *trans* to *cis* necessary to protonate the leaving group cysteine during interchange.

Our hypothesis is that the catalytic cycle for TR is dominated by a leaving group effect. The first leaving group (Sec in mTR3) must either be in position for protonation from the catalytic His during the ring opening step or have a significantly lower pK_a . An alternative brought to light in the Introduction and in Chapter 3 is the question of nucleophilicity. While there is no disagreement in the likely nucleophilic difference between Sec and Cys or that the flanking serines in *DmTR* may increase nucleophilicity, the question is the fold contribution. Whitesides (173) and Hupe (156) have characterized the rates of thiol-disulfide exchange as a function of pK_a , as reviewed in (174, 175). Using a series of alkyl and aromatic nucleophiles of determined pK_a , Hupe and co-workers determined an ~ 3.2 fold change in rate per pK_a unit (156). While these systems are simplistic in that they do not account for protein conformations, it is rather striking that it requires a >3 pK_a unit shift for a given nucleophile to produce a 10-fold change in

rate. This is important in that a three pK_a unit difference is that which has been estimated for Cys compared to Sec (125).

It has been postulated that the Sec residue is the attacking nucleophile in the reduction of Trx (109). This is due to the selenolate of a Sec residue being more nucleophilic than the thiolate of a Cys residue. Indirect evidence supporting this hypothesis is the hydrogen peroxidase activity of the enzyme (63, 68), which is abolished upon mutation of Sec to Cys (109). However another role for Sec is as the leaving group position of the dyad during the ring opening step as we have argued in our model. Placing the Cys residue in the leaving group position by switching positions of the Sec and Cys residues should significantly decrease the activity towards all three substrates in this study, as the C-terminal selenysulfide would be more difficult to reduce. This is what we observed in our results in Chapter 3.

The kinetic profile of the hydrogen peroxidase activity of the WT enzyme is more like that of a chemical reaction (2nd order kinetics) rather than an enzymatic reaction. Therefore one would expect the position of Sec to have little impact on the peroxidase activity. However, switching positions of the two atoms (S and Se) results in a 30 fold decrease in peroxidase activity when selenium content is normalized. A probable explanation for this is that the selenysulfide in this mutant is poorly reduced in the assay. This interpretation is further supported by the near WT activity of the Ala insertion mutants for all three substrates. These mutants would maintain Cys in the interchange position and Sec in the leaving group position of the ring opening step according to our model.

BINDING OR CHEMISTRY ($k_{\text{cat}}/K_{\text{m}}$).

The structural interpretation here raises the question of what is actually being observed in the peptide complementation assays in Chapter 4. Since the assay conditions do not reach saturation, the representation of the plot is in the form of $k_{\text{cat}}/K_{\text{m}}$. Can we distinguish between binding or conformation and chemistry in our data? In terms of our interpretation, we have developed a model that results in the chemistry being dependent on binding the correct conformation of the peptide in the ring opening step. In this interpretation, the only assumption is that the selenium is not a binding determinant for the peptide, which is quite reasonable. The support for this comes from the agreement in the fold difference in the $k_{\text{cat}}/K_{\text{m}}$ of the peptide pairs in the peptide complementation assays when compared to the fold difference in the Trx assays for the equivalent mutants (Chapter 4, **Table 14**).

In the Trx assay, there is very little difference in the apparent K_{m} for Trx between the GCUG, GCCG and SCCS mutants of mTR3 (Chapter 3). Similar results are observed for the Trx activity with mutants of *Dm*TR published by Gromer *et al.* (65), which included the C-terminal mutants GCUG, GCCG and SCUS in comparison with the wild type SCCS. Therefore, the >200 fold difference in $k_{\text{cat}}/K_{\text{m}}$ for the mutants of mTR3 is attributed to the >200 fold difference in k_{cat} . This is the same order of magnitude difference in the $k_{\text{cat}}/K_{\text{m}}$ determined in the peptide complementation assays (308 fold for the GCUG/GCCG and 88 fold for the GCUG/SCCS). The agreement of these numbers supports our model that the ring opening step is where Sec is required for mammalian TR and that it is likely a function of the chemistry.

Our model can be understood by relating the results for the truncated TR assays in a more simplified form (**Table 19**) to that which has been observed in the literature for GR (**Table 20**). The truncated forms of mTR3 and *Dm*TR have good activity towards DTNB (thiol $pK_a = 4.75$ (159)) and GCUG (Sec $pK_a = 5.2$ (125)). The peptide GCCG is a substrate for *Dm*TR as the tetrapeptide binding pocket for *Dm*TR allows for the C⁺ conformation whereas mTR3 does not. Neither enzyme has activity for cystine, since there is no ring structure to place the leaving group in the correct orientation for protonation by the catalytic His. This is the same interpretation that can be made for GR. The thiol pK_a for glutathione is 8.6 (175), however GR binds GSSG in the correct disulfide orientation for the catalytic cycle to occur. This is not the case for the mixed disulfides GS-SCy (160) and GS-STNB (95) with each only having a single glutathione moiety and not likely to have the disulfide in the correct orientation for protonation of the first leaving group. Only the latter (GS-STNB) is a substrate for GR since it has the low pK_a TNB- leaving group, just like the tetrapeptide GCUG has the low pK_a leaving group of Sec.

OUR MODEL AND A MECHANISTIC EVOLUTIONARY ADVANTAGE

Incorporation of Sec into mammalian TR may be an evolutionary advantage beyond a broader substrate range. In the proposed mechanism of GR, His 464' would protonate both the leaving group GSHII and then GSHI upon resolution of the interchange mixed disulfide. Incorporation of selenocysteine would eliminate the need for the first leaving group protonation step and only require protonation upon resolution

of the interchange. Upon re-oxidation of the vicinal disulfide with transfer of electrons to Trx, the peptide bond would likely be in the *trans* conformation. Incorporation of Sec as the first leaving group would remove the necessity for *cis/trans* conformational switching. The differences in the two ring opening steps we hypothesize here are shown in **Figure 57** (mTR3) and **Figure 58** (*DmTR*).

SUPPORT FROM THE STOPPED-FLOW TR LITERATURE

Minimal characterization has been done for the WT mammalian enzyme with the stopped-flow technique described in Chapter 1 (79). The initial characterization of *DmTR* (78) and analysis of mutants of *PfTR* (93) provide significant support to the model we have presented here. In the *DmTR* study (78), a k_{cat} was determined for Trx as $\sim 5 \text{ s}^{-1}$. For the reductive half-reaction, three rate constants were determined; $k_1 \sim 100 \text{ s}^{-1}$, $k_2 \sim 49 \text{ s}^{-1}$, and $k_3 \sim 21 \text{ s}^{-1}$. The first two rate constants are essentially the reductive half-reaction of GR with formation of the FADH⁻ - NADP⁺ charge-transfer complex then the formation of the thiolate-FAD charge-transfer complex EH₂(B) (Please refer to **Figure 10** in Chapter 1 for the remainder of this discussion). Therefore, the third rate constant must be the reduction of the C-terminal disulfide terminating at EH₄(B). This indicates that reduction of the C-terminal disulfide is rate limiting in the reductive half-reaction. This is not surprising as with GR the protonation of the first leaving group in the oxidative half-reaction is rate limiting (88, 95). A single rate constant was determined for the oxidative half-reaction for *DmTR* of $\sim 11 \text{ s}^{-1}$ (65). This led the authors to conclude that a step in the

oxidative half-reaction was rate limiting overall. This, however, does not necessarily mean the nucleophilic attack on Trx, as was clarified in the analysis *PfTR*.

The *PfTR* work is most interesting as it includes the mutants of the His-Glu dyad (93). The results for the reductive half-reaction are similar to that of *DmTR*. Again k_1 is the largest at $425 - 815 \text{ s}^{-1}$ depending on the mutant or the pH. This is the formation of the $\text{FADH}^- - \text{NADP}^+$ charge-transfer complex and is only weakly affected by the mutations. As with *DmTR*, k_2 is $\sim 50 \%$ of k_1 for the WT *PfTR* and significantly affected by the mutations, between ~ 30 to 150 fold. The k_3 for *PfTR*, the reduction of the C-terminus by the N-terminus, is $\sim 5 \%$ of k_2 and again is dramatically reduced by either mutation. With *PfTR* the reduction of the C-terminus is rate limiting in the reductive half-reaction, to an even greater extent than in *DmTR*.

For *PfTR*, three rate constants were estimated for the oxidative half-reaction. The k_1 was the fastest of the three and similar to k_3 of the reductive half-reaction with the His and Glu mutants $\sim 50 \%$ of wild type. The other two rate constants were very slow with $k_2 \sim 10 \%$ of k_1 , and k_3 rate limiting (wild type). Each of these constants was significantly lower for the mutants. In this analysis of *PfTR* it was proposed that k_1 is the reduction of Trx ($\text{EH}_4(\text{B})$ to $\text{EH}_2(\text{B})$) and that the other two rate constants are $\text{EH}_2(\text{B})$ back to E_{ox} . Therefore, in both half-reactions, the reduction of the C-terminus would be rate limiting and thereby rate limiting overall. This interpretation can then be extrapolated to the *DmTR* results where the step in the oxidative half-reaction that is rate limiting likely involves the $\text{EH}_2(\text{B})$ to E_{ox} steps. The k_1 for *PfTR* being unaffected by the His or Glu mutations indicates that the dyad is not involved in the transfer of electrons to Trx as suggested by Brandt (100), but is essential to the reduction of the C-terminus.

CONTRADICTIONS TO THE TR LITERATURE

While there is a contribution of the flanking Ser residues to the activity of *DmTR*, it is only a 7 fold increase over the activity of flanking Gly residues (65). Therefore, the Ser can hardly be seen as critical when compared to the >100 fold loss in activity upon mutation of the Sec in mTR3 (157) or mutation of the catalytic base in *PfTR* (93). The other point of contention with our model is that the proposal for the Ser residues facilitating thiolate formation is that it is based on the tetrapeptide modeled in all *trans* configurations (65). Comparing the NMR structures of the SCCS(ox) tetrapeptide, the hydroxyls of the Ser residues face the eight-membered ring only in the *trans* configuration and not in the *cis* configuration (**Figure 59**). Based on our analysis, the Ser hydroxyls would not be correctly oriented in the *cis* configuration during the ring opening step.

It is still feasible that the hydroxyls could impact the oxidative half-reaction by increasing the nucleophilicity of the attacking thiolate. The seven fold loss in activity for *DmTR* could be accounted for by a decrease in pK_a of the attacking thiolate. However, it cannot account for the loss in activity for the SCCS mutant of mTR3, which is even below that of the GCCG mutant. The same results were also demonstrated for human TR where the SCCS mutant shows less activity than the GCCG mutant (154). The results from the human TR SCCS mutant (hTR-SCCS) were interpreted by the authors to be a function of the oxidative half-reaction. Both half-reactions were slow in comparison to WT with the oxidative half-reaction determined to be 200 fold slower in the SCCS

mutant. A closer inspection of the data presented does raise a question of the reaction conditions (**Figure 60**). Comparing the reductive half-reaction (**A**) spectra 6 to the oxidative half-reaction (**B**) spectra 2, it would appear that the latter has not reached $\text{EH}_4(\text{B})$. One of the primary characteristics of $\text{EH}_4(\text{B})$ is an enhanced thiolate-flavin charge-transfer complex at 540 nm (93) which is much lower in **Figure 60B** spectra 2 than **Figure 60A** spectra 6. The 460 nm peak also does not appear shifted to shorter wavelengths as would be expected. **Figure 60C** is the oxidative half-reaction of *PfTR* for spectral reference (93).

SEC AS LEAVING GROUP OR INTERCHANGE

The TR field is split as to the function of Sec in the catalytic cycle. While its role as the nucleophile for Trx reduction is universally accepted, there are those who suggest that Sec (36, 109) is the leaving group upon ring opening and those who suggest that it is the interchange (35). However, prior to the data we present here, no biochemical evidence was provided for either hypothesis. The high activity of the mTR3-GCAUG and mTR3-GCAAUG mutants would support our model that Sec is the leaving group position and not the interchange position. If Sec were the interchange, the insertion of residues would be expected to prevent the interchange step from occurring during ring opening.

The Sec-relative position in *DmTR* (Cys490') has been suggested as the interchange (78) and is in partial disagreement with our model. This suggestion was generated from the difference in spectral properties of Cys489'Ser and Cys490'Ser mutants. The Cys489'Ser mutant showed a persistent FAD-thiolate charge-transfer

complex. It was suggested that this was due to a stable mixed-disulfide between the interchange thiol Cys57 and Cys490'. In our modeling, there is no chemical distinction in the SCCS or GCCG peptides as both residues in the dyad are Cys. Therefore, it is quite possible that Cys490' forms the interchange with Cys57. This would suggest that the two enzymes have different mechanisms, which we suspect is unlikely.

SUPPORTING EXPERIMENTS

The data produced in these studies and proposal for Sec as the leaving group in the ring opening step for mammalian TRs is a testable model generating an extended list of experiments of which the most direct will be discussed here. The first suggestion is the production of *DmTR*-SCAUS by semisynthesis. Recovering activity compared to the *DmTR*-SCACS mutant would support our model. In both mutants, there are still the flanking serines except that there is not the vicinal disulfide. We suggested, based on the high activity of mTR3-GCAUG and mTR3-GCAAUG, that the Sec position is the leaving group and that we have not moved the interchange position or dramatically affected the attack on Trx. Similar results for *DmTR*-SCAUS would make for a convincing argument that both enzymes have a similar mechanism. Standard molecular biology techniques can be used to test the effect of the residues from helix 3 proposed as the conformational and peptide determinants for the two enzymes. The Thr114 *DmTR* substitution for His or Tyr in mammalian TR would be the position of choice. A collection of full length and truncated mutants was generated for *DmTR* that were not

evaluated enzymatically but whose likely functions have been discussed. These mutations provide opportunities for future crystallographic studies.

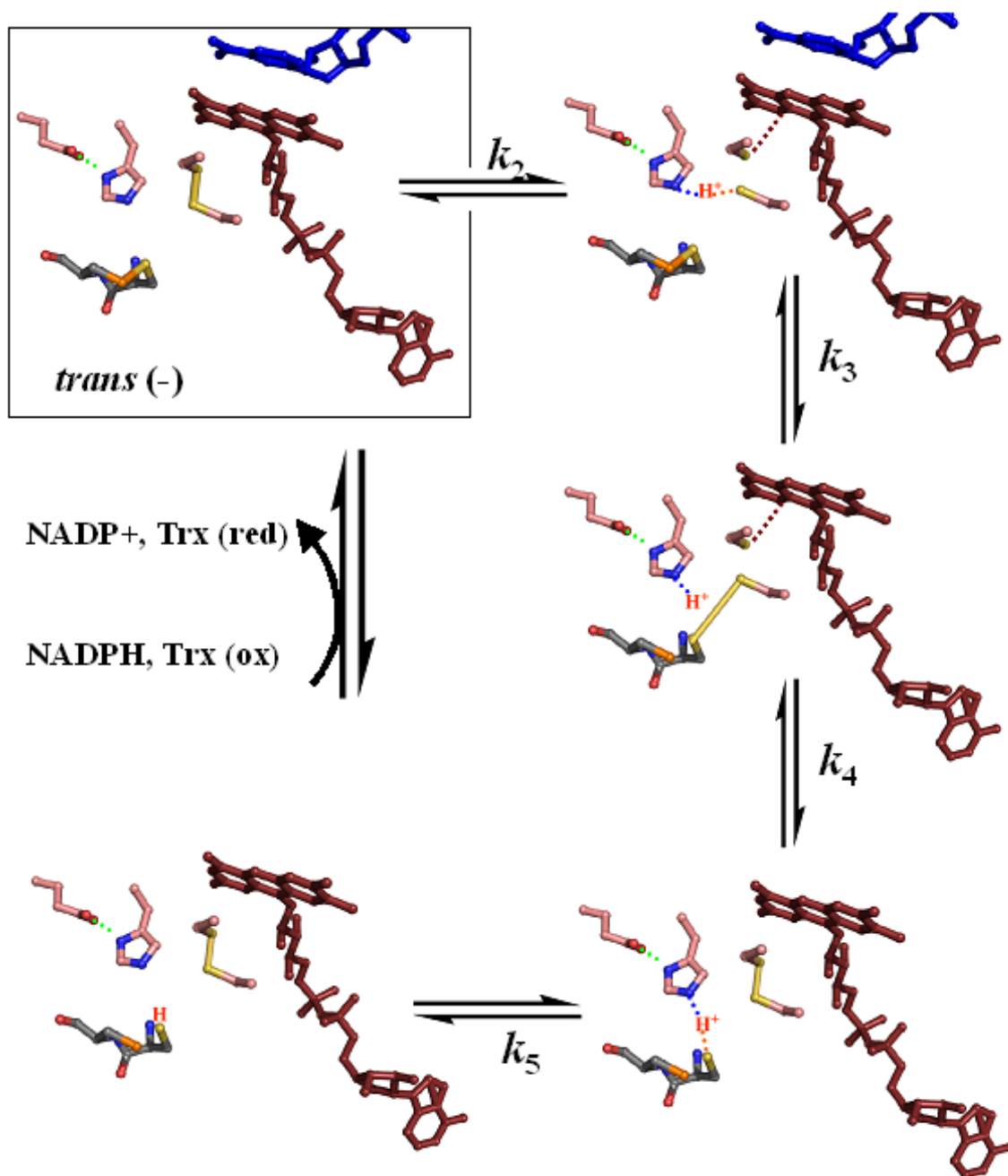


Figure 57. Model for mTR3 ring opening steps.

The steps of ring opening within the reductive half-reaction for mTR3 with the C-terminal tetrapeptide GCUG in the *trans* (-) conformation. Binding of NADPH and formation of the FADH-NADP⁺ charge-transfer complex (Boxed k_1), thiolate-FAD charge-transfer complex (k_2), formation of the interchange mixed disulfide with Sec (orange) **not** requiring protonation (k_3), resolution of the mixed disulfide (k_4) and protonation of the Cys (k_5).

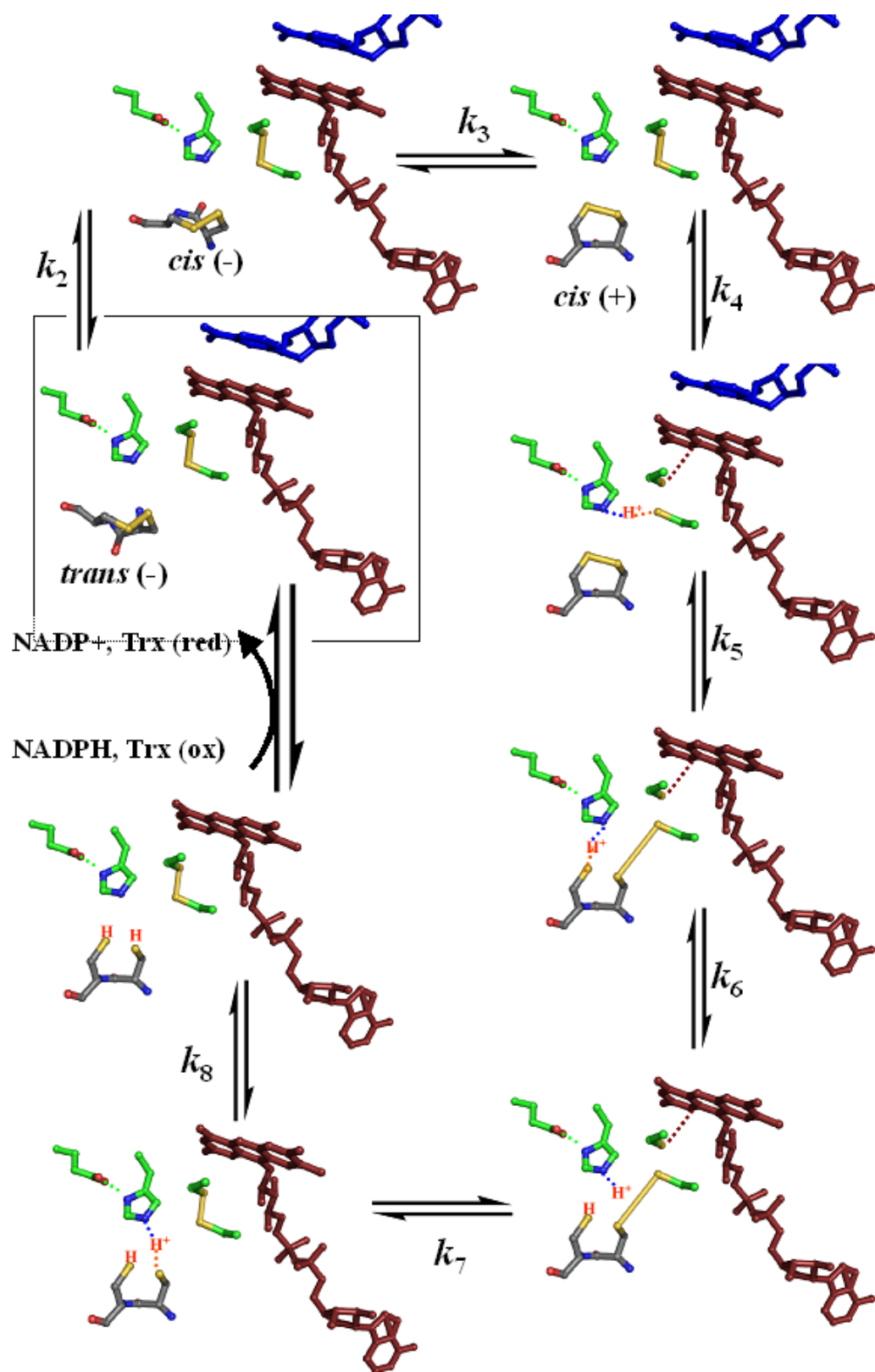


Figure 58. Model for *Dm*TR ring opening steps.

The steps of ring opening within the reductive half-reaction for *Dm*TR with the tetrapeptide SCCS in the *cis* (+) conformation. Binding of NADPH and formation of the FADH-NADP⁺ charge-transfer complex (Boxed k_1). The peptide in the *trans* (-) conformation must undergo conformational change the *cis* (-) (k_2) then *cis* (+) (k_3). The thiolate-FAD charge-transfer complex (k_4), formation of the interchange mixed disulfide (k_5) with Cys48' **requiring** protonation (k_6), resolution of the mixed disulfide (k_7) and protonation of the Cys49' (k_8).

Table 19. Substrates for truncated TR.

Enzyme	DTNB	GCUG	GCCG	^c CyS-SCy
^a <i>Dm</i> TR-S	+	+	+	-
^b mTR-G	+	+	-	-

^a*Drosophila melanogaster* TR missing the C-terminal tripeptide Cys-Cys-Ser.

^bMouse mitochondrial TR missing the C-terminal tripeptide Cys-Sec-Gly.

^cCystine.

Table 20. Substrates for glutathione reductase.

Enzyme	^a GS-SG	^b GS- STNB	^c GS-SCy	^d CyS-SCy
GR	+	+	-	-

^aThe natural substrate diglutathione (GSSG).

^bGlutathione-TNB mixed disulfide taken from (95).

^cGlutathione-cysteine mixed disulfide taken from (160).

^dCystine taken from (160).

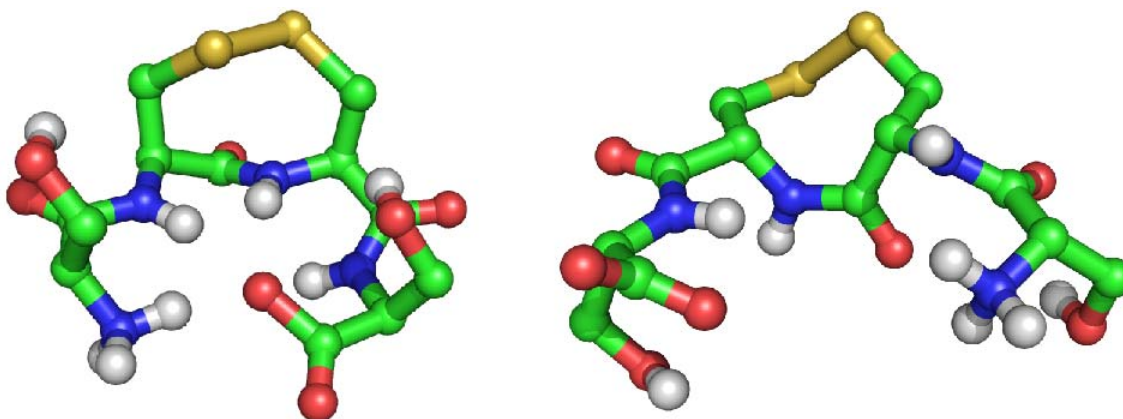


Figure 59. Orientation of flanking serine hydroxyls.

Orientation of the flanking Ser hydroxyls in the SCCS(ox) tetrapeptide in *trans* configuration (left) and the *cis* configuration (right). The Ser hydroxyls would not be correctly oriented to impact thiolate formation during the ring opening step when in the *cis* configuration.

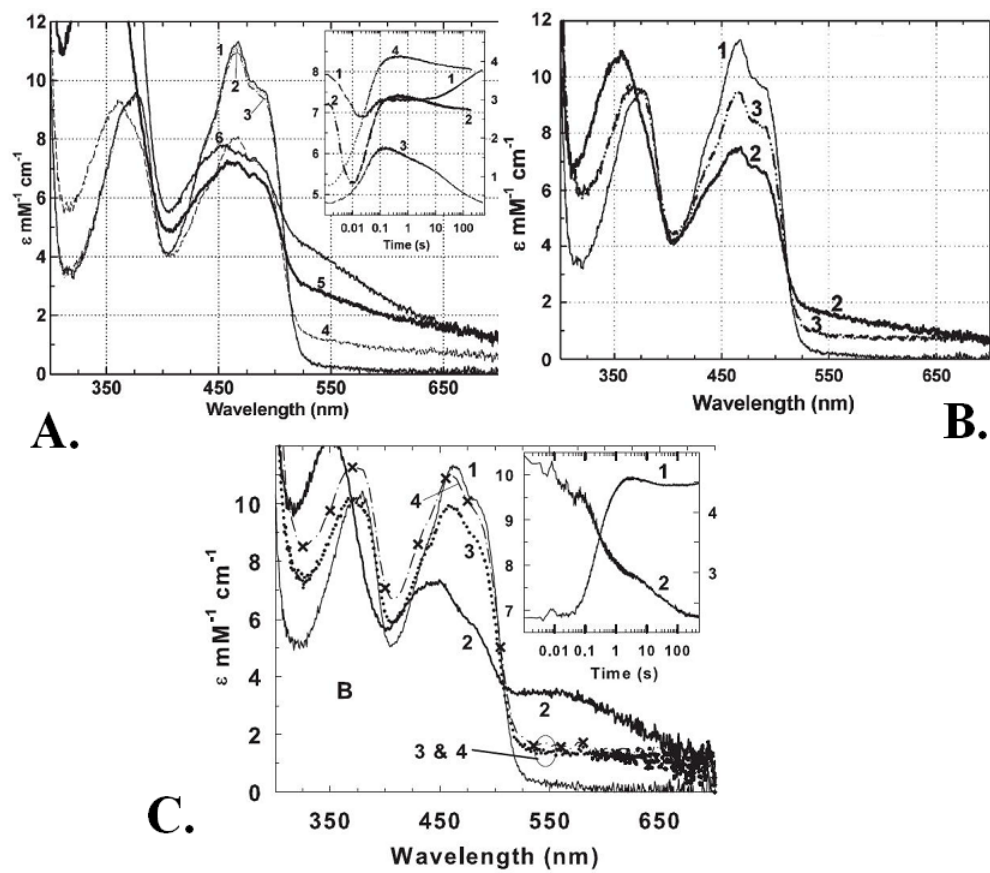


Figure 60. Interpretation of human TR-SCCS.

Interpretation of the human Ser-Cys-Cys-Ser TR mutant (hTR-SCCS) from (154) **reprinted with permission (176)**. **A** is the reductive half-reaction of hTR-SCCS. Spectra 1 is oxidized hTR-SCCS, spectra 4 is the addition of 1.7 equivalents of NADPH, spectra 5 is 3.3 equivalents of NADPH, spectra 6 is 7.7 equivalents of NADPH. **B** is the Oxidative half-reaction of hTR-SCCS. Spectra 1 is the oxidized hTR-SCCS, spectra 2 is reduction with 2.1 equivalents of NADPH, spectra 3 is reoxidation after addition of Trx. **C** is the oxidative half-reaction of wild type TR from *Plasmodium falciparum* (PfTR) as a reference (93). Spectra 1 is the oxidized PfTR, spectra 2 is reduction with 2.2 equivalents of NADPH, spectra 3 and 4 are time points following addition of Trx. It is possible that the slow oxidative half-reaction in the experiment is the incomplete reduction of hTR-SCCS, based on the lack of shift in the 460 nm peak to shorter wavelength and the weaker thiolate FAD charge-transfer complex at 540 nm.

REFERENCES

1. Han, D., Canali, R., Garcia, J., Aguilera, R., Gallaher, T. K., and Cadenas, E. (2005) Sites and mechanisms of aconitase inactivation by peroxynitrite: modulation by citrate and glutathione, *Biochemistry* 44, 11986-11996.
2. Hagg, D., Englund, M. C., Jernas, M., Schmidt, C., Wiklund, O., Hulten, L. M., Ohlsson, B. G., Carlsson, L. M., Carlsson, B., and Svensson, P. A. (2006) Oxidized LDL induces a coordinated up-regulation of the glutathione and thioredoxin systems in human macrophages, *Atherosclerosis* 185, 282-289.
3. Rajavashisth, T. B., Andalibi, A., Territo, M. C., Berliner, J. A., Navab, M., Fogelman, A. M., and Lusis, A. J. (1990) Induction of endothelial cell expression of granulocyte and macrophage colony-stimulating factors by modified low-density lipoproteins, *Nature* 344, 254-257.
4. Robertson, K. A., Bullock, H. A., Xu, Y., Tritt, R., Zimmerman, E., Ulbright, T. M., Foster, R. S., Einhorn, L. H., and Kelley, M. R. (2001) Altered expression of *Ape1/ref-1* in germ cell tumors and overexpression in NT2 cells confers resistance to bleomycin and radiation, *Cancer Res.* 61, 2220-2225.
5. Hirota, K., Matsui, M., Iwata, S., Nishiyama, A., Mori, K., and Yodoi, J. (1997) AP-1 transcriptional activity is regulated by a direct association between thioredoxin and Ref-1, *Proc. Natl. Acad. Sci. U. S. A.* 94, 3633-3638.
6. Becker, K., Gromer, S., Schirmer, R. H., and Müller, S. (2000) Thioredoxin reductase as a pathophysiological factor and drug target, *Eur. J. Biochem.* 267, 6118-6125.
7. Arnér, E. S., and Holmgren, A. (2000) Physiological functions of thioredoxin and thioredoxin reductase, *Eur. J. Biochem.* 267, 6102-6109.
8. Holmgren, A. (1989) Thioredoxin and glutaredoxin systems, *J. Biol. Chem.* 264, 13963-13966.
9. Holmgren, A. (1985) Thioredoxin, *Annu. Rev. Biochem.* 54, 237-271.
10. Fairlamb, A. H., Blackburn, P., Ulrich, P., Chait, B. T., and Cerami, A. (1985) Trypanothione: a novel bis(glutathionyl)spermidine cofactor for glutathione reductase in trypanosomatids, *Science* 227, 1485-1487.

11. Kanzok, S. M., Fechner, A., Bauer, H., Ulschmid, J. K., Müller, H. M., Botella-Munoz, J., Schneuwly, S., Schirmer, R., and Becker, K. (2001) Substitution of the thioredoxin system for glutathione reductase in *Drosophila melanogaster*, *Science* 291, 643-646.
12. Jaeger, T., and Flohe, L. (2006) The thiol-based redox networks of pathogens: unexploited targets in the search for new drugs, *Biofactors* 27, 109-120.
13. Davioud-Charvet, E., Becker, K., Landry, V., Gromer, S., Loge, C., and Sergheraert, C. (1999) Synthesis of 5,5'-dithiobis(2-nitrobenzamides) as alternative substrates for trypanothione reductase and thioredoxin reductase: a microtiter colorimetric assay for inhibitor screening, *Anal. Biochem.* 268, 1-8.
14. Krauth-Siegel, R. L., and Schoneck, R. (1995) Flavoprotein structure and mechanism. 5. Trypanothione reductase and lipoamide dehydrogenase as targets for a structure-based drug design, *FASEB J.* 9, 1138-1146.
15. Davioud-Charvet, E., McLeish, M. J., Veine, D. M., Giegel, D., Arscott, L. D., Andricopulo, A. D., Becker, K., Müller, S., Schirmer, R. H., Williams, C. H., Jr., and Kenyon, G. L. (2003) Mechanism-based inactivation of thioredoxin reductase from *Plasmodium falciparum* by Mannich bases. Implication for cytotoxicity, *Biochemistry* 42, 13319-13330.
16. Thelander, L., and Reichard, P. (1979) Reduction of ribonucleotides, *Annu. Rev. Biochem.* 48, 133-158.
17. Arnér, E. S., and Holmgren, A. (2006) The thioredoxin system in cancer, *Semin. Cancer Biol.* 16, 420-426.
18. Holmgren, A. (1979) Glutathione-dependent synthesis of deoxyribonucleotides. Characterization of the enzymatic mechanism of *Escherichia coli* glutaredoxin, *J. Biol. Chem.* 254, 3672-3678.
19. Holmgren, A. (1979) Glutathione-dependent synthesis of deoxyribonucleotides. Purification and characterization of glutaredoxin from *Escherichia coli*, *J. Biol. Chem.* 254, 3664-3671.
20. Wilson, L. G., Asahi, T., and Bandurski, R. S. (1961) Yeast sulfate-reducing system. I. Reduction of sulfate to sulfite, *J. Biol. Chem.* 236, 1822-1829.
21. Asahi, T., Bandurski, R. S., and Wilson, L. G. (1961) Yeast sulfate-reducing system. II. Enzymatic reduction of protein disulfide, *J. Biol. Chem.* 236, 1830-1835.

22. Koc, A., Mathews, C. K., Wheeler, L. J., Gross, M. K., and Merrill, G. F. (2006) Thioredoxin is required for deoxyribonucleotide pool maintenance during S phase, *J. Biol. Chem.* 281, 15058-15063.
23. Liu, S. Y., and Stadtman, T. C. (1997) Heparin-binding properties of selenium-containing thioredoxin reductase from HeLa cells and human lung adenocarcinoma cells, *Proc. Natl. Acad. Sci. U. S. A.* 94, 6138-6141.
24. Tamura, T., and Stadtman, T. C. (1996) A new selenoprotein from human lung adenocarcinoma cells: purification, properties, and thioredoxin reductase activity, *Proc. Natl. Acad. Sci. U. S. A.* 93, 1006-1011.
25. Mustacich, D., and Powis, G. (2000) Thioredoxin reductase, *Biochem. J.* 346 Pt 1, 1-8.
26. Hirota, K., Murata, M., Sachi, Y., Nakamura, H., Takeuchi, J., Mori, K., and Yodoi, J. (1999) Distinct roles of thioredoxin in the cytoplasm and in the nucleus. A two-step mechanism of redox regulation of transcription factor NF-kappaB, *J. Biol. Chem.* 274, 27891-27897.
27. Matthews, J. R., Wakasugi, N., Virelizier, J. L., Yodoi, J., and Hay, R. T. (1992) Thioredoxin regulates the DNA binding activity of NF-kappa B by reduction of a disulphide bond involving cysteine 62, *Nucleic Acids Res* 20, 3821-3830.
28. Rigobello, M. P., Scutari, G., Boscolo, R., and Bindoli, A. (2002) Induction of mitochondrial permeability transition by auranofin, a gold(I)-phosphine derivative, *Br. J. Pharmacol.* 136, 1162-1168.
29. Gladyshev, V. N., Stadtman, T. C., Hatfield, D. L., and Jeang, K. T. (1999) Levels of major selenoproteins in T cells decrease during HIV infection and low molecular mass selenium compounds increase, *Proc. Natl. Acad. Sci. U. S. A.* 96, 835-839.
30. May, J. M. (2002) Recycling of vitamin C by mammalian thioredoxin reductase, *Methods Enzymol.* 347, 327-332.
31. May, J. M., Morrow, J. D., and Burk, R. F. (2002) Thioredoxin reductase reduces lipid hydroperoxides and spares alpha-tocopherol, *Biochem. Biophys. Res. Commun.* 292, 45-49.
32. Williams, C. H., Jr., Zanetti, G., Arscott, L. D., and McAllister, J. K. (1967) Lipoamide dehydrogenase, glutathione reductase, thioredoxin reductase, and thioredoxin, *J. Biol. Chem.* 242, 5226-5231.

33. Murzin, A. G., Brenner, S. E., Hubbard, T., and Chothia, C. (1995) SCOP: a structural classification of proteins database for the investigation of sequences and structures, *J. Mol. Biol.* 247, 536-540.
34. Karplus, P. A., and Schulz, G. E. (1989) Substrate binding and catalysis by glutathione reductase as derived from refined enzyme: substrate crystal structures at 2 Å resolution, *J. Mol. Biol.* 210, 163-180.
35. Biterova, E. I., Turanov, A. A., Gladyshev, V. N., and Barycki, J. J. (2005) Crystal structures of oxidized and reduced mitochondrial thioredoxin reductase provide molecular details of the reaction mechanism, *Proc. Natl. Acad. Sci. U. S. A.* 102, 15018-15023.
36. Sandalova, T., Zhong, L., Lindqvist, Y., Holmgren, A., and Schneider, G. (2001) Three-dimensional structure of a mammalian thioredoxin reductase: implications for mechanism and evolution of a selenocysteine-dependent enzyme, *Proc. Natl. Acad. Sci. U. S. A.* 98, 9533-9538.
37. Bond, C. S., Zhang, Y., Berriman, M., Cunningham, M. L., Fairlamb, A. H., and Hunter, W. N. (1999) Crystal structure of *Trypanosoma cruzi* trypanothione reductase in complex with trypanothione, and the structure-based discovery of new natural product inhibitors, *Structure* 7, 81-89.
38. Mattevi, A., Obmolova, G., Kalk, K. H., van Berkel, W. J., and Hol, W. G. (1993) Three-dimensional structure of lipoamide dehydrogenase from *Pseudomonas fluorescens* at 2.8 Å resolution. Analysis of redox and thermostability properties, *J. Mol. Biol.* 230, 1200-1215.
39. Dym, O., and Eisenberg, D. (2001) Sequence-structure analysis of FAD-containing proteins, *Protein Sci.* 10, 1712-1728.
40. Waksman, G., Krishna, T. S., Williams, C. H., Jr., and Kuriyan, J. (1994) Crystal structure of *Escherichia coli* thioredoxin reductase refined at 2 Å resolution. Implications for a large conformational change during catalysis, *J. Mol. Biol.* 236, 800-816.
41. Rossmann, M. G., Moras, D., and Olsen, K. W. (1974) Chemical and biological evolution of nucleotide-binding protein, *Nature* 250, 194-199.
42. Bottoms, C. A., Smith, P. E., and Tanner, J. J. (2002) A structurally conserved water molecule in Rossmann dinucleotide-binding domains, *Protein Sci.* 11, 2125-2137.

43. Karplus, P. A., and Schulz, G. E. (1992) Refined Three-Dimensional Structure of Glutathione Reductase in *Chemistry and Biochemistry of Flavoenzymes* (Muller, F., ed) (CRC Press, Inc., Boca Raton, FL) 3, 121-211.
44. Arscott, L. D., Thorpe, C., and Williams, C. H., Jr. (1981) Glutathione reductase from yeast. Differential reactivity of the nascent thiols in two-electron reduced enzyme and properties of a monoalkylated derivative, *Biochemistry* 20, 1513-1520.
45. Mittl, P. R., Berry, A., Scrutton, N. S., Perham, R. N., and Schulz, G. E. (1994) Anatomy of an engineered NAD-binding site, *Protein Sci.* 3, 1504-1514.
46. Scrutton, N. S., Berry, A., and Perham, R. N. (1990) Redesign of the coenzyme specificity of a dehydrogenase by protein engineering, *Nature* 343, 38-43.
47. Pai, E. F., and Schulz, G. E. (1983) The catalytic mechanism of glutathione reductase as derived from x-ray diffraction analyses of reaction intermediates, *J. Biol. Chem.* 258, 1752-1757.
48. Berry, A., Scrutton, N. S., and Perham, R. N. (1989) Switching kinetic mechanism and putative proton donor by directed mutagenesis of glutathione reductase, *Biochemistry* 28, 1264-1269.
49. Lennon, B. W., Williams, C. H., Jr., and Ludwig, M. L. (2000) Twists in catalysis: alternating conformations of Escherichia coli thioredoxin reductase, *Science* 289, 1190-1194.
50. Karplus, P. A., and Schulz, G. E. (1987) Refined structure of glutathione reductase at 1.54 Å resolution, *J. Mol. Biol.* 195, 701-729.
51. Deonarain, M. P., Scrutton, N. S., and Perham, R. N. (1992) Engineering surface charge. 1. A method for detecting subunit exchange in Escherichia coli glutathione reductase, *Biochemistry* 31, 1491-1497.
52. Deonarain, M. P., Scrutton, N. S., and Perham, R. N. (1992) Engineering surface charge. 2. A method for purifying heterodimers of Escherichia coli glutathione reductase, *Biochemistry* 31, 1498-1504.
53. Scrutton, N. S., Deonarain, M. P., Berry, A., and Perham, R. N. (1992) Cooperativity induced by a single mutation at the subunit interface of a dimeric enzyme: glutathione reductase, *Science* 258, 1140-1143.
54. Bashir, A., Perham, R. N., Scrutton, N. S., and Berry, A. (1995) Altering kinetic mechanism and enzyme stability by mutagenesis of the dimer interface of glutathione reductase, *Biochem. J.* 312 (Pt 2), 527-533.

55. Krnajski, Z., Gilberger, T. W., Walter, R. D., and Müller, S. (2000) Intersubunit interactions in *Plasmodium falciparum* thioredoxin reductase, *J. Biol. Chem.* *275*, 40874-40878.
56. Hudaky, I., Gaspari, Z., Carugo, O., Cemazar, M., Pongor, S., and Perczel, A. (2004) Vicinal disulfide bridge conformers by experimental methods and by ab initio and DFT molecular computations, *Proteins* *55*, 152-168.
57. Carugo, O., Cemazar, M., Zahariev, S., Hudaky, I., Gaspari, Z., Perczel, A., and Pongor, S. (2003) Vicinal disulfide turns, *Protein Eng.* *16*, 637-639.
58. Creighton, C. J., Reynolds, C. H., Lee, D. H., Leo, G. C., and Reitz, A. B. (2001) Conformational analysis of the eight-membered ring of the oxidized cysteinyl-cysteine unit implicated in nicotinic acetylcholine receptor ligand recognition, *J. Am. Chem. Soc.* *123*, 12664-12669.
59. Wang, X., Connor, M., Smith, R., Maciejewski, M. W., Howden, M. E., Nicholson, G. M., Christie, M. J., and King, G. F. (2000) Discovery and characterization of a family of insecticidal neurotoxins with a rare vicinal disulfide bridge, *Nat. Struct. Biol.* *7*, 505-513.
60. Hunter, H. N., Fulton, D. B., Ganz, T., and Vogel, H. J. (2002) The solution structure of human hepcidin, a peptide hormone with antimicrobial activity that is involved in iron uptake and hereditary hemochromatosis, *J. Biol. Chem.* *277*, 37597-37603.
61. Blake, C. C., Ghosh, M., Harlos, K., Avezoux, A., and Anthony, C. (1994) The active site of methanol dehydrogenase contains a disulphide bridge between adjacent cysteine residues, *Nat. Struct. Biol.* *1*, 102-105.
62. Engst, S., and Miller, S. M. (1998) Rapid reduction of Hg(II) by mercuric ion reductase does not require the conserved C-terminal cysteine pair using HgBr₂ as the substrate, *Biochemistry* *37*, 11496-11507.
63. Gladyshev, V. N., Jeang, K. T., and Stadtman, T. C. (1996) Selenocysteine, identified as the penultimate C-terminal residue in human T-cell thioredoxin reductase, corresponds to TGA in the human placental gene, *Proc. Natl. Acad. Sci. U. S. A.* *93*, 6146-6151.
64. Bock, A., Forchhammer, K., Heider, J., Leinfelder, W., Sawers, G., Veprek, B., and Zinoni, F. (1991) Selenocysteine: the 21st amino acid, *Mol. Microbiol.* *5*, 515-520.

65. Gromer, S., Johansson, L., Bauer, H., Arscott, L. D., Rauch, S., Ballou, D. P., Williams, C. H., Jr., Schirmer, R. H., and Arnér, E. S. (2003) Active sites of thioredoxin reductases: why selenoproteins?, *Proc. Natl. Acad. Sci. U. S. A.* *100*, 12618-12623.
66. Williams, C. H., Arscott, L. D., Müller, S., Lennon, B. W., Ludwig, M. L., Wang, P. F., Veine, D. M., Becker, K., and Schirmer, R. H. (2000) Thioredoxin reductase two modes of catalysis have evolved, *Eur. J. Biochem.* *267*, 6110-6117.
67. Stoll, V. S., Simpson, S. J., Krauth-Siegel, R. L., Walsh, C. T., and Pai, E. F. (1997) Glutathione reductase turned into trypanothione reductase: structural analysis of an engineered change in substrate specificity, *Biochemistry* *36*, 6437-6447.
68. Zhong, L., Arnér, E. S., and Holmgren, A. (2000) Structure and mechanism of mammalian thioredoxin reductase: the active site is a redox-active selenolthiol/selenenylsulfide formed from the conserved cysteine-selenocysteine sequence, *Proc. Natl. Acad. Sci. U. S. A.* *97*, 5854-5859.
69. Massey, V. (2000) The chemical and biological versatility of riboflavin, *Biochem. Soc. Trans.* *28*, 283-296.
70. Ghisla, S., Massey, V., Lhoste, J. M., and Mayhew, S. G. (1974) Fluorescence and optical characteristics of reduced flavines and flavoproteins, *Biochemistry* *13*, 589-597.
71. Massey, V., and Ganther, H. (1965) On the interpretation of the absorption spectra of flavoproteins with special reference to D-amino acid oxidase, *Biochemistry* *4*, 1161-1173.
72. Michaelis, L., Schubert, M. P., and Smythe, C. V. (1936) Potentiometric Study of Flavins, *J. Biol. Chem.* *116*, 587-607.
73. Massey, V., and Palmer, G. (1966) On the existence of spectrally distinct classes of flavoprotein semiquinones. A new method for the quantitative production of flavoprotein semiquinones, *Biochemistry* *5*, 3181-3189.
74. Stewart, R. C., and Massey, V. (1985) Potentiometric studies of native and flavin-substituted Old Yellow Enzyme, *J. Biol. Chem.* *260*, 13639-13647.
75. Stankovich, M. T., Schopfer, L. M., and Massey, V. (1978) Determination of glucose oxidase oxidation-reduction potentials and the oxygen reactivity of fully reduced and semiquinoid forms, *J. Biol. Chem.* *253*, 4971-4979.

76. Deponte, M., Urig, S., Arscott, L. D., Fritz-Wolf, K., Reau, R., Herold-Mende, C., Koncarevic, S., Meyer, M., Davioud-Charvet, E., Ballou, D. P., Williams, C. H., Jr., and Becker, K. (2005) Mechanistic studies on a novel, highly potent gold-phosphole inhibitor of human glutathione reductase, *J. Biol. Chem.* *280*, 20628-20637.
77. Reed, J. K. (1973) Studies on the kinetic mechanism of lipoamide dehydrogenase from rat liver mitochondria, *J. Biol. Chem.* *248*, 4834-4839.
78. Bauer, H., Massey, V., Arscott, L. D., Schirmer, R. H., Ballou, D. P., and Williams, C. H., Jr. (2003) The mechanism of high M_r thioredoxin reductase from *Drosophila melanogaster*, *J. Biol. Chem.* *278*, 33020-33028.
79. Arscott, L. D., Gromer, S., Schirmer, R. H., Becker, K., and Williams, C. H., Jr. (1997) The mechanism of thioredoxin reductase from human placenta is similar to the mechanisms of lipoamide dehydrogenase and glutathione reductase and is distinct from the mechanism of thioredoxin reductase from *Escherichia coli*, *Proc. Natl. Acad. Sci. U. S. A.* *94*, 3621-3626.
80. Matthews, R. G., Ballou, D. P., Thorpe, C., and Williams, C. H., Jr. (1977) Ion pair formation in pig heart lipoamide dehydrogenase: rationalization of pH profiles for reactivity of oxidized enzyme with dihydrolipoamide and 2-electron-reduced enzyme with lipoamide and iodoacetamide, *J. Biol. Chem.* *252*, 3199-3207.
81. Matthews, R. G., and Williams, C. H., Jr. (1976) Measurement of the oxidation-reduction potentials for two-electron and four-electron reduction of lipoamide dehydrogenase from pig heart, *J. Biol. Chem.* *251*, 3956-3964.
82. Wilkinson, K. D., and Williams, C. H., Jr. (1979) Interactions of guanidinium chloride and pyridine nucleotides with oxidized and two-electron-reduced lipoamide dehydrogenase from *Escherichia coli*, *J. Biol. Chem.* *254*, 863-871.
83. Wilkinson, K. D., and Williams, C. H., Jr. (1979) Evidence for multiple electronic forms of two-electron-reduced lipoamide dehydrogenase from *Escherichia coli*, *J. Biol. Chem.* *254*, 852-862.
84. Massey, V., and Veeger, C. (1960) On the reaction mechanism of lipoyl dehydrogenase, *Biochim. Biophys. Acta* *40*, 184-185.
85. Massey, V., Gibson, Q. H., and Veeger, C. (1960) Intermediates in the catalytic action of lipoyl dehydrogenase (diaphorase), *Biochem. J.* *77*, 341-351.

86. Williams, C. H., Jr. (1992) Lipoamide Dehydrogenase, Glutathione Reductase, Thioredoxin Reductase, and Mercuric Ion Reductase - A Family of Flavoenzyme Transhydrogenases in *Chemistry and Biochemistry of Flavoenzymes* (Muller, F., ed) (CRC Press, Inc., Boca Raton, FL) 3, 121-211.
87. Massey, V., and Williams, C. H., Jr. (1965) On the reaction mechanism of yeast glutathione reductase, *J. Biol. Chem.* 240, 4470-4480.
88. Rietveld, P., Arscott, L. D., Berry, A., Scrutton, N. S., Deonarain, M. P., Perham, R. N., and Williams, C. H., Jr. (1994) Reductive and oxidative half-reactions of glutathione reductase from *Escherichia coli*, *Biochemistry* 33, 13888-13895.
89. Huber, P. W., and Brandt, K. G. (1980) Kinetic studies of the mechanism of pyridine nucleotide dependent reduction of yeast glutathione reductase, *Biochemistry* 19, 4569-4575.
90. Untucht-Grau, R., Schulz, G. E., and Schirmer, R. H. (1979) The C-terminal fragment of human glutathione reductase contains the postulated catalytic histidine, *FEBS Lett.* 105, 244-248.
91. Krauth-Siegel, R. L., Arscott, L. D., Schonleben-Janas, A., Schirmer, R. H., and Williams, C. H., Jr. (1998) Role of active site tyrosine residues in catalysis by human glutathione reductase, *Biochemistry* 37, 13968-13977.
92. Adamson, S. R., Robinson, J. A., and Stevenson, K. J. (1984) Inhibition of pyruvate dehydrogenase multienzyme complex from *Escherichia coli* with a radiolabeled bifunctional arsenoxide: evidence for an essential histidine residue at the active site of lipoamide dehydrogenase, *Biochemistry* 23, 1269-1274.
93. McMillan, P. J., Arscott, L. D., Ballou, D. P., Becker, K., Williams, C. H., Jr., and Müller, S. (2006) Identification of acid-base catalytic residues of high-Mr thioredoxin reductase from *Plasmodium falciparum*, *J. Biol. Chem.* 281, 32967-32977.
94. Arscott, L. D., Veine, D. M., and Williams, C. H., Jr. (2000) Mixed disulfide with glutathione as an intermediate in the reaction catalyzed by glutathione reductase from yeast and as a major form of the enzyme in the cell, *Biochemistry* 39, 4711-4721.
95. Wong, K. K., Vanoni, M. A., and Blanchard, J. S. (1988) Glutathione reductase: solvent equilibrium and kinetic isotope effects, *Biochemistry* 27, 7091-7096.
96. Bilzer, M., Krauth-Siegel, R. L., Schirmer, R. H., Akerboom, T. P., Sies, H., and Schulz, G. E. (1984) Interaction of a glutathione S-conjugate with glutathione

- reductase. Kinetic and X-ray crystallographic studies, *Eur. J. Biochem.* 138, 373-378.
97. Benen, J., van Berkel, W., Dieteren, N., Arscott, D., Williams, C., Jr., Veeger, C., and de Kok, A. (1992) Lipoamide dehydrogenase from *Azotobacter vinelandii*: site-directed mutagenesis of the His450-Glu455 diad. Kinetics of wild-type and mutated enzymes, *Eur. J. Biochem.* 207, 487-497.
 98. Williams, C. H., Jr., Allison, N., Russell, G. C., Prongay, A. J., Arscott, L. D., Datta, S., Sahlman, L., and Guest, J. R. (1989) Properties of lipoamide dehydrogenase and thioredoxin reductase from *Escherichia coli* altered by site-directed mutagenesis, *Ann. N. Y. Acad. Sci.* 573, 55-65.
 99. Gromer, S., Wessjohann, L. A., Eubel, J., and Brandt, W. (2006) Mutational studies confirm the catalytic triad in the human selenoenzyme thioredoxin reductase predicted by molecular modeling, *Chembiochem* 7, 1649-1652.
 100. Brandt, W., and Wessjohann, L. A. (2005) The functional role of selenocysteine (Sec) in the catalysis mechanism of large thioredoxin reductases: proposition of a swapping catalytic triad including a Sec-His-Glu state, *Chembiochem* 6, 386-394.
 101. Gilberger, T. W., Walter, R. D., and Muller, S. (1997) Identification and characterization of the functional amino acids at the active site of the large thioredoxin reductase from *Plasmodium falciparum*, *J. Biol. Chem.* 272, 29584-29589.
 102. Kryukov, G. V., Castellano, S., Novoselov, S. V., Lobanov, A. V., Zehtab, O., Guigo, R., and Gladyshev, V. N. (2003) Characterization of mammalian selenoproteomes, *Science* 300, 1439-1443.
 103. Xu, X. M., Carlson, B. A., Mix, H., Zhang, Y., Saira, K., Glass, R. S., Berry, M. J., Gladyshev, V. N., and Hatfield, D. L. (2006) Biosynthesis of Selenocysteine on Its tRNA in Eukaryotes, *PLoS Biol* 5, e4.
 104. Yuan, J., Palioura, S., Salazar, J. C., Su, D., O'Donoghue, P., Hohn, M. J., Cardoso, A. M., Whitman, W. B., and Soll, D. (2006) RNA-dependent conversion of phosphoserine forms selenocysteine in eukaryotes and archaea, *Proc. Natl. Acad. Sci. U. S. A.* 103, 18923-18927.
 105. Pinsent, J. (1954) The need for selenite and molybdate in the formation of formic dehydrogenase by members of the coli-aerogenes group of bacteria, *Biochem. J.* 57, 10-16.
 106. Stadtman, T. C. (1996) Selenocysteine, *Annu. Rev. Biochem.* 65, 83-100.

107. Enoch, H. G., and Lester, R. L. (1975) The purification and properties of formate dehydrogenase and nitrate reductase from *Escherichia coli*, *J. Biol. Chem.* 250, 6693-6705.
108. Cone, J. E., Del Rio, R. M., Davis, J. N., and Stadtman, T. C. (1976) Chemical characterization of the selenoprotein component of clostridial glycine reductase: identification of selenocysteine as the organoselenium moiety, *Proc. Natl. Acad. Sci. U. S. A.* 73, 2659-2663.
109. Zhong, L., and Holmgren, A. (2000) Essential role of selenium in the catalytic activities of mammalian thioredoxin reductase revealed by characterization of recombinant enzymes with selenocysteine mutations, *J. Biol. Chem.* 275, 18121-18128.
110. Ip, C. (1998) Lessons from basic research in selenium and cancer prevention, *J. Nutr.* 128, 1845-1854.
111. Mugesh, G., du Mont, W. W., and Sies, H. (2001) Chemistry of biologically important synthetic organoselenium compounds, *Chem. Rev.* 101, 2125-2179.
112. Jacobs, M., and Forst, C. (1981) Toxicological effects of sodium selenite in Sprague-Dawley rats, *J. Toxicol. Environ. Health* 8, 575-585.
113. Jacobs, M., and Forst, C. (1981) Toxicological effects of sodium selenite in Swiss mice, *J. Toxicol. Environ. Health* 8, 587-598.
114. Bjornstedt, M., Hamberg, M., Kumar, S., Xue, J., and Holmgren, A. (1995) Human thioredoxin reductase directly reduces lipid hydroperoxides by NADPH and selenocystine strongly stimulates the reaction via catalytically generated selenols, *J. Biol. Chem.* 270, 11761-11764.
115. May, J. M., Cobb, C. E., Mendiratta, S., Hill, K. E., and Burk, R. F. (1998) Reduction of the ascorbyl free radical to ascorbate by thioredoxin reductase, *J. Biol. Chem.* 273, 23039-23045.
116. Kumar, S., Bjornstedt, M., and Holmgren, A. (1992) Selenite is a substrate for calf thymus thioredoxin reductase and thioredoxin and elicits a large non-stoichiometric oxidation of NADPH in the presence of oxygen, *Eur. J. Biochem.* 207, 435-439.

117. Gromer, S., Arscott, L. D., Williams, C. H., Jr., Schirmer, R. H., and Becker, K. (1998) Human placenta thioredoxin reductase. Isolation of the selenoenzyme, steady state kinetics, and inhibition by therapeutic gold compounds, *J. Biol. Chem.* 273, 20096-20101.
118. Bjornstedt, M., Kumar, S., and Holmgren, A. (1992) Selenodiglutathione is a highly efficient oxidant of reduced thioredoxin and a substrate for mammalian thioredoxin reductase, *J. Biol. Chem.* 267, 8030-8034.
119. Clark, L. C., Combs, G. F., Jr., Turnbull, B. W., Slate, E. H., Chalker, D. K., Chow, J., Davis, L. S., Glover, R. A., Graham, G. F., Gross, E. G., Krongrad, A., Lesher, J. L., Jr., Park, H. K., Sanders, B. B., Jr., Smith, C. L., and Taylor, J. R. (1996) Effects of selenium supplementation for cancer prevention in patients with carcinoma of the skin. A randomized controlled trial. Nutritional Prevention of Cancer Study Group, *JAMA* 276, 1957-1963.
120. Ganther, H. E. (1999) Selenium metabolism, selenoproteins and mechanisms of cancer prevention: complexities with thioredoxin reductase, *Carcinogenesis* 20, 1657-1666.
121. Jacob, J., Schirmer, R. H., and Gromer, S. (2005) The conserved histidine 106 of large thioredoxin reductases is likely to have a structural role but not a base catalyst function, *FEBS Lett.* 579, 745-748.
122. Lacey, B. M., and Hondal, R. J. (2006) Characterization of mitochondrial thioredoxin reductase from *C. elegans*, *Biochem. Biophys. Res. Commun.* 346, 629-636.
123. Gilberger, T. W., Bergmann, B., Walter, R. D., and Müller, S. (1998) The role of the C-terminus for catalysis of the large thioredoxin reductase from *Plasmodium falciparum*, *FEBS Lett.* 425, 407-410.
124. Wang, P. F., Arscott, L. D., Gilberger, T. W., Müller, S., and Williams, C. H., Jr. (1999) Thioredoxin reductase from *Plasmodium falciparum*: evidence for interaction between the C-terminal cysteine residues and the active site disulfide-dithiol, *Biochemistry* 38, 3187-3196.
125. Huber, R. E., and Criddle, R. S. (1967) Comparison of the chemical properties of selenocysteine and selenocystine with their sulfur analogs, *Arch. Biochem. Biophys.* 122, 164-173.
126. Hondal, R. J. (2005) Incorporation of selenocysteine into proteins using peptide ligation, *Protein Pept Lett* 12, 757-764.

127. Hondal, R. J., Nilsson, B. L., and Raines, R. T. (2001) Selenocysteine in native chemical ligation and expressed protein ligation, *J. Am. Chem. Soc.* *123*, 5140-5141.
128. Hondal, R. J., and Raines, R. T. (2002) Semisynthesis of proteins containing selenocysteine, *Methods Enzymol.* *347*, 70-83.
129. Kato, M., Chuang, J. L., Tso, S. C., Wynn, R. M., and Chuang, D. T. (2005) Crystal structure of pyruvate dehydrogenase kinase 3 bound to lipoyl domain 2 of human pyruvate dehydrogenase complex, *EMBO J.* *24*, 1763-1774.
130. Weichsel, A., Gasdaska, J. R., Powis, G., and Montfort, W. R. (1996) Crystal structures of reduced, oxidized, and mutated human thioredoxins: evidence for a regulatory homodimer, *Structure* *4*, 735-751.
131. Chenna, R., Sugawara, H., Koike, T., Lopez, R., Gibson, T. J., Higgins, D. G., and Thompson, J. D. (2003) Multiple sequence alignment with the Clustal series of programs, *Nucleic Acids Res* *31*, 3497-3500.
132. Tujebajeva, R. M., Copeland, P. R., Xu, X. M., Carlson, B. A., Harney, J. W., Driscoll, D. M., Hatfield, D. L., and Berry, M. J. (2000) Decoding apparatus for eukaryotic selenocysteine insertion, *EMBO Rep* *1*, 158-163.
133. Fagegaltier, D., Hubert, N., Yamada, K., Mizutani, T., Carbon, P., and Krol, A. (2000) Characterization of mSelB, a novel mammalian elongation factor for selenoprotein translation, *EMBO J.* *19*, 4796-4805.
134. Richards, F. M., and Vithayathil, P. J. (1959) The preparation of subtilisin-modified ribonuclease and the separation of the peptide and protein components, *J. Biol. Chem.* *234*, 1459-1465.
135. Evans, T. C., Jr., Benner, J., and Xu, M. Q. (1998) Semisynthesis of cytotoxic proteins using a modified protein splicing element, *Protein Sci.* *7*, 2256-2264.
136. Valiyaveetil, F. I., Sekedat, M., MacKinnon, R., and Muir, T. W. (2006) Structural and functional consequences of an amide-to-ester substitution in the selectivity filter of a potassium channel, *J. Am. Chem. Soc.* *128*, 11591-11599.
137. Valiyaveetil, F. I., Sekedat, M., Muir, T. W., and MacKinnon, R. (2004) Semisynthesis of a functional K⁺ channel, *Angew. Chem. Int. Ed. Engl.* *43*, 2504-2507.
138. Ottesen, J. J., Huse, M., Sekedat, M. D., and Muir, T. W. (2004) Semisynthesis of phosphovariants of Smad2 reveals a substrate preference of the activated T beta RI kinase, *Biochemistry* *43*, 5698-5706.

139. Evans, T. C., Jr., and Xu, M. Q. (1999) Intein-mediated protein ligation: harnessing nature's escape artists, *Biopolymers* 51, 333-342.
140. Gogarten, J. P., and Hilario, E. (2006) Inteins, introns, and homing endonucleases: recent revelations about the life cycle of parasitic genetic elements, *BMC Evol Biol* 6, 94.
141. Noren, C. J., Wang, J., and Perler, F. B. (2000) Dissecting the Chemistry of Protein Splicing and Its Applications, *Angew. Chem. Int. Ed. Engl.* 39, 450-466.
142. Cotton, G. J., Ayers, B., Xu, R., and Muir, T. W. (1999) Insertion of a Synthetic Peptide into a Recombinant Framework: a Protein Biosensor, *J. Am. Chem. Soc.* 121, 1100-1101.
143. Harris, K. M., Flemer, S., Jr., and Hondal, R. J. (2007) Studies on deprotection of cysteine and selenocysteine side-chain protecting groups, *J Pept Sci* 13, 81-93.
144. Fairbanks, G., Steck, T. L., and Wallach, D. F. (1971) Electrophoretic analysis of the major polypeptides of the human erythrocyte membrane, *Biochemistry* 10, 2606-2617.
145. Arnér, E. S., Zhong, L., and Holmgren, A. (1999) Preparation and assay of mammalian thioredoxin and thioredoxin reductase, *Methods Enzymol.* 300, 226-239.
146. Chivers, P. T., Prehoda, K. E., Volkman, B. F., Kim, B. M., Markley, J. L., and Raines, R. T. (1997) Microscopic pKa values of Escherichia coli thioredoxin, *Biochemistry* 36, 14985-14991.
147. Gill, S. C., and von Hippel, P. H. (1989) Calculation of protein extinction coefficients from amino acid sequence data, *Anal. Biochem.* 182, 319-326.
148. Turanov, A. A., Su, D., and Gladyshev, V. N. (2006) Characterization of alternative cytosolic forms and cellular targets of mouse mitochondrial thioredoxin reductase, *J. Biol. Chem.* 281, 22953-22963.
149. Urig, S., Lieske, J., Fritz-Wolf, K., Irmeler, A., and Becker, K. (2006) Truncated mutants of human thioredoxin reductase 1 do not exhibit glutathione reductase activity, *FEBS Lett.* 580, 3595-3600.
150. Luthman, M., and Holmgren, A. (1982) Rat liver thioredoxin and thioredoxin reductase: purification and characterization, *Biochemistry* 21, 6628-6633.

151. Arnér, E. S., Sarioglu, H., Lottspeich, F., Holmgren, A., and Bock, A. (1999) High-level expression in *Escherichia coli* of selenocysteine-containing rat thioredoxin reductase utilizing gene fusions with engineered bacterial-type SECIS elements and co-expression with the selA, selB and selC genes, *J. Mol. Biol.* 292, 1003-1016.
152. Bauer, H., Gromer, S., Urbani, A., Schnolzer, M., Schirmer, R. H., and Muller, H. M. (2003) Thioredoxin reductase from the malaria mosquito *Anopheles gambiae*, *Eur. J. Biochem.* 270, 4272-4281.
153. Inoue, H., Nojima, H., and Okayama, H. (1990) High efficiency transformation of *Escherichia coli* with plasmids, *Gene* 96, 23-28.
154. Johansson, L., Arscott, L. D., Ballou, D. P., Williams, C. H., Jr., and Arnér, E. S. (2006) Studies of an active site mutant of the selenoprotein thioredoxin reductase: The Ser-Cys-Cys-Ser motif of the insect orthologue is not sufficient to replace the Cys-Sec dyad in the mammalian enzyme, *Free Radic. Biol. Med.* 41, 649-656.
155. Ellman, G. L. (1959) Tissue sulfhydryl groups, *Arch. Biochem. Biophys.* 82, 70-77.
156. Wilson, J. M., Bayer, R. J., and Hupe, D. J. (1977) Structure-Reactivity Correlations for the Thiol-Disulfide Interchange Reaction, *J. Am. Chem. Soc.* 99, 7922-7926.
157. Eckenroth, B., Harris, K., Turanov, A. A., Gladyshev, V. N., Raines, R. T., and Hondal, R. J. (2006) Semisynthesis and characterization of mammalian thioredoxin reductase, *Biochemistry* 45, 5158-5170.
158. Zhang, R. M., and Snyder, G. H. (1989) Dependence of formation of small disulfide loops in two-cysteine peptides on the number and types of intervening amino acids, *J. Biol. Chem.* 264, 18472-18479.
159. Danehy, J. P., Elia, V. J., and Lavelle, C. J. (1971) The Alkaline Decomposition of Organic Disulfides. IV. A Limitation on the Use of Ellman's Reagent, 2,2'Dinitro-5,5'-dithiodibenzoic Acid, *J Org. Chem.* 36, 1003-1005.
160. Carlberg, I., and Mannervik, B. (1975) Purification and characterization of the flavoenzyme glutathione reductase from rat liver, *J. Biol. Chem.* 250, 5475-5480.
161. Otwinowski, Z., and Minor, W. (1997) Processing of x-ray diffraction data collected in oscillation mode., in *Methods in Enzymology, Part A* (Carter, C. W., and Sweet, R. M., Eds.), pp 307-326, Academic Press, San Diego.

162. Brunger, A. T., Adams, P. D., Clore, G. M., DeLano, W. L., Gros, P., Grosse-Kunstleve, R. W., Jiang, J. S., Kuszewski, J., Nilges, M., Pannu, N. S., Read, R. J., Rice, L. M., Simonson, T., and Warren, G. L. (1998) Crystallography & NMR system: A new software suite for macromolecular structure determination, *Acta Crystallographica D Biological Crystallography* 54, 905-921.
163. Jones, T. A., Zou, J. Y., Cowan, S. W., and Kjeldgaard, M. (1991) Improved methods for building protein models in electron density maps and location of errors in these models., *Acta Crystallogr. A* 47, 110-119.
164. Collaborative Computational Project, N. (1994) The CCP4 Suite: Programs for Protein Crystallography, *Acta Crystallographica D Biological Crystallography* D50, 760-763.
165. Winn, M. D., Isupov, M. N., and Murshudov, G. N. (2001) Use of TLS parameters to model anisotropic displacements in macromolecular refinement, *Acta Crystallogr. D. Biol. Crystallogr.* 57, 122-133.
166. Occena, L. G., and Schmoltdt, D. L. (1995) GRASP - A Prototype Interactive Graphic Sawing Program - (MU-IE Technical Report). *MU-IE Technical Report 019501*, 1-17.
167. DeLano, W. L. (2002) The PyMOL Molecular Graphics System, in *The PyMOL Molecular Graphics System*, DeLano Scientific, Palo Alto.
168. Zhang, Y., Bond, C. S., Bailey, S., Cunningham, M. L., Fairlamb, A. H., and Hunter, W. N. (1996) The crystal structure of trypanothione reductase from the human pathogen *Trypanosoma cruzi* at 2.3 Å resolution, *Protein Sci.* 5, 52-61.
169. Hansen, R. E., Ostergaard, H., and Winther, J. R. (2005) Increasing the reactivity of an artificial dithiol-disulfide pair through modification of the electrostatic milieu, *Biochemistry* 44, 5899-5906.
170. Avizonis, D. Z., Farr-Jones, S., Kosen, P. A., and Basus, V. J. (1996) Conformations and dynamics of the essential cysteinyl-cysteine ring derived from the acetylcholine receptor, *J. Am. Chem. Soc.* 118, 13031-13039.
171. Wang, P. F., Veine, D. M., Ahn, S. H., and Williams, C. H., Jr. (1996) A stable mixed disulfide between thioredoxin reductase and its substrate, thioredoxin: preparation and characterization, *Biochemistry* 35, 4812-4819.
172. May, J. M., Mendiratta, S., Hill, K. E., and Burk, R. F. (1997) Reduction of dehydroascorbate to ascorbate by the selenoenzyme thioredoxin reductase, *J. Biol. Chem.* 272, 22607-22610.

173. Shaked, Z., Szajewski, R. P., and Whitesides, G. M. (1980) Rates of thiol-disulfide interchange reactions involving proteins and kinetic measurements of thiol pKa values, *Biochemistry* 19, 4156-4166.
174. Gilbert, H. F. (1990) Molecular and cellular aspects of thiol-disulfide exchange, *Adv. Enzymol. Relat. Areas Mol. Biol.* 63, 69-172.
175. Gilbert, H. F. (1997) Thiol/disulfide exchange and redox potentials of proteins, in *Bioelectrochemistry of Biomacromolecules*, eds. Lenaz, G. & Milazzo, G. (Birkhauser, Basel) 256-324.
176. **Reprinted from Free Radical Biology & Medicine, V., Johansson, L., Arscott, L.D., Ballou, D.P., Williams Jr., C.H., Arnér, E.S.J., Studies of an active site mutant of the selenoprotein thioredoxin reductase: The Ser-Cys-Cys-Ser motif of the insect orthologue is not sufficient to replace the Cys-Sec dyad in the mammalian enzyme, p. 649-56, Copyright 2006, with permission from Elsevier.**

APPENDIXES

A. ABBREVIATIONS

AMP, adenosine monophosphate; β -Me, 2-mercaptoethanol; CATC, the sequence Cys-Ala-Thr-Cys; CCG, the tripeptide Cys-Cys-Gly; CeTR; *Caenorhabditis elegans* TR; CID, collision induced dissociation; CISS; the sequence Cys-Ile-Ser-Ser; CNS, Crystallography and NMR system; CUG, the tripeptide Cys-Sec-Gly; DEAE, diethylaminoethyl; *DmTR*, *Drosophila melanogaster* TR; dNTP, deoxyribonucleotide triphosphate; DTNB, 5,5'-Dithio-bis(2-nitrobenzoic acid); DTT, dithiothreitol; EDTA, ethylenediaminetetraacetic acid; EH₂, 2-electron reduced (1 NADPH equivalent) flavoprotein; EH₄, 4-electron reduced (2 NADPH equivalent) flavoprotein; E_{ox}, oxidized flavoprotein; EPL, expressed protein ligation; ESI-MS, electrospray ionization mass spectrometry; FAD, flavin adenine dinucleotide; Fmoc, 9-fluoroenylmethoxycarbonyl; GCCG, the tetrapeptide Gly-Cys-Cys-Gly; GCUG, the tetrapeptide Gly-Cys-Sec-Gly; GITS, the sequence Gly-Ile-The-Ser; GR, glutathione reductase; GSH, reduced glutathione (γ -glutamylcysteinylglycine); GSH I, interchange glutathione; GSH II, first leaving group glutathione; GSSG, oxidized diglutathione; HPLC, high pressure liquid chromatography; H₂O₂, hydrogen peroxide; ICP-MS, inductively coupled plasma mass spectrometry; IPTG, isopropyl- β -D-thiogalactopyranoside; LB, Luria-Betami Media; LipDH, dihydrolipoamide dehydrogenase; MALDI-TOF, matrix-assisted laser desorption ionization time of flight mass spectrometry; MES, 2-(4-Morpholio)-Ethane Sulfonic

Acid; M_r , molecular weight; MOPS; 3-(N-Morpholino) Propane-Sulfonic Acid; mTR3, mouse mitochondrial TR; NADH, reduced nicotinamide adenine dinucleotide; NADP⁺, oxidized nicotinamide adenine dinucleotide phosphate; NADPH, reduced nicotinamide adenine dinucleotide phosphate; NF- κ B, nuclear factor κ B; NMA, *N*-methylmeraptoacetamide; NMR, nuclear magnetic resonance; PDB, Protein Data Bank; PEG, polyethylene glycol; *Pf*TR, TR from *Plasmodium falciparum*; RMSD, root mean squared deviation; RNR, ribonucleotide reductase; SCCS, the tetrapeptide Ser-Cys-Cys-Ser; Sec, selenocysteine; SDS-PAGE, sodium dodecyl sulfate polyacrylamide gel electrophoresis; SECIS, selenocysteine insertion sequence; TB, terrific broth; TNB-, thiobis(2-nitrobenzoic acid) anion; TR, thioredoxin reductase; Trx, thioredoxin; TryR, trypanothine reductase; U, the one-letter abbreviation for selenocysteine; WT, wild type; Xa, protease Xa.

B. COMPREHENSIVE LIST OF MATERIALS

Solvents for peptide synthesis were purchased from EMD Biosciences (San Diego, CA). Fmoc amino acids were purchased from Synpep Corp. (Dublin, CA). Resins for solid-phase synthesis were purchased from Novabiochem (San Diego, CA). All PCR primers were purchased from Integrated DNA Technologies Inc., and PAGE purified (Coralville, IA). Restriction endonucleases Nco I, Sap I, Hind III, Eco RI, Nde I, Sal I, Kpn I, Vent DNA polymerase, plasmids pTYB1 and pTYB3, chitin agarose beads, T4 DNA ligase, and reaction buffers were supplied by New England Biolabs (Ipswich, MA). All restriction enonucleases, Vent DNA Polymerase, and T4 DNA ligase were used with the supplied buffers according to manufacturers guidelines. Recombinant *E. coli* thioredoxin was purchased from American Diagnostica (Greenwich, CT). DTNB, NADPH, NADP+, Bovine Pancreatic Insulin and N-Methylmercaptoacetamide (NMA) were purchased from Sigma-Aldrich (St. Louis, MO). Hydrogen peroxide 30% solution was purchased from J.T Baker (Phillipsburg, NJ). The PEG 6000 used for crystallization was purchased from Fluka (Sigma-Aldrich). All other chemicals were purchased from either Sigma-Aldrich or Fisher Scientific and were of reagent grade or better.

C. LIST OF PCR PRIMERS

CLONING OF MOUSE TR3 WITH pTYB3

Upstream mTR3 (labeled TRup2).

Downstream mTR3-GCCG 5'-

ACAGCCGCTCTTCAGCAGCCACAGCAACCAGTCACA-3' (labeled TRCYS).

Downstream mTR3-SCCS 5'-

ACAGCCGCTCTTCAGCAGGAACAGCAAGAAGTCACAGTAGGCTCC-3' (labeled TRser).

Downstream mTR3-GSCG 5'-

ACAGCCGCTCTTCAGCAGCCACAGGAACCAGTCACA-3' (labeled mTR-C488S).

QuickChange Stratagene Mutagenesis Forward mTR3-Cys52Ser/Cys57Ser 5'-

GGTGGCACCTCTGTCAACGTGGGTTCCATACCCAAGAAGC-3' (labeled mTRC52-57A-fwd).

QuickChange Stratagene Mutagenesis Reverse mTR3-Cys52Ser/Cys57Ser 5'-

GCTTCTTGGGTATGGAACCCACGTTGACAGAGGTGCCACC-3' (labeled mTRC52-57A-Rev).

CLONING OF DROSOPHILA TR WITH pTYB1

Upstream primer 5' – AACAGACATATGGCGCCCGTGCAAGG – 3' (labeled dmup2).

Downstream *Dm*TR-SCCS 5'-

ACAGCCGGTACCCTTGGCAAAGCAGCTGCAGCAGCTGGCCGG -3' (labeled
dmdown2L).

Downstream truncated *Dm*TR-S₄₈₈ 5'-

ACAGCCGGTACCCTTGGCAAAGCAGCTGGCCGGCGTGGGG-3' (labeled
dmdown2s).

Downstream *Dm*TR-SCACS 5'-

ACAGCCGGTACCCTTGGCAAAGCAGCTGCAGGCGCAGCTGGCCGGCGTGGG-
3' (labeled *Dm*TR-CAC).

Downstream *Dm*TR-SCAACS 5'-

ACAGCCGGTACCCTTGGCAAAGCAGCTGCAGGCGGCGCAGCTGGCCGGCGTG
GG-3' (labeled *Dm*TR-CAAC).

QuickChange Stratagene Mutagenesis Forward *Dm*TR His464Ala 5'-

CAACACCGTGGGCATCGCCCCACTACCGCCGAAGAG-3' (labeled
HIS464forward).

QuickChange Stratagene Mutagenesis Reverse *Dm*TR His464Ala 5'-

CTCTTCGGCGGTAGTGGGGGCGATGCCACGGTGTTG-3' (labeled
HIS464reverse).

QuickChange Stratagene Mutagenesis Forward *Dm*TR His106Ala 5'-

CTGGTGCAGTCCGTACAGAACGCCATTAAGTCCGTCAACTGG-3' (labeled
His106f2).

QuickChange Stratagene Mutagenesis Reverse *Dm*TR His106Ala 5'-
CCAGTTGACGGACTTAATGGCGTTCTGTACGGACTGCACCAG-3' (labeled
His106rev2).

QuickChange Stratagene Mutagenesis Forward *Dm*TR Glu469Ala 5'-
CACTACCGCCGCAGAATTCACCCGGCTG-3' (labeled E469Aforward).

QuickChange Stratagene Mutagenesis Reverse *Dm*TR Glu469Ala 5'-
CAGCCGGGTGAATTCTGCGGCGGTAGTG-3' (labeled E469Areverse).

CLONING OF THIOREDOXIN

QuickChange Stratagene Mutagenesis Forward Trx Cys36Ser 5'-
GGTGCGGTTCGGTCCAAAATGATCGC-3' (*labeled TrxC35Sfw).

QuickChange Stratagene Mutagenesis Reverse Trx Cys36Ser 5'-
GCGATCATTTTGGACGGACCGCACC-3' (labeled TrxC35Srev).

*Cys36 is correct, the C35 was a typo in ordering.